To the Graduate Council:

I am submitting herewith a dissertation written by Anne M. Kroman entitled "Fracture Biomechanics of the Human Skeleton." I have examined the final electronic copy of this dissertation for form and content and recommend that it be accepted in partial fulfillment of the requirements for the degree of Doctor of Philosophy, with a major in Anthropology.

Murray K. Marks
Major Professor

We have read this dissertation
and recommend its acceptance:

Walter Klippel

Lyle Konigsberg

Mohamed Mahfouz

Accepted for the Council:

Carolyn R. Hodges

Vice Provost and
Dean of the Graduate School

(Original signatures are on file with official student records.)

FRACTURE BIOMECHANICS OF THE HUMAN SKELETON

A Dissertation
Presented for the
Doctor of Philosophy Degree

The University of Tennessee, Knoxville

Anne M. Kroman
August 2007

DEDICATION

This dissertation is dedicated to my amazing parents,

Jim and Deb Kroman

for all of their love and support.

I would also like to dedicate this dissertation to all of the individuals who donated their remains to science.

ACKNOWLEDGEMENTS

This dissertation is due in part to the unselfish support and help of countless people. First and foremost, I would like to thank my committee, Drs. Marks, Klippel, Konisberg, and Mahfouz. They are an amazing group of people and have been an inspiration through my entire academic career. To my chair, Dr. Murray Marks, thanks for everything through the years. You have been a wonderful inspiration and a friend, and I'll remember all the laughs that we shared. "Face down on a hill" still cracks me up! I look forward to more laughs and stories. I also owe a huge thanks to the people that peaked my interest in forensic anthropology at got me on to the path of trauma analysis. I owe all of you more than I could ever say! To Dr. Hugh Berryman, thank you for your great insight into trauma and all the help through the years! To Dr. Ranald Donaldson, thank you so much for your incredible support, brilliant mind, and your amazing friendship. I owe you and Daphne, and Fergus more than I could ever say! To Dr. Steven Symes, thank you for everything. You were my inspiration and my foundation for looking at trauma in forensic anthropology. I owe you so much more than I can ever say – words are not enough.

In addition to all the help and support I've gotten from the faculty at The University of Tennessee, I've been so lucky to receive so much assistance, guidance, and encouragement from many other brilliant minds. I owe a big thanks to Dr. David Porta who has been a wonderful mentor, friend and a shining example of the type of researcher I hope to be. And to Nancy Porta, thanks so

much for the laughs and the unwavering support through some of the crazy times with Thing 1 and Thing 2.

I also feel so lucky for the wonderful support from Dr. Stefan Duma. I owe Stefan and all his students at Virginia Tech for the tons and help and lots of good times. Also, thanks to Chrissy Duma for being a great friend and for giving wonderful advice and perspective.

I am also blessed in all of my friends – I could not have finished this with out your love, encouragement and support. Liz DiGangi – thank you for sharing my frustrations and listing to my rants and laughing about it all. You are an amazing professor and an inspiration. Meta Pike – thank you for being a wonderful friend! I miss you! You are always there to listen to my crazy stories and you always can relate! You are a beautiful person, inside and out. Natalie Shirley – thank you so much for being a wonderful friend. I'm so glad that we have become close, and I look forward to many more years of hanging out, trying on ridiculous looking expensive clothes, ranting about trauma, and drinking good wine! Megan Moore – Megan, what can I say. It makes me smile just to type in your name. You are so incredibly supportive and such a positive person. Thank you for everything and always being there. Sue Myster – I could not have done this with out you. You have always been there every step of the way. You're a wonderful person and I'm so glad to have you as a friend. Emily Dixon – a.k.a. Schmemily Nelson. Oh good lord. There is no way I can put into words what you mean to me. You have been my best friend since high school, and most of

the things that we went through and the trouble we got into is not fit to print! Repress and smile! I love you and miss you!

I owe everything to my wonderful family which is the best family that anyone could ever ask for. I am blessed with a whole slew of wonderful aunts, uncles, and cousins who have been there through it all. To Pat, John, Andy, and Kate – thanks for all the laughs and all the amazing meals. To Denise, Roger, Joe, Jenny, and Jill – thank you for being a wonderful, loving, supportive group of people! To Barb – you are an amazing person, and an amazing inspiration and the best Irish godmother that anyone could ask for! Thank you so much for being so strong and so unselfishly loving! To Doug – I can't thank you enough for all the side splitting laughs and the late night kitchen table chats. You are one of my favorite people, and I'm lucky to count you as a friend! I look forward to a lifetime more of inspiration, bottles of good wine, and talks with you! To my grandparents – thank you for everything. Even though you are gone, the fact that I know how proud you would be keeps me going.

Thank you so much, Mom and Dad for all you have done and for being amazing parents, wonderful people, and my best friends. I truly could not have gotten this far in life with out your constant love and support. I will never be able to thank you enough.

I would also like to give a big thanks to the entire Kress family, especially Tom, Dee, and Wendy. Thank you for being so supportive in all aspects of my life and making me feel loved and welcome.

My final thank you is reserved for someone very special. Tyler, thank you for everything. I can't possibly tell you how much you mean to me. You are my everything. You have all my love.

ABSTRACT

Trauma analysis is a growing area of physical and forensic anthropology. The analysis of fracture patterns is useful in determining cause and manner of death, as well as making inferences about past populations. Traditionally, anthropologists have categorized bone trauma into the discrete categories of blunt, ballistic, and sharp trauma. While these descriptors provide a practical approach, anthropologists need to change the way that trauma is perceived and analysis of fractures is conducted. Bone trauma is best viewed as a continuum (rather than discrete independent categories), with the variables of force, acceleration/deceleration, and surface area of impacting interface governing the appearance of the resulting fractures. The application of this new way of thinking will allow anthropologists to better understand bone fracture and injury to the body as a relationship between the engineering inputs and the anatomical outputs.

This new way of thinking is applied to the human skeleton and tested through a series of experimental studies and injury data analyses. The studies include fracture propagation and patterning in the skull, the response of the thorax/upper body to propeller induced trauma, force tolerance for human phalanges, and mechanics of lower limb fractures. The results from these studies assist in reiterating the importance of variables (or “engineering inputs”), such as force, surface area of impacting interface, and acceleration/deceleration,

on the resulting injury and fracture patterns (“anatomical outputs”) of the human body.

As expected, the magnitude of force clearly influences the severity of fractures. However, comparison of force magnitude is not a “one-to-one” comparison. Surface area between the impacting object and the bone is a crucial variable. It essentially explains differences between blunt and sharp trauma. An example of the surface area variable in this experimental testing involved the propeller impacts to the buttocks and upper body. Note, though, as failure occurs, surface area interfacing can change, resulting in sharp trauma wounds that could contain characteristics of blunt trauma, or vice versa. Intrinsic properties of the bone (such as geometry, location, quality of bone) and its anisotropic and viscoelastic nature should also be considered along with these other engineering variables.

TABLE OF CONTENTS

CHAPTER 1: INTRODUCTION 1
Bone Trauma and Forensic Anthropology 2
Mechanical Properties of Bone 5
Definitions and Basic Principles of Biomechanics 6
Biomechanics of Human Bone 10
Re-evaluation of Bone Trauma Paradigm: Engineering inputs and anatomical outputs 17

CHAPTER 2: CRANIAL TRAUMA 20
Relevance of Cranial Trauma 21
Forensic and Physical Anthropology 21
Impact Biomechanics 21
Fracture Biomechanics of the Cranium 22
Fracture Pattern Testing in the Cranial Vault 26
Introduction 26
Materials and Methods 27
Results 31
Discussion 34
Conclusion 36
Fracture Pattern Testing in the Cranial Base 37
Introduction 37
Materials and Methods 39
Results 41
Conclusions 44

CHAPTER 3: TRAUMA TO THE THORAX 48
Relevance of Thoracic Trauma 49
Forensic and Physical Anthropology 49
Impact Biomechanics 49
Impact Testing of the Thorax from Boat Propellers 50
Introduction 50
Materials and Methods 51
Human Test Results 60
Porcine Test Results 86
Discussion 90
Conclusion 91

CHAPTER 4: UPPER EXTREMITY TRAUMA 92
Relevance of Upper Extremity Trauma 93
Forensic and Physical Anthropology 93
Impact Biomechanics 94
Experimental Testing of Phalanges 94
Introduction 94
Materials and Methods 95
Results and Discussion: Static Testing 95
Results and Discussion: Dynamic Testing 97
Results and Discussion: Field Testing 105

CHAPTER 5: LOWER EXTREMITY TRAUMA 107
Relevance of Lower Extremity Trauma 108
Forensic and Physical Anthropology 108
Impact Biomechanics 108
Relevant Anatomy of the Ankle 109
Lower Extremity and Ankle Injury Classifications 111
Lauge-Hansen Classification System 112
Danis_Weber Classification System 119
Other relevant mechanisms of injury 121
Personal Watercraft Injury Study 127
Introduction 127
Materials and Methods 130
Results 133
Conclusions 159

CHAPTER 6: CONCLUSION 160
Recommendations for physical and forensic anthropologists 161

BIBLIOGRAPHY 165

APPENDIX 175
Appendix A : Fracture Propagation in the Cranial Vault 176
Appendix B: Propeller Impact Testing 193
Appendix C: Personal Watercraft Study 224

VITA 283

LIST OF FIGURES

Figure 1.1 Illustration of the effect of tensile, compressive, and shear stress on a beam. 8

Figure 1.2 Anisotropic materials have physical properties that vary with direction; in this case, the model of bone is stronger in vertical direction (large arrows) than in transverse direction (small arrows). 12

Figure 1.3 Elastic deformation of bone. 14

Figure 1.4 Plastic deformation of bone. 14

Figure 1.5 Diagram showing a characteristic stress-strain curve showing the elastic and plastic deformation phases and failure point (after Turner and Burr 1993: 597). 16

Figure 2.1 Fracture propagation in both the inner (right) and outer (left) tables of the cranium. After Moritz 1954: 342. 24

Figure 2.2 Concentric and Radiating fractures from blunt force trauma impact site to the left parietal (10X). 25

Figure 2.3 Dorsal view of human head ready for testing with impact area on left parietal with intact soft tissue, and clean bone on the rest of the cranium... 29

Figure 2.4 Dorsal view of the skull (test five) during the impact event taken from the high speed video. The line of fracture propagation shown at the white arrows (read left to right) and is radiating out from the point of impact. 35

Figure 2.5 Orientation of the head during impact. The vault and brain have been removed, and the internal surface of the cranial base is visible. The impactor (visible in the photo) is lined up to impact the right temporal region. 40

Figure 2.6 View of the cranial base from test one post testing. A radiating fracture is visible (black arrow) that terminates into foramen magnum. 43

Figure 2.7 View of the skull from test two after some soft tissue removal. A complete hinge fracture is visible traveling anterior to the petrous portions and through sella turica. 45

Figure 2.8 Fractures radiating out of the left and right internal auditory meatus (black arrows). 46

Figure 3.1 View of a portion of the torodial pool at the CRESE facility showing the centrifuge arm with motor attached. 53

Figure 3.2 Outboard motor mounted to the platform over the water. 54

Figure 3.3 Underwater viewing windows and halogen lights for high speed filming. 55

Figure 3.4 Mirror placed at a 45 degree angle to allow for lateral viewing of the specimen. 56

Figure 3.5 Schematic of RingProp propeller. 57

Figure 3.6 Schematic of standard propeller. 57

Figure 3.7 Cavitation/ Laceration type injury to the lateral aspect of the right thigh in human specimen 1 from test 9.H1R5R shown here in the post-test view. 64

Figure 3.8 Laceration injury to parietal scalp in human specimen 1 from test 9.H1R5R. No fractures were present. 65

Figure 3.9 Parallel depressions (shown at red arrows) on the back of human specimen 1 from test 10.H1S5L from the blades of the propeller. 67

Figure 3.10 Diagram illustrating location of rib fractures in human specimen 1 from test 10.H1S5L. 68

Figure 3.11 Location of rib fractures (black arrows) in human specimen 1 from test 10.H1S5L 69

Figure 3.12 Laceration to the rectal region. 70

Figure 3.13 Patterned brusing and exposure of the right humerus in human specimen 2 from test 12.H2S5R 72

Figure 3.14 Diagram illustrating location of rib fractures in human specimen 2 from test 12.H2S5R. 73

Figure 3.15 Dissection showing fracture of rib seven (black arrow) in human specimen 2 from test 12.H2S5R 74

Figure 3.16 Laceration to temporal region with mild involvement of the temporalis muscle. 75

Figure 3.17 Large scooping laceration to left buttocks in human specimen 3 from test 13.H3R7L. There was no damage to the muscle, nerve, or bone tissue from the impact..... 76

Figure 3.18 Twelve parallel lacerations on the right side of human specimen three from test 14.H3S7R..... 78

Figure 3.19 Diagram illustrating the location of rib fractures from the anterior view in human specimen three from test 14.H3S7R..... 78

Figure 3.20 Diagram illustrating the location of rib fractures from the posterior view in human specimen 3 from test 14.H3S7R..... 79

Figure 3.21 Multiple rib fractures and lacerated lung in human specimen 3 from test 14.H3S7R..... 80

Figure 3.22 Reflection of the fractured ribs on the right side of human specimen 3 from test 14.H3S7R revealed a penetrated plural cavity. 81

Figure 3.23 Lacerations, fractured zygoma, and comminuted skull fracture from standard propeller blade impacts in human specimen 3 from test 14.H3S7R. 82

Figure 3.24 Laceration to right cerebral hemisphere in area of propeller blade impact in human specimen 3 from test 14.H3S7R. 83

Figure 3.25 Laceration to the lateral superior right thigh in human specimen 4 from test 15.H4R7R. Dissection reveled that there was no injury to the musculature or bone..... 84

Figure 3.26 Lacerations to the left buttock region and the posterior scalp in human specimen 4 from test 16.H4S7L. 85

Figure 4.1 Test set up for the static finger testing..... 96

Figure 4.2 Test set up for dynamic finger impact testing. 98

Figure 4.3 Soft tissue lacerations in hand one..... 100

Figure 4.4 Longitudinal fractures of the phalanges in hand two..... 101

Figure 4.5 Longitudinal fracture to the intermediate phalanx of the fifth ray. 103

Figure 4.6 Fracture to the condyles of the proximal phalanx of the thumb. 104

Figure 4.7 Fuji film reading with the pressure reported in psi. 106

Figure 5.1 Injury mechanics for supination-adduction injury. From Trafton et al 1992. 115

Figure 5.2 Injury mechanics behind supination-external rotation. From Trafton et al 1992..... 116

Figure 5.3 Injury mechanism for pronation-abduction. From Trafton et al 1992. 117

Figure 5.4 Injury mechanics for pronation-external rotation injury. From Trafton et al 1992..... 118

Figure 5.5 Fractures to the ankle from an axial load..... 122

Figure 5.6 Fractures to the foot from an axial load. 123

Figure 5.7 Fractures to the knee from an axial load. 124

Figure 5.8 Sprial fracture from torsional loading. 126

Figure 5.9 Injury data from PWC from 1989 to 1992. 129

Figure 5.10 Breakdown of PWC injury location. 131

Figure 5.11 1998 NTSB Injury data for PWC accidents..... 132

Figure 5.12 Radiographs from case 16 illustrating fractures from an external rotation injury. 140

Figure 5.13 Radiograph showing fractures resulting from a bending mechanism. 141

Figure 5.14 Radiograph showing fracture from an axial load. 142

Figure 5.15 Locations of all PWC fractures involving the right femur. 144

Figure 5.16 Locations of all PWC fractures involving the left femur..... 145

Figure 5.17 Locations of all PWC fractures involving the right tibia and fibula. 146

Figure 5.18 Locations of all PWC fractures involving the left tibia and fibula.... 147

Figure 5.19 Location of all PWC fractures involving the left foot..... 148

Figure 5.20 Locations of PWC fractures to the tibia and fibula. 150

Figure 5.21 Locations of PWC fractures to the femur. 151

Figure 5.22 Comparison of location of fracture between soccer and PWC use. 153

Figure 5.23 Comparison of fracture locations between skiboarding and PWC use. 154

Figure 5.24 Comparison between fracture location between PWC use and soccer. 155

Figure 5.25 Comparison of fracture patterns between PWC case 16 (on left) to a MVA (on right). 156

Figure 5.26 Comparison between fracture patterns in PWC case 21 (left) and a football player (right). 157

Figure 5.27 Comparison of fracture patterns between PWC case 15 and a slip and fall. 158

LIST OF TABLES

Table 3.1 Cadaver Data……59

Table 3.2 Human Test Matrix…….. 61

Table 3.3 Porcine Test Matrix……. 62

Table 3.4 Soft Tissue Injury Summary…….. 87

Table 3.5 Osseous tissue injury summary ……... 88

Table 3.6 Soft tissue injury summary……. 89

Table 3.7 Osseous tissue injury summary…… 90

Table 5.1 Abbreviations used in the following tables…… 134

Table 5.2 Case Summaries…….. 135

Table 5.3 Results Quantified……. 138

CHAPTER 1: INTRODUCTION

Bone Trauma and Forensic Anthropology

As the field of forensic anthropology has grown, bone trauma has become an increasingly vital component in the analysis of skeletal remains. Anthropologists are working side by side with forensic pathologists in increasing numbers and are being called on to examine trauma to the skeleton for evidence of cause or manner of death. Correct fracture pattern interpretation is used to determine such things as type of trauma (i.e., blunt, ballistic, or sharp), number of impacts to the body, location of impact, and amount of force applied to the body to name just a few. All of these conclusions are drawn by relying on the science of physics and knowledge of the material properties of bone to correctly understand and "read" the fractures.

While an important variable in forensic anthropology, trauma analysis is fundamentally different from its cohorts of age, ancestry, stature, and sex. Gone are the typologies, regression equations, and scoring of traits by present or absent. Gone are the subtle populational variations and secular change that exists in modern humans. In their place is a complex world of physics, and the countless intrinsic and extrinsic variables that govern how the human body responds to force. Interest in trauma analysis as a component of forensic anthropology has grown tremendously in recent years; however there have been some associated growing pains (Byers 2002). Problems arise from approaching trauma analysis in a similar manner to approaching sex estimation. Physical anthropologist have been trained to view things in terms of classifications – certain traits expressed in a skeleton lead us to the conclusion of a discrete

category (i.e., male or female). This “typological” background has colored the way that trauma is viewed. Trauma tables are used as teaching tools with a list of characteristics that allow anthropologists to classify the trauma as blunt, sharp, or ballistic. For example, a table may list the characteristics of delamination, concentric fractures, and plastic deformation under “blunt trauma.” These are all valid perceptions of osseous response to a blunt trauma impact. However, this can mislead some anthropologists into thinking that those indicators are the “signs” of blunt trauma alone, similar to the way that a wide sciatic notch is a “sign” of a female. The problem then deepens when the general categories that are used to talk about trauma (i.e., blunt, ballistic, and sharp) are viewed as exclusive weapons based categories. Byers (2002) runs into this major problem when he classifies any projectile (i.e., anything that flies through the air) as ballistic and ballistic trauma. This mode of thinking reduces everything to discrete categories. For example, all bullets create ballistic trauma, all hammers create blunt trauma, all knives create sharp trauma and they can all be neatly separated based on their own individual fracture characteristics (the male/female approach). However, confusion arises when there are mixed signals and the trauma can not be easily classified. What happens when an incised wound ends in a large radiating fracture? What happens when a bullet impact looks like blunt trauma? These types of questions have led to the bizarre creation of new categories of trauma, such as “sharp-blunt trauma” or “blunt-ballistic trauma.”

Trauma to the skeleton is best conceptualized as a physics based continuum, rather than a series of discrete categories. This continuum is

governed by a series of variables relating to the intrinsic properties of bone and the extrinsic characteristics of the force applied. The key extrinsic factors are force of the impact, surface area of impacting interface, and the acceleration/deceleration rate. The goal of this dissertation is to explore the influence of these variables on the creation of fractures in the skeleton. In other words, to understand the relationship between the "engineering inputs" and the "anatomical outputs" of traumatic events.

Most of the proceeding trauma research in forensic anthropology has relied on forensic case studies as data sets. While invaluable information can be learned from these cases and the majority of this work is exceptional, case studies are inherently limited. In many instances there is no information as to the exact circumstances of the death and the cause of the skeletal trauma. What information there is may be general at best. Experimental impact testing provides us with a means to fill in the gaps created by case based research and fine tune our understanding of fracture mechanics. Recently, anthropologists have begun to explore the use of experimental testing for trauma analysis (Bartelink et al 2001, Calce and Rogers 2007, Kroman 2004, Kroman et al 2005, Kroman et al 2006, Porta et al 2006). Testing can provide answers to questions regarding controversial theories, such as fracture propagation in the skull (Kroman 2004, Kroman et al 2005), explore new technology (such as SEM analysis) (Bartelink et al 2001), and even correlate penetration ballistic penetration depths in live human soft tissue (Porta et al 20060. Experimental

testing provides a wonderful counterpart to case studies, with cases bring about the fascinating questions and testing helping to resolve them.

This dissertation is segmented into the major regions of the body; head, thorax, upper extremity, and lower extremity. Within each section there is a general overview of examples of relative trauma to that region. The overview is in no way exhaustive of the vast literature for every body region. Browner et al (1992) provides excellent volumes to this extent. For each region, specific questions regarding bone trauma mechanics is formulated and tested, using the key variables of force of impact, surface area of impacting interface, and acceleration/deceleration rate.

Mechanical Properties of Bone

Biomechanics involves an understanding of the physical science of forces and energies to living tissue. The application of biomechanics to skeletal material is necessary to understand bone fractures in a rational context. An understanding of biomechanics and the physical properties of bone lends valuable insight into the mechanics of fracture creation and propagation. The creation of fractures depends on several factors. The first relates to the extrinsic characteristics of the impacting force. Second, intrinsic characteristics of bone influence the creation and propagation of fractures, including both the material and structural properties (Gonza 1982).

Definitions and Basic Principles of Biomechanics

To understand how bone responds to forces and how fractures occur, a scientist must understand some basic physics terminology of biomechanics. Some basic definitions of important concepts follow. For further review see Brinckmann et al (2002), Cowin (1989), Evans (1970), Frost (1967), Low and Reed (1996), and Roark and Young (1975).

Force

The impacting force or load type plays an important role in fracture creation and propagation. Force is defined as an "action or influence" that is "applied to a free body" (Turner and Burr 1993: 595). In other words, a force is anything that alters the state of motion of an object (Low and Reed 1996). Two kinds of forces exist; the type that influences an object by direct contact and the kind of force that influences an object from a distance (i.e., gravitational) (Cowin 1989). A direct force simply pushes or pulls an object. Newton's first law of motion states that a force must be applied to change the velocity or direction of movement of an object. Newton's second law of motion states that the resulting change in momentum of the object is proportional to the force applied (Low and Reed 1996). For example, the more force that is applied in hitting a baseball with a bat, the faster the ball will travel. Force (F) is proportional to the product of mass (m) and acceleration (a).

$$F \propto ma$$

Force is expressed in newtons (N) or pounds (lbs) and is a "vector quantity." It is characterized by its direction, magnitude, and area of application. Direction of the force to the bone is particularly important in trauma biomechanics as explained later.

Load

A load is a force, or combination of forces that is sustained by an object (Frost 1967, Low and Reed 1996). For example, the weight of the body on the foot is a load.

Stress

When examining load type, a common term used is "stress." Stress is defined as "force per unit area" (Turner and Burr 1993: 595), thus expressed as:

$$Stress = force/area$$

A unit of stress is newtons per square meter or pascals. The unit of 1 newton per square meter (Nm^{-2}) is 1 pascal.

Stress is further subdivided into the three areas: compressive, tensile, and shear (Figure 1.1) (Alms 1961, Turner and Burr 1993, Nordin and Frankel 1980). Compressive stress develops when a load acts to make an object or material shorter. Likewise, tensile stress forms when load works to stretch an object or material. Shear stress results when one area of an object or material slides into another area. These three types of stress do not usually exist in isolation. No matter how simple the loading scheme, compressive, tensile, and shear stress often occur in combination.

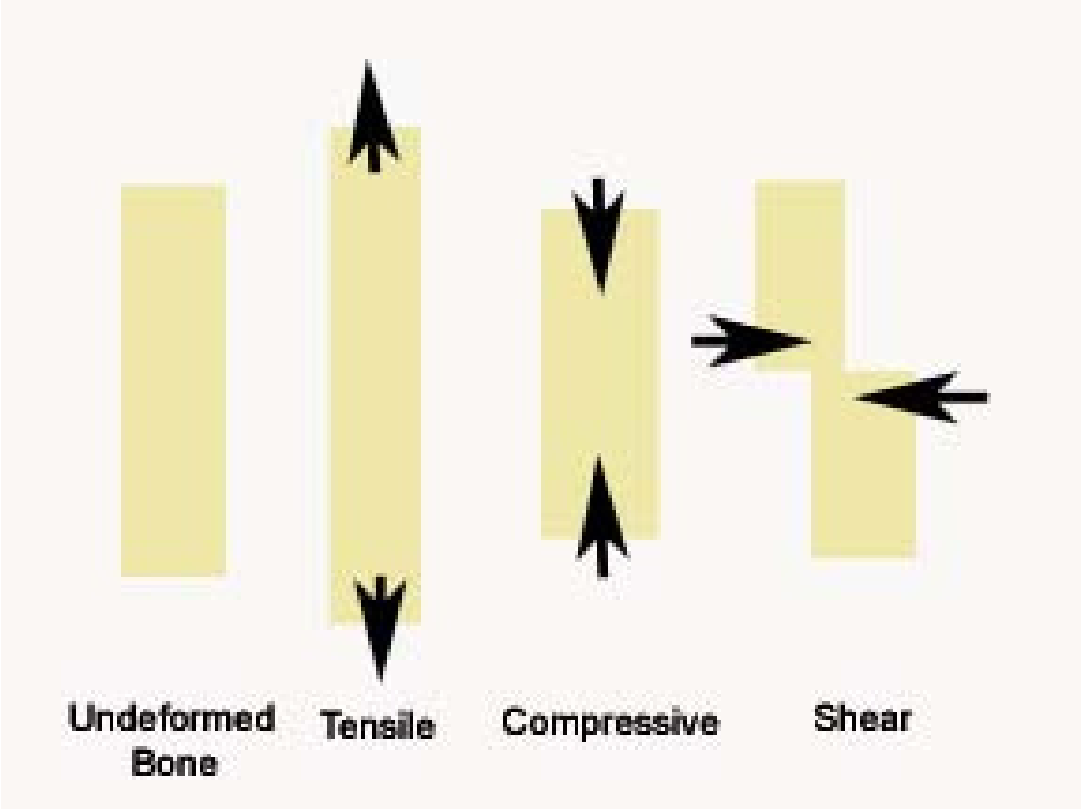

Figure 1.1 Illustration of the effect of tensile, compressive, and shear stress on a beam.

Strain

Strain is related to stress as expressed in Hooke's Law and is dependant on the mechanical property of a material (specifically the modulus of elasticity). Strain is expressed as "percentage change in length, or relative deformation" (Turner and Burr 1993).

Strain = increased length/ original length

Since strain is a ratio at lengths, it is a unit less quantity.

Poisson's ratio

Poisson's ratio describes the ratio of change due to strain in length and width (Turner and Burr 1993). Ashman et al (1984) reports a range in Poisson's ratio between .28 and .45 for bone. To summarize, if 1% strain is applied to a human femur in the longitudinal direction, a corresponding strain in the transverse direction will be between 28% and 45% (Turner and Burr 1993).

Young's modulus (or Modulus of Elasticity)

The ratio of stress to strain in the elastic region of a material is known as Young's modulus, denoted with the variable E (Low and Reed 1996). Young's modulus is often used to depict how brittle or stiff a material is.

Fracture

In bone trauma, fracture is the term used for failure of bone. A fracture occurs when there is a complete separation of molecules (Low and Reed 1996). a break in the bone or cartilage (usually on the superior and posterior ends of

bones); usually is a result of trauma; a fracture can, however, be the result of an acquired disease of bone such as osteoporosis or the result of abnormal formation of bone in a congenital disease of bone such as osteogenesis imperfecta. Fractures are classified by their character and location. Examples of classification include "spiral fracture of the femur," "greenstick fracture of the radius," "impacted fracture of the humerus," "linear fracture of the ulna," "oblique fracture of the metatarsal," "compression fracture of the vertebrae," and "depressed fracture of the skull."

Biomechanics of Human Bone

To completely understand bone trauma biomechanics, it is just as important to understand the properties of bone as it is to understand basic biomechanics.

Bone Tissue Structure

Vertebrate skeletal systems contain two types of bone, cortical or compact, and cancellous or spongy (Harkess et al 1984). Cortical bone is stiff and more dense while cancellous bone is porous and lightweight with a characteristic fragile honeycomb appearance. Cortical and cancellous bone differ greatly in reaction to force. Cortical bone has a higher Young's modulus, indicating greater stiffness (Nordin and Frankel 1980). It exhibits a lesser amount of strain for a given stress before failure, as compared to cancellous bone. Cancellous bone is less stiff, therefore for a given stress the strain is less

than for cortical bone. Cortical bone fails when strain exceeds 2%, while cancellous bone can withstand up to 7% (Nordin and Frankel 1980).

Bone Histology

Bone is composed of cells and an extracellular matrix. The cells of the bone include osteoblasts, osteoclasts, and osteocytes (Bouvier 1989). Osteoblasts are cuboidal cells responsible for the secretion of bone matrix. Osteoclasts are larger, multinucleated cells responsible for the absorption of bone. Osteocytes are osteoblasts that are trapped within the bone, and responsible for maintenance. The circular structures that house the osteocytes are known as osteons.

Anisotropy and Viscoelasticity of Bone

Both cortical and cancellous bones are anisotropic materials (for review see Antich 1993, Bonfield et al 1985, Evans 1973, Johnson 1985, Keaveny and Hayes 1993, Nordin and Frankel 1980, Turner and Burr 1993). Characteristically, anisotropic materials have different material properties based on direction (Figure 1.2). This differs from isotropic materials which are more homogenous having the same material properties in all directions. Human cortical bone has a particular type of anisotropy referred to as transverse isotropy, because it has the same resistance to force in all transverse directions, and a higher resistance in the longitudinal direction (Keaveny and Hayes 1993). The histology of bone contributes to its anisotropy. Human bone is stronger in the longitudinal dimension (the direction the osteons run) than in the transverse

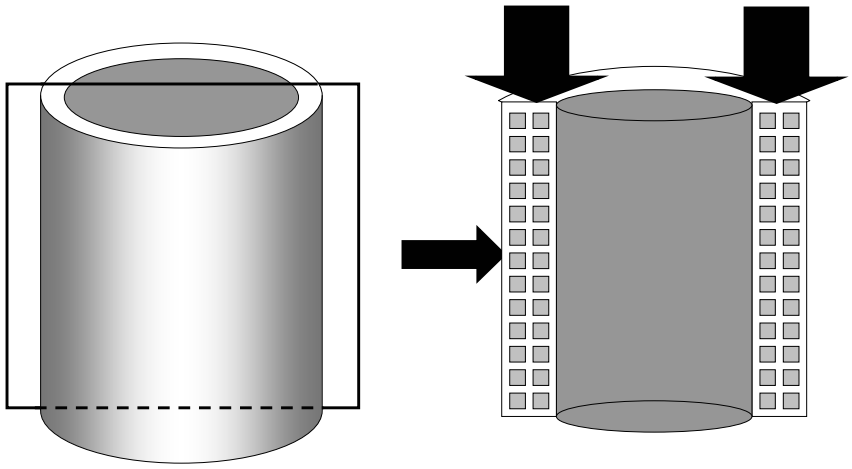

Figure 1.2 Anisotropic materials have physical properties that vary with direction; in this case, the model of bone is stronger in vertical direction (large arrows) than in transverse direction (small arrows).

direction. Human bone is also stronger in compression than tension or shear. This is often explained because limbs and bones are frequently exposed to compressive stresses from daily activity, therefore have adapted a higher resistance to compression than tension.

Human bone is also a viscoelastic material (for review see Bonfield and Li 1965, Keaveny and Hayes 1993, Piekarski 1970, Turner and Burr 1993). A viscoelastic material behaves in different ways depending on the rate and the length of loading (i.e., strain rate). Histologically, fractures induced by low strain rate follow the interstitial bone around the osteons, while at a higher load they travel indiscriminately through the bone (Piekarski 1970).

The viscoelastic properties of bone also play an important role in trauma interpretation. Resulting fracture patterns can be quite different due to the rate of loading. Keaveny and Hayes (1993) state that at high rates of loading bone can behave like a brittle material skipping the stage of plastic deformation and failing quickly under the force.

Bone Deformation

Materials under stress pass through two stages before failure. These are elastic and plastic deformation (Low and Reed 1996). In elastic deformation material can return to its original form, once pressure is released (Figure 1.3). For example, a sponge always changes shape when squeezed, but then returns to its original form when released. Plastic deformation is a level of deformation from which the material will never recover (Figure 1.4). For

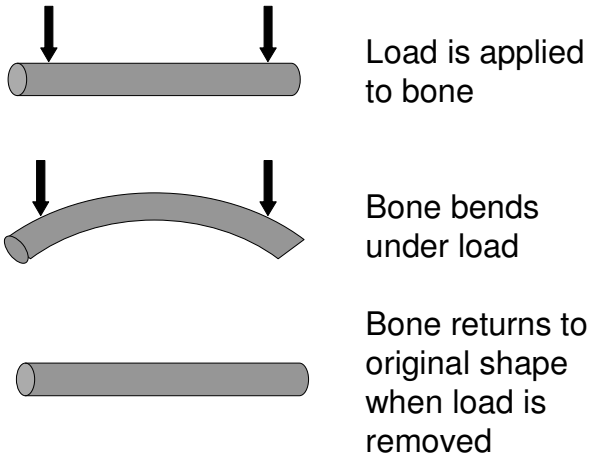

Figure 1.3 Elastic deformation of bone.

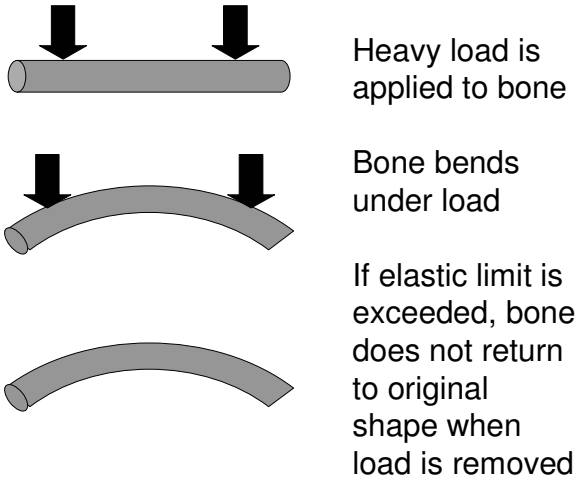

Figure 1.4 Plastic deformation of bone.

example, if a sponge tears when stretched as opposed to returning to its original form.

Bone under stress and strain reacts in a predictable manner as outlined extensively by Keaveny and Hayes (1993), Nordin and Frankel (1980), Turner and Burr (1993). The deformation of the material has a direct relationship to the force of the load exerted upon it. This relationship is depicted as a stress-strain or load-deformation curve (Figure 1.5). Load-deformation curves depict the stages that bone undergoes through out loading. The elastic deformation region is the first area of the load-deformation curve. When bone is in elastic deformation and the load is removed the bone will return to its former shape with no visual structural alteration. Bone enters the plastic deformation stage when a load has been reached that causes permanent visual structural alteration. After release of the force, bone in the plastic deformation stage cannot return to its original shape even though a visible fracture may not have occurred.

Load-deformation curves provide information on the amount of energy absorbed, load sustained, and deformation achieved before failure (Nordin and Frankel 1980). The amount of energy absorbed is calculated by the area underneath the curve, and the load and deformation sustained at failure.

The overall structural stiffness is demonstrated by the slope of the curve. Stiffness is calculated according to the modulus of elasticity or Young's modulus. The stiffer the material, the higher the moduli value will be. Young's modulus is important in bone fracture mechanics to illustrate stiffness or ductility which has a great influence on fracture mechanics. Brittle materials deform very little

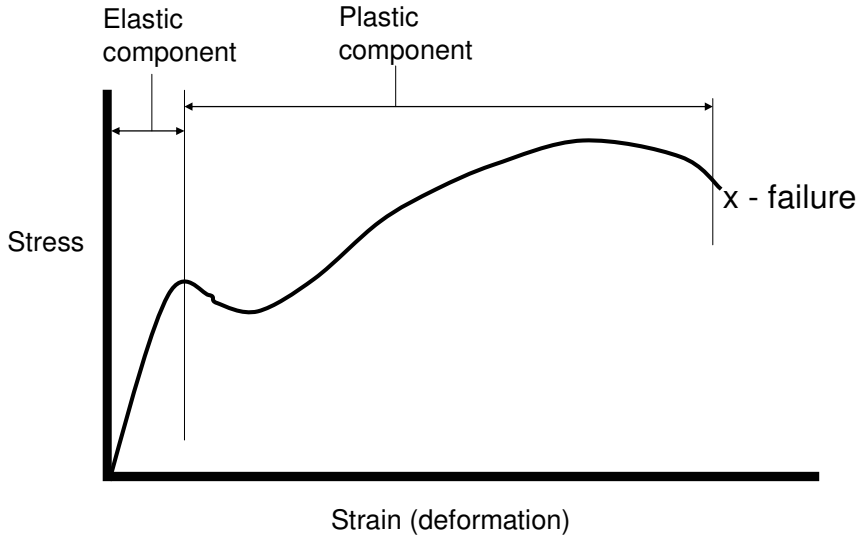

Figure 1.5 Diagram showing a characteristic stress-strain curve showing the elastic and plastic deformation phases and failure point (after Turner and Burr 1993: 597).

before failure, while ductile materials can withstand a great deal of elastic deformation.

Reaction to Tension

When loads are applied in a direction opposite of each other an outward from the bone surface, tension is created. Maximum tensile stress occurs in a direction perpendicular from the applied force (Nordin and Frankel 1980). This force causes the material to narrow and lengthen. In bones, failure occurs at a microscopic level by the pulling apart of the osteons at the cement lines (Nordin and Frankel 1980).

Re-evaluation of Bone Trauma Paradigm: Engineering inputs and anatomical outputs

The phrases “engineering inputs and anatomical outputs” were coined by Kress (1996) as a new way of thinking about injury causation. Their applicability to forensic anthropology is great. In rethinking bone trauma as a continuum, rather than discrete categories, the three key extrinsic factors (or engineering inputs) of focus are force, surface area of impact interface, and acceleration/deceleration.

Force is a very relevant variable for obvious reasons. The amount of external force applied to the body can influence the level of injury. The human body is subjected to a variety of benign forces every day, such as gravity, with out any injuries occurring.

The surface area of the impact interface relates to the concept of stress. For example, imagine holding a twelve pound bowling ball on the palm of your hand. The force on your hand is twelve pounds, not near enough to cause injury. This is because the twelve pounds is spread out over a large region (i.e., a large interface surface area). The stress can be calculated by dividing the force by the area to give the pounds per square inch (psi). The stress of holding a twelve pound bowling ball in your hand is 1.33 psi. This value is below the threshold for injury. Now imagine a knife point between the bowling ball and your hand. The force still remains twelve pounds, but now injury would occur. The calculated stress rises to 120,000 psi with a far smaller interface surface area.

The acceleration/deceleration of an object is also an important variable. While a great deal of attention is given to speed in trauma analysis, the essential component of time is missing. For example, commercial airplanes reach very high speeds with out causing injury to the passengers. While they may have a change in velocity of over 500 mph, this occurs at a slow rate over a long distance and the passengers only feel an acceleration of approximately 0.5 g. A car can crash and go from 60 to 0 (a much lower total change in velocity than the airplane) and cause massive injuries. This is due to the fact that the car stops in a fraction of a second. This causes the occupants to be subjected to very high deceleration forces (100 g).

When trying to understand the fracture patterns or “anatomical outputs” seen from an injury, it is essential to remember the possible range of “engineering inputs” that may have come into play. The experimental testing in

this dissertation is designed to illustrate how these variables interact and influence the fracture patterns that are seen.

CHAPTER 2: CRANIAL TRAUMA

Relevance of Cranial Trauma

Forensic and Physical Anthropology

Skull trauma interests forensic anthropologists because the skull is often injured in cases of interpersonal violence (Galloway 1999). The head is a frequent target for blunt and ballistic trauma in cases of homicide. It can also be an area of inflicted sharp trauma in cases where of attempt to conceal identity by removal of the face or dentition.

When examining fracture patterns from blunt trauma to the skull, anthropologists are most often called to assess the point of impact, the number of blows delivered, the sequence of blows delivered, and the level of force or energy. By keeping the concept of "engineering inputs and anatomical outputs" in mind, and considering the key variables of surface area, force, and acceleration, it is possible to use the resulting blunt force trauma fracture patterns to extrapolate information as to the injurious event.

Impact Biomechanics

The skull is also an area that is of primary concern in the fields of safety and impact biomechanics. Head injuries frequently occur in motor vehicle accidents, as well as sports injuries. Research into the mechanism of these injuries is the foundation behind helmet safety testing and standards (Allsop 1993, Halstead 2001). In all of these areas of research, a correct forensic examination of the injuries to the skull is needed to determine the exact

mechanism of injury in order to determine fault, either for civil or criminal matters (Beier 1983).

In a frontal crash motor vehicle accident, fractures of the face, mandible, and neurocranium are common. Crash data analysis has shown that injuries to the head and face can account for 40% of all vehicular crash injuries (Allsop 1993). During the impact, the motor vehicle rapidly decelerates. This deceleration occurs slightly before the occupant in the vehicle fully decelerates. This difference causes the "second impact" (i.e., the collision between the occupant and the interior of the vehicle (Kress 1996). In these instances, the skull can make contact with the steering wheel or windshield. Because of the frequency of head and face injuries resulting from motor vehicle crashes, there has been a strong effort in the field of impact biomechanics for cadaveric testing to better understand tolerance levels for the skull, as well as fracture etiology (Kress 1996).

Fracture Biomechanics of the Cranium

The analysis of cranial trauma differs slightly from the analysis of injured long bones. While the same principles of biomechanics govern cranial fractures, the differences in the structure and architecture of the cranium deserve special consideration. The skull is composed of 22 separate skeletal elements that act as an entire system. The bones of the neurocranial vault are characterized as flat or irregular bones and are formed in three layers; the inner and outer cortex

(similar to cortical or lamellar bone) and the diploe, or spongy, cancellous bone in between.

The construction of these distinct layers affects the manner in which fractures propagate through the skull. A blow delivered to the outer surface, subjects the inner cortex to a greater degree of tension than the outer cortex. A micro-fracture often occurs on the inner surface directly below the impact site and then spreads to the outer surface and propagates from impact (Figure 2.1) (Mortiz 1954). The fractures traveling out from the point of impact in a linear direction are radiating fractures. As they move, secondary areas of tension and compression are created, and circumventing fractures i.e. concentric fractures transect the radiating fractures (Figure 2.2). Depressed skull fractures occur when a significant, localized force to the skull that causes a collapse of the diploe layer, and there is complete penetration of the skull.

A study by Melvin et al (1969) examined the fracture force for the frontal and parietal bones. Major conclusions from the study suggested that the amount of force needed to fracture bones of the vault was directly related to their thickness (Melvin et al 1969). In the cadaveric samples used, the parietal fractured at a lower force than the frontal, and was subsequently found to be thinner. No differences were found between the left and right parietals for the same location in the same individual (Melvin et al 1969). Another earlier impact study reported similar results, with the frontal bone fracture occurring at an average of 1,108 lbs over 18 tests, and the parietal region failing at an average of 784 lbs over 18 tests (Nahum et al 1968).

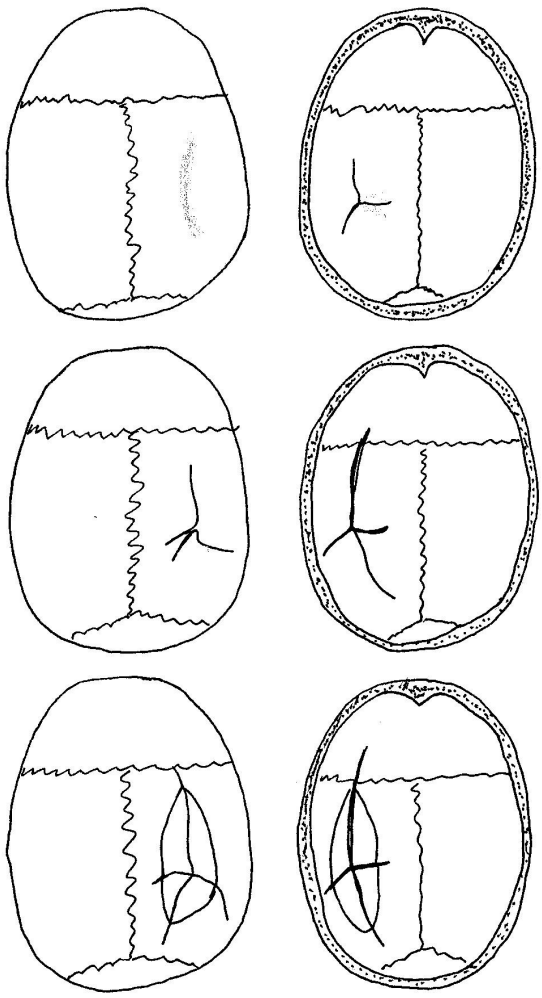

Figure 2.1 Fracture propagation in both the inner (right) and outer (left) tables of the cranium. After Moritz 1954: 342.

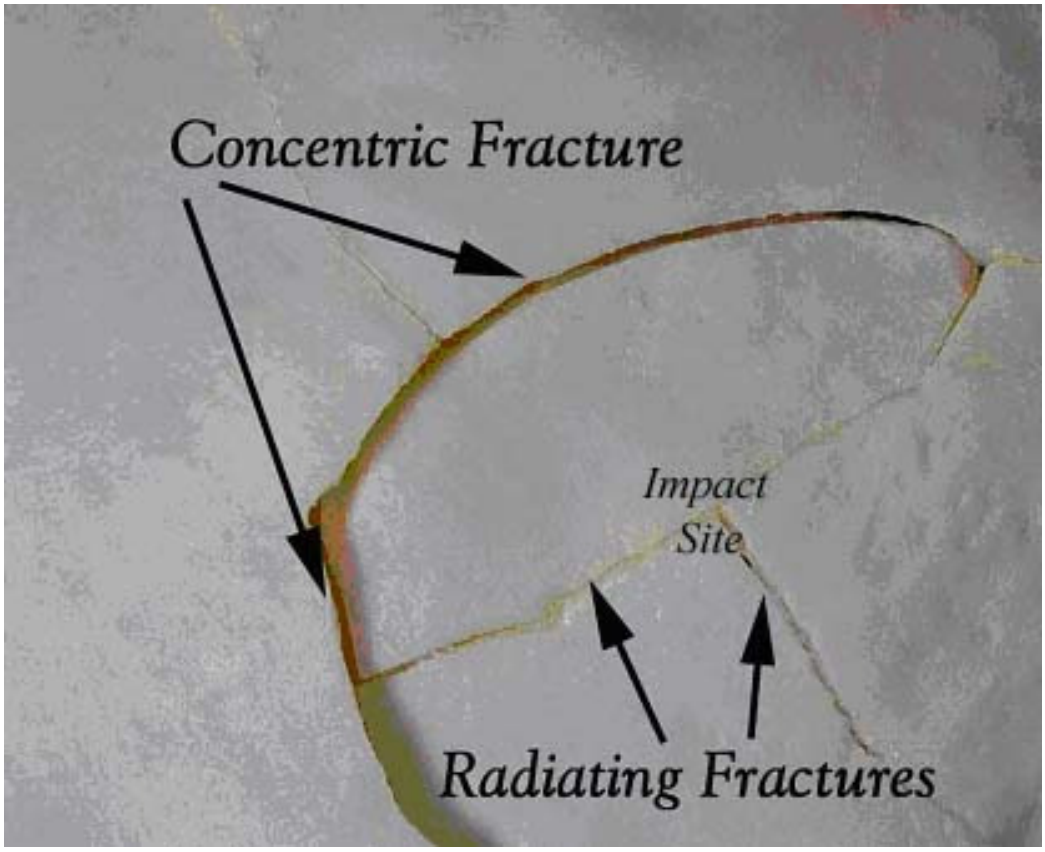

Figure 2.2 Concentric and Radiating fractures from blunt force trauma impact site to the left parietal (10X).

When the skull is entrapped between the impact and another surface, contrecoup fracture can occur. The coup/contrecoup phenomenon was first described by Hippocrates over 2000 years ago, and is described as a pattern of injury resulting from both the impacting blow and the resulting impact against the opposing surface (Hein and Schulz 1990). Contrecoup injuries are seen in the brain, when a blow causes the brain to shift and impact the opposite side of the skull. Analysis of coup/contrecoup fractures requires that the anthropologist take into account both blunt force trauma from the initial impact, and the blunt force trauma from the entrapping surface.

Fracture Pattern Testing in the Cranial Vault

Introduction

In forensic anthropology, there is great importance on correctly determining the point of impact for blunt force trauma to the skull (Berryman et al 1998). Historically, however, there has been some confusion in the literature as to the nature in which fracture propagation occurs in the cranial vault. Numerous well regarded sources in the literature (Berryman et al 1998, DiMaio and DiMaio 2001, Galloway 1999, and Knight 1996) report that radiating fractures can initiate at a location very remote from the point of impact. This was reported in a series of papers by E.S. Gurdjian and colleagues from the 1940's and 1950's (Gurdjian and Lissner 1945, Gurdjian et al 1947, Gurdjian et al 1949, Gurdjian et al 1950a, and Gurdjian et al 1950b).

Despite the fact that it was widely reported that fractures start at a remote location and travel backwards to the point of impact, a few astute researchers noticed that this theory did not seem to hold up (Symes et al 1989). This controversy between the literature (Galloway 1999, etc.) and the practicing forensic anthropologists dealing with trauma everyday (Symes et al 1989, etc.) provided the impetus to conduct testing to try and solve this puzzle once and for all.

Materials and Methods

To answer the questions addressed in this study, a cadaveric impact testing model was chosen. Using human tissue is the best way to replicate blunt force trauma. Impact testing affords the unique opportunity to monitor the cranium's response during impact. Advancements in instrumented impact testing allow quantification of data such as axial load, strain and deflection versus time.

Instrumented impact testing, as employed in this research, is commonly used to determine load vs. deformation of a material such as bone under high speed impact. The standard protocol for this testing involves utilization of a steel "drop tower" structure that allows for controlled and monitored descent of a weight with an attached instrumented load cell. The load cell feeds a constant data stream to a computer which monitors applied load and collects information on deflection, elastic stiffness, maximum load, absorbed energy, damage, and load at failure (Turner and Burr 1993). The impactor cell records the data throughout descent and impact, which is recorded as the impact load *P*, a

continuous function of *t* time (Turner and Burr 1993). In this test setup, data were recorded from four separate load cells for the entire impact event.

Specimens

To test fracture propagation in the neurocranium, five cadaver heads, two females and three males ranging in age from 61-89, were obtained from Virginia Tech Biomechanics Impact Lab in Blacksburg VA. The unembalmed heads had been previously frozen. After a thaw period of 36 hours, each head was prepared for study. An area of the scalp was left intact with the hair, skin, and muscle over the exact impact site (Figure 2.3). The remaining soft tissue was reflected back in four flaps to enable proper fracture viewing and imaging.

Head weights ranged between 4.01 kg (8.84 lbs) to 6.44 kg (14.20 lbs). All skulls were impacted in the parietal region, corresponding to Gurdjian's Anterior Parietal region (Gurdjian et al 1950b). Four were impacted on the left side and one on the right. The skull tested on the right side had a small degree of soft tissue damage to the left side that may have affected results. The parietal was chosen as the impact site for several reasons. First, in order to properly video capture the fracture progress, a site was selected that enabled viewing. Second, the parietal is of fairly uniform thickness. Third, there are no thick muscle attachment sites as in the occipital, and it is not nearly as thin and likely to punch through as the frontal. For these reasons, the high parietal was chosen to help ensure good radiating fracture propagation instead of having a simple depression fracture. Major suture structures were also avoided as they tend to absorb energy and alter fracture propagation.

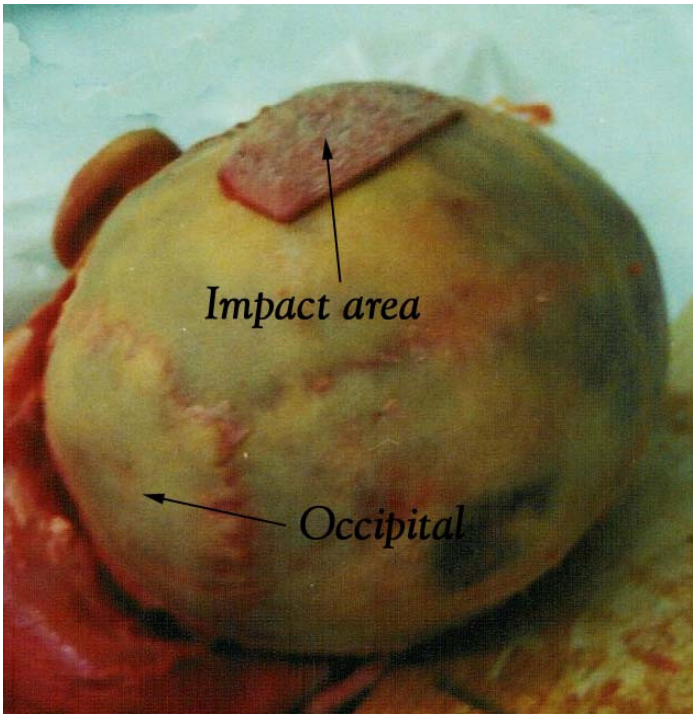

Figure 2.3 Dorsal view of human head ready for testing with impact area on left parietal with intact soft tissue, and clean bone on the rest of the cranium.

The heads were placed in the drop tower structure and struck from a range of 1.95 meters (6.41 feet) to 2.82 meters (9.25 feet). An "overlap" was created to allow the impactor to fall further than the initial point of contact with the skull. Styrofoam squares were placed in the drop tower to slow down the impactor after the drop. The overlap height ranged from 5.08 cm (2 in) to 8.89 cm (3.5 in). The drop mass was consistently 10.43 kg (23 lbs). The skulls were stabilized underneath by a wooden support beam that was scored collinearly along the impact direction in order that the beam would completely fail well before fracture initiation of the skulls. In other words, the wooden support board provided a means to hold the skull in position for impact. One test used a semi-rigid boundary to see if a different amount of energy was needed to produce a fracture in that situation.

Load cells monitored impact throughout each test. A trigger switch placed on the top of the impact site triggered sensor monitoring from the time of immediate contact. Force was measured off the right and left supports, and the axial impactor arm, which allowed for the determination of associated forces over time.

Each test was filmed with high-speed video to show the exact fracture propagation. The video was placed to capture fracture propagation through the posterior parietal and occipital region. The high speed video filmed faster than the fracture travels through bone (approximately 4,000 frames per second), allowing approximately 1.25 centimeters (cm) of fracture propagation per frame. This speed enabled viewing of fracture travel while still providing good resolution

and definition. The video input was recorded digitally and input into the data acquisition computer.

After impact, each skull was cleaned, photographed, and diagramed. The skull was examined for fractures in all areas, including locations remote to impact. All fractures were described, measured, and charted (For complete test photos and data see Appendix A).

Results

Test One

The left parietal was impacted from a drop height of 1.95 meters (6.41 feet) and a weight of 10.43 kg (23 lbs). The impact caused two radiating fractures. The main radiating fracture traveled from the point of impact to terminate into the squamosal suture, a total distance of 6.35 cm (2.5 inches). A secondary fracture radiated laterally a distance of 3.175 cm (1.25 inches). All fractures recorded were radiating from the impact site. The axial load reached a force of 1,200 lbs.

Test Two

Test specimen 2 is a 61 year old female with a head weight of 3.3kg (8.84 lbs). The left parietal was impacted from a drop height of 2.82 meters (9.25 feet) with a drop mass of 10.43 kg (23 lbs). Fractures formed at the point of impact and radiated into the squamosal suture traveling a total distance of 8.89 cm (3.5 inches). Additional small fractures in the outer cortex were noted in a circular

concentric pattern around the point of impact. No additional fractures radiating from locations other than the impact site were noted. The maximum axial load force was 1,140 lbs.

Test Three

The cranium was impacted on the right parietal from a drop height of 2.82 meters (9.25 feet) with a drop mass of 10.43 kg (23 lbs). The right parietal was used to avoid an area of soft tissue damage directly over the potential impact site on the left parietal. The only resulting fracture was a very small fracture affecting the outer table in a small stellate pattern directly under the main impact site. No radiating or concentric fractures occurred at the impact site and no other fractures were notes radiating from any locations remote to impact. The axial force was recorded at 1,400 lbs.

Test Four

The cranium was impacted from a drop height of 2.82 meters (9.25 feet) with a drop mass of 10.43 kg (23 lbs). The left parietal was impacted with no visible fractures. The data show a peak at 1400 lbs of force.

Test Five

Test five investigated the difference in fracture patterns between unconstrained impacted crania and one with a semirigid boundary. This test was conducted to see if the constraint of the skull would produce the fracture patterns similar to Gurdjian's findings. The board that stabilized the other four test

subjects until impact was not scored in this test. The board doesn't completely constrain the skull but provided enough resistance to measure the differences. The semirigid boundary was the only variable altered in the test. The drop height and drop mass remained constant.

At impact, the board failed allowing the skull to move in the direction of the impact. However, the presence of the semirigid boundary drastically changed the results of the test. The fracture pattern was different with two main areas of fractures occurring on the left parietal (site of impact) and the right parietal. Fractures were more complex with many radiating and concentric fractures present. Bilateral fractures were also present through the frontozygomatic sutures. The complex fracture patterns failed to occur at remote locations and travel back towards the impact site. Damage to the left side of the cranium resulted from direct impact and damage to the right resulted from the semirigid boundary provided by the board. There was a noticeable difference between the data collected by the load cell data between the unconstrained and constrained tests. The event for the constrained test lasted considerable longer with several fracture events visible in the graph. The main peak occurred at 840 lbs of force but there were other major failures. Analysis of the high speed video showed that the first peak indicated the failure in the area of the impact site with radiating fractures creating the release in pressure as indicated by the sharp drop after peak one. The semirigid boundary created additional peaks in energy, indicating failure of the right parietal (side opposite from impact), and failure of the facial skeleton.

Results from High Speed Video

In the experimental design, all tests were recorded with high speed video. The video allowed us to witness the fracture propagation clearly demonstrating the point of fracture and direction of travel. Unlike Gurdjian's testing, the high speed video results allowed for clear indication of fracture direction dispersal. Video analysis revealed that the fractures initiated at the point of impact and radiated out. No out bending was observed in the video. The frame by frame sequence of images showed fractures traveling from the impact site (it can be seen that the impactor is already in contact with the skull) in a posterior direction towards the occipital (Figure 2.4). The results of video analysis are valuable by providing a means of viewing the fracture event as it occurs.

Discussion

While Gurdjian's studies (1949, 1950a, 1950b) were far ahead of the time and certainly set a standard for the experimental study of fracture mechanics, they suffered from some inherent problems. These issues surfaced when it was noted that predictions made from experimental models were not seen in real case studies. An overwhelming amount of forensic evidence indicates that fractures in the skull initiate at the point of impact. In fact, the detailed fracture patterns that Gurdjian described for each area of the skull bear little resemblance to forensic cases.

While bone has a degree of elasticity, it is not as elastic as the Gurdjian theory predicts (Turner and Burr 1993). The considerable amount of out bending

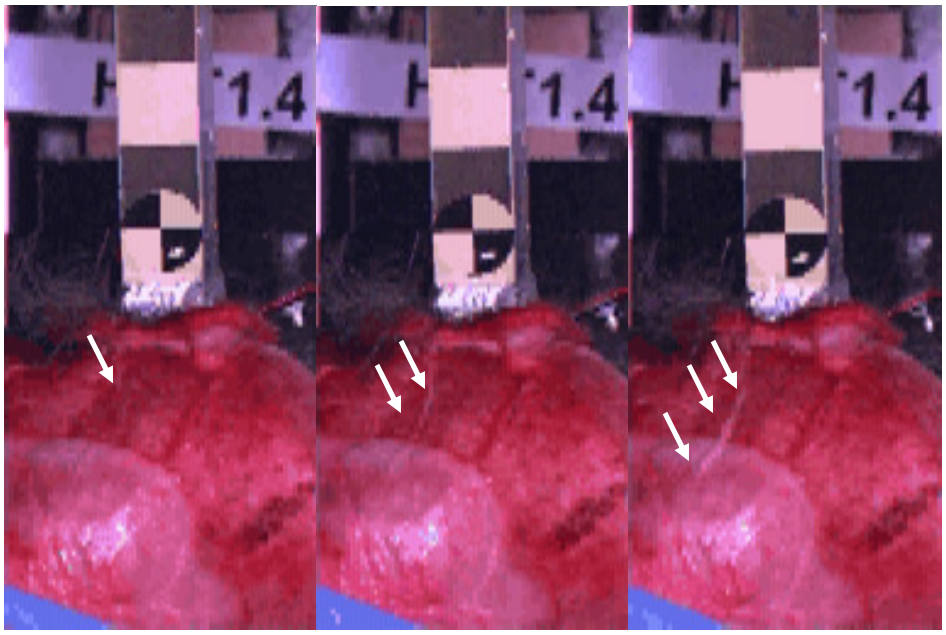

Figure 2.4 Dorsal view of the skull (test five) during the impact event taken from the high speed video. The line of fracture propagation shown at the white arrows (read left to right) and is radiating out from the point of impact.

described by research is indicative of a material far more elastic than bone. The drastic degree of bending illustrated by DiMaio and DiMaio (2001) and Galloway (1999) and the tearing described by Berryman and Symes (1998) are more likely to describe a rubber ball impact rather than a human skull. Galloway (1999) even describes the human skull as a "semi-elastic ball." As a viscoelastic material, bone deformation is dependent on the rate of loading. At a rate of loading common to blunt force trauma, bone fails before in-bending and out-bending occurred (Keaveny and Hayes 1993).

Conclusion

The results from this study (Kroman 2003) demonstrate that failure occurs first in the immediate area of impact with radiating fracture traveling from this point. No areas of drastic inbending or out bending were created. There was no indication of fracture beginning at any region other than the point of impact as proposed by Gurdjian and coauthors (1950b). Fractures were documented as radiating from the point of impact and this propagation was captured on high speed video.

The results of this study refute Gurdjian's notion that fracture initiation begins at a location remote to the point of impact. All fractures, regardless of the constraint of the cranium radiated out from the impact site. This should be taken into consideration by anthropologists and pathologists when conducting fracture pattern analysis and trauma interpretation.

Fracture Pattern Testing in the Cranial Base

Introduction

Fractures of the cranial base represent severe trauma to the head and often result in a monumental amount of neurological damage due to the numerous nerves and vessels permeating this area. These fractures are also referred to as “hinge” fractures when they are severe enough to transect the entire cranial base, creating movement between the anterior and posterior regions of the skull usually through the temporal fossa.

Debate and controversy surrounds the etiology of these complex fractures. Hinge or cranial base fractures have been attributed to high energy projectile or ballistic trauma. Betz et al (1997) even provide a connection between the type of base trauma and the type of ballistic projectile used. They attribute the creation of the fracture to “intercranial overpressure” resulting from energy released from the bullet. Increase in intercranial pressure due to a ballistic injury at close contact is also thought to be the cause of small fractures of the orbital roof via a mechanism thought to be a violent increase of pressure in the brain due to the sudden release of gases (Spitz and Fisher 1980). Betz and colleagues (1997) hypothesize these “indirect” fractures caused by increased intercranial pressure will more often be found in the cranial base than the vault. They argue that this is due to the fact that the base of the skull is “inhomogeneous and less resistant to stretching than the vault” (Betz et al 1997). However, a great deal of controversy still surrounds this notion (Spitz and Fisher

1980), and little attention is given to the prospect of the creation of hinge fractures from blunt force trauma.

Another argument regarding the creation of cranial base fractures is that they are the result of “indirect” trauma or a blow to a remote region of the skull (Schuknecht and Graetz 2005). The term “indirect” trauma implies that the created fracture does not radiate out from the point of impact but is generated from forces caused by a blow to a different region of the vault or base. Another type of indirect trauma seen as responsible for the creation of cranial base fractures is a large force over a large area of the skull, leading to a “burst” fracture (Schuknecht and Graetz 2005). These types of burst fractures have been reported in the literature to be common in the cranial base, particularly the petrous portion (Schuknecht and Graetz 2005).

Spitz and Fisher (1980) contend that cranial base fractures can also be due to a blow to the side of the head or from side to side compression of the skull. They also note that cranial base, or hinge fractures tend to run in the direction of the force. Basilar skull fractures have also been attributed to blows to the front of the head or as the result of compression of the spine (Galloway 1999, Rogers 1992). Harvey and Jones (1980), on the other hand, report that fractures of the cranial base are an unreliable indicator of the location of the blow and that they can occur for a variety of locations of impacts, including direct blows to the chin.

The conflicting theories, both popular in the current forensic literature, that A) cranial base fractures are the result of high energy projectile or ballistic trauma

(Betz et al 1997), and B) they occur from a blow to a remote region of the skull, and are properly described as indirect or burst fractures (Schuknecht and Graetz 2005); have provided the impetus to investigate the creation of cranial base fractures in an experimental setting.

In light of the above mentioned controversy in the forensic literature, when deciding to test fracture propagation through the cranial base, two test questions were formulated: 1) Can cranial base fractures be generated from blunt force lateral impacts to the skull? 2) How do fractures travel through the cranial base? Is there a "bursting' (as proposed by Schuknecht and Graetz 2005) or simply a radiating linear fracture?

Materials and Methods

To test fracture propagation in the cranial base, two unembalmed cadaver heads were used. The unembalmed heads had been previously frozen. After a thaw period of 36 hours, each head was prepared for study. The heads had previously had the cranial vault and brain tissue removed. Previous tests of intact, unembalmed human heads under similar conditions confirm that force values for creating basilar skull fractures are comparable with or without the cranial vault and brain. The absence of the cranial vault and the brain enabled a unique opportunity to directly view the internal surface of the cranial base during the impact testing. Each of the heads was impacted with a lateral impact, with the point of impact at the temporal region (Figure 2.5). The head was stabilized on a platform beneath the impactor in a constrained manner. To ensure that the

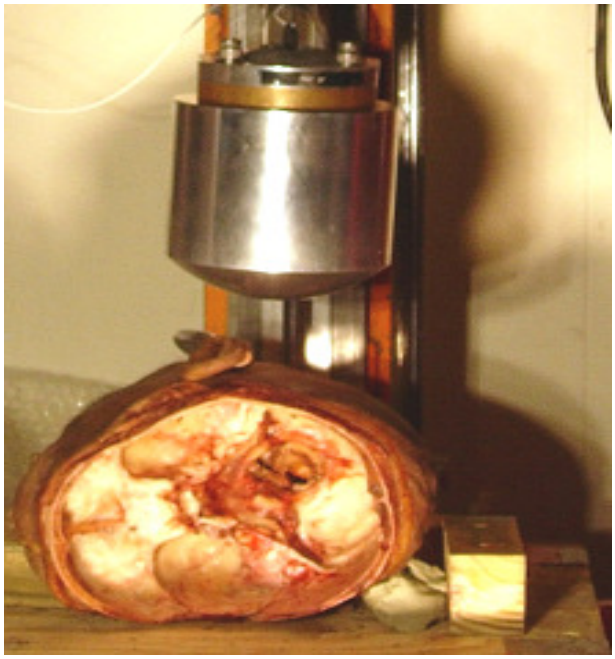

Figure 2.5 Orientation of the head during impact. The vault and brain have been removed, and the internal surface of the cranial base is visible. The impactor (visible in the photo) is lined up to impact the right temporal region.

biomechanical characteristics of the impact were no compromised, a layer of hair, skin and muscle was retained for the area of impact.

A standard engineering drop tower system was used to ensure that each impact was controlled and monitored. The drop tower system is controlled by a computer which monitors the acceleration of the impactor over the time of the impact. A rounded impactor with a mass of 2.09 kg (4.6 lbs) was used. The drop height ranged from 2.02 meters (6.63 feet) to 3.03 meters (9.94 feet).

Each test was filmed with high-speed video to show the exact fracture propagation. The video was placed to capture fracture propagation through the internal surface of the cranial base. The video input was recorded digitally and input into the data acquisition computer.

After impact, each skull was cleaned, photographed, and diagramed. The skull was examined for fractures in all areas, including locations remote to impact. All fractures were described, measured, and charted.

Results

The results from the study provided a great amount of information about the creation of cranial base fractures and how they travel through the cranial base. The force for each impact was also calculated based on a derived equation. This "energy balance" equation ($F\Delta = hW$), comes from the 1st Law of Thermodynamics. The "energy balance" calculation models "potential energy" ($h \times W$) as being converted or equated to work ($F \times \Delta$). The variables are defined as follows: h = distance the object falls (in this study this is a known variable, i.e.

the drop height of the impactor); W = weight of the object (known weight of the impactor); F = force of the object during the impact; and Δ = the distance the head deflected or moved during the impact. In the equation $F\Delta = hW$ there are two unknowns, F and Δ.

This equation can be useful if there is a desire (as in this study) to quantify the amount of force imparted to the head during the impact in order to correlate the force value with the resultant fracture pattern. In other words, this is one way to relate engineering inputs (force value) to anatomical outputs (fracture pattern).

The unknown variable Δ is derived by analyzing the computer output for each impact test. The velocity of the impactor was found using the formula for velocity (v) in which $v = \sqrt{2gh}$ where g = gravitational constant ($9.81 m/s^2$) and h = drop height. The Δt (amount of time of the impact event) was determined from the plots created from the impact of acceleration vs. time. The final equation used was d = rt where d = distance, r = rate (calculated from 1/2v), and t = time. The final value for d was the distance that the head was deflected, and therefore can be substituted back in to the original equation $F = hW/\Delta$ to find the force value.

Test one

Test one was conducted with the impactor dropped from a height of 2.02 meters (6.63 feet). A complete cranial base fracture was created. There were also small radiating fractures seen on the orbital roof, as well as a radiating fracture terminating into the foramen magnum (Figure 2.6). The impact velocity was 20.66 ft/sec, and the calculated force of the impact was 1,181 lbs.

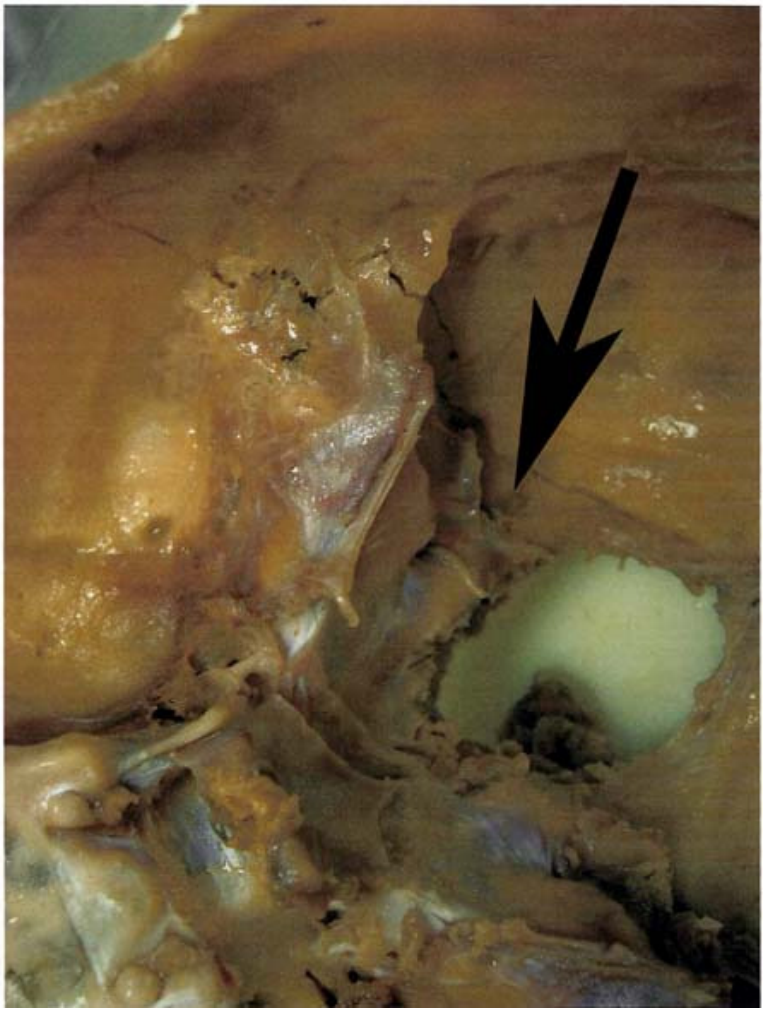

Figure 2.6 View of the cranial base from test one post testing. A radiating fracture is visible (black arrow) that terminates into foramen magnum.

Test two

Test two was conducted to have a higher peak force than in test one. The impactor was dropped from a height of 3.03 meters (9.94 feet). In this test a classic hinge fracture was created, bisecting the pituitary fossa (Figure 2.7). Radiating fractures were also seen coming from both the external and internal auditory meatus (Figure 2.8). The impact velocity was 25.30 ft/sec, and the calculated force of impact was 1,444 lbs.

Results from high speed video

The results from the high speed video provided information regarding how hinge fractures are created and how they travel through the cranial base. There was no "bursting" seen as the fractures were created. The fractures radiated out from the point of impact all the way across the cranial base. One interesting aspect of viewing the fracture travel was to note the great amount of separation that occurred in the video from test two. It also appears that there was movement of the petrous portion of the temporal bone in a superior direction during the fracture event. It becomes clear why these types of fractures are accompanied by such a high amount of soft tissue damage, and are often fatal.

Conclusions

The results of this experimental study help to answer a few of the questions regarding the creation and the propagation of cranial base or hinge

Figure 2.7 View of the skull from test two after some soft tissue removal. A complete hinge fracture is visible traveling anterior to the petrous portions and through sella turica.

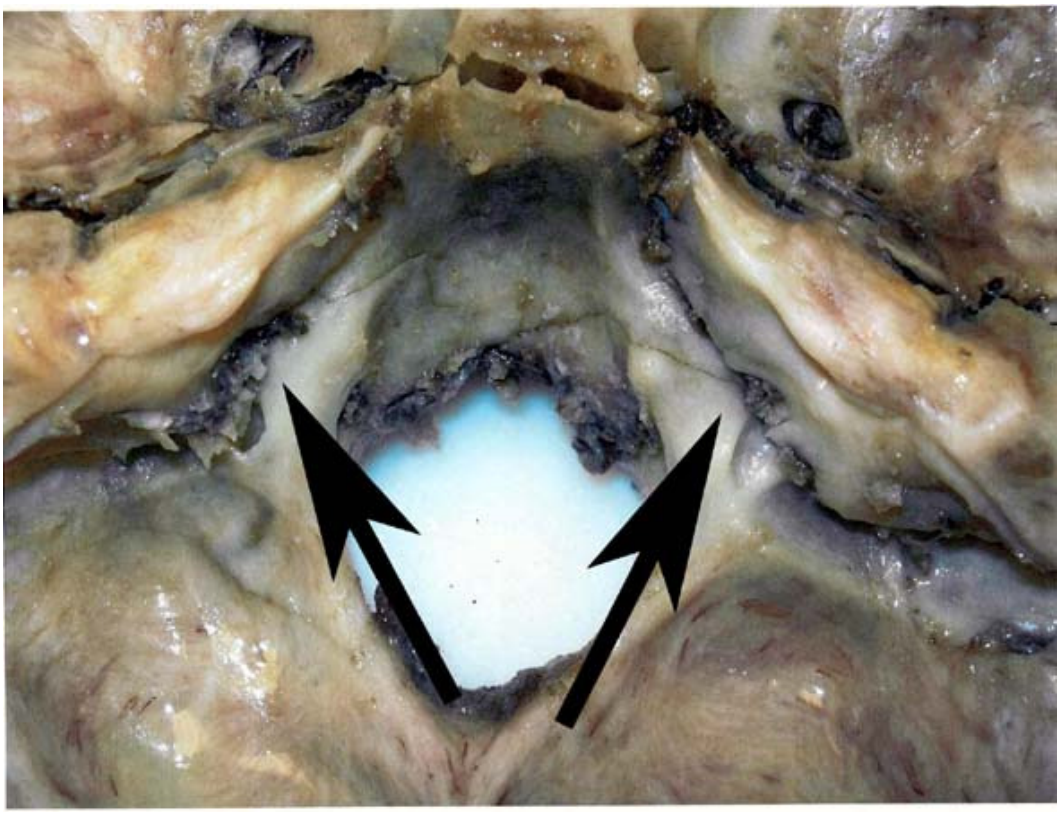

Figure 2.8 Fractures radiating out of the left and right internal auditory meatus (black arrows).

fractures. Classic hinge fractures were created from blunt force trauma from impacts to the lateral aspect of the skull.

While it was determined that lateral impacts could indeed create cranial base fractures, no other impact sites were tested in this study to validate or refute the theories of Galloway (1999), Rogers (1992), Schuknecht and Graetz (2005), and Harvey and Jones (1980). Future research is planned to try and elucidate which, if any, remote locations of impact will cause hinge fractures of the cranial base.

The results from the high speed video clearly showed that hinge fractures travel across the cranial base radiating out from the site of impact, similar to what was seen in fractures of the cranial vault. No evidence of “bursting” was seen. The test definitively proved that cranial base fractures can be created from blunt force lateral impacts to the head and are not exclusively the results of increased intercranial pressure.

CHAPTER 3: TRAUMA TO THE THORAX

Relevance of Thoracic Trauma

Forensic and Physical Anthropology

The thoracic region is another region of the human body that is often under close examination by forensic anthropologists. The rib cage can display trauma from ballistic trauma, blunt trauma, and sharp trauma. The thorax, unlike the skull or long bones, can be tricky to understand from a biomechanical aspect. Instead of operating as independent entities, the ribs have to be understood as part of a whole, and governed by the biomechanics of the thorax as a system including the spine, sternum, and rib cage. Another important area of consideration with regards to the rib cage and forensics is the area of child abuse (for review see Marks and Mileusnic 2007, Symes et al 2002a, Symes et al 2002b). Rib fractures in young children and infants can be indicative of abuse, either from a direct impact or from a squeezing or compression of the thorax.

Impact Biomechanics

This region is also of special interest and consideration for safety standards in the automotive industry. In a motor vehicle accident, the driver can strike the steering wheel causing massive thoracic injury. Of thoracic injuries of both drivers and passengers in motor vehicle accidents, fractures were the most common (Cavanaugh 1993). There is also an area of concern regarding the interaction between the passenger and the restraint systems of belts and air bags. These systems have been designed to minimize the injuries from a crash,

but careful consideration has to be given to the amount of force they themselves inflict on the occupant.

Impact Testing of the Thorax from Boat Propellers

Introduction

Boating injuries are common in the United States, with the National Center for Injury Prevention reporting approximately 50,000 boating related injuries in a one year period. Of these, approximately 43.2% are caused by boat propellers. These propeller injuries also have a high rate of serious trauma and fatality with 7% of the propeller injuries resulting in death. Even boats traveling at relatively slow speeds can create a large amount of soft and hard tissue damage from a propeller strike.

The classic propeller design leaves fairly characteristic wound patterns, often described in the literature as “multiple, deep, parallel lacerations”, however the mechanics of these injuries are subject to some debate. The confusion arises from the numerous variables that effect the severity of the injury, such as the propeller design (analogous to shape or surface area), the boat velocity (acceleration/deceleration), and the rotations per minuet of the boat motor (force). These factors influence how the body responds to the impact, and whether the impact displays a more stereotypical “sharp trauma” appearance, or a classic “blunt trauma” appearance (Kroman et al 2007).

The two propellers used for the testing were a traditional propeller with three separate blades and one “ring style” propeller in which there is a ring

surrounding and attached to the three propeller tips. These two different designs provided useful variables to test the differences in injury pattern. For instance, the component of the propeller interfacing with the body is different, with the blade edge impacting in the traditional propeller and the ring impacting in the ring style propeller. Also, there is a difference in impact velocity between the striking edge, even in boats traveling the same speed. For instance, in a boat with a low velocity of 5-10 mph, the blades of the traditional style propeller effectively can often have a higher angular velocity defined by their spinning in accordance to the rotations per minuet (RPMs) of the boat motor. In the ring style propeller, the component impacting the body – the ring – is only traveling at the speed of the boat.

There is also a difference between how the two propeller designs engage the body during impact. The null hypothesis of this research was that these variables would have no effect the injury pattern seen.

This experimental research afforded the opportunity to study the effect of propeller shape on the severity of injury to humans and marine mammals, as well as an enhanced understanding of how the human thorax responds to force and the resulting fracture patterns.

Materials and Methods

Testing was performed in a unique facility at SUNY University at Buffalo. The Center for Research and Education in Special Environments (CRESE) provides a controlled environment that allows for safety, privacy, and

repeatability such that real-world boating accidents could be simulated as closely as possible. The facility houses a toroidal pool that is 8' wide, 8' deep, and 200' in circumference (Figure 3.1). The water was maintained at 73 degrees throughout the testing. A large centrifuge is located at the center of the pool and a platform is suspended over the pool from the centrifuge arm (Figure 3.2). An outboard boat motor was mounted to the platform. Instrumentation allowed for inputting and recording of motor travel speed an RPM.

The motor was towed at 5 or 7.4 mph around the pool to the impact site for the human tests. The motor was towed at 1, 5, 7.4, and 15 mph around the pool to the impact site for the porcine tests. The pool has three 4 foot by 4 foot underwater window through which videotaping can be conducted (Figure 3.3). The monitoring bride can be fully instrumented and is direct wired to computer processing for control, data collection and data processing. A mirror was positioned under the water in front of the viewing windows to allow for inferior and lateral viewing of the specimen (Figure 3.4).

The motor used for testing was a Honda BF50 engine. The engine has two valves per cylinder, and a gear shift ratio of 2.08:1. The full throttle RMP range was 5500 – 6000 RPMs. The ring style propeller used was a RingProp™ C03-040050 model propeller. The RingProp has three blades made of aluminum which are joined together by a hydrofoil ring (Figure 3.5). The standard propeller used also had three aluminum blades with out the hydrofoil ring (Figure 3.6).

Ten cadaver specimens were used, 6 porcine specimens and 4 humans. The human cadavers were obtained from the University of Buffalo Anatomy

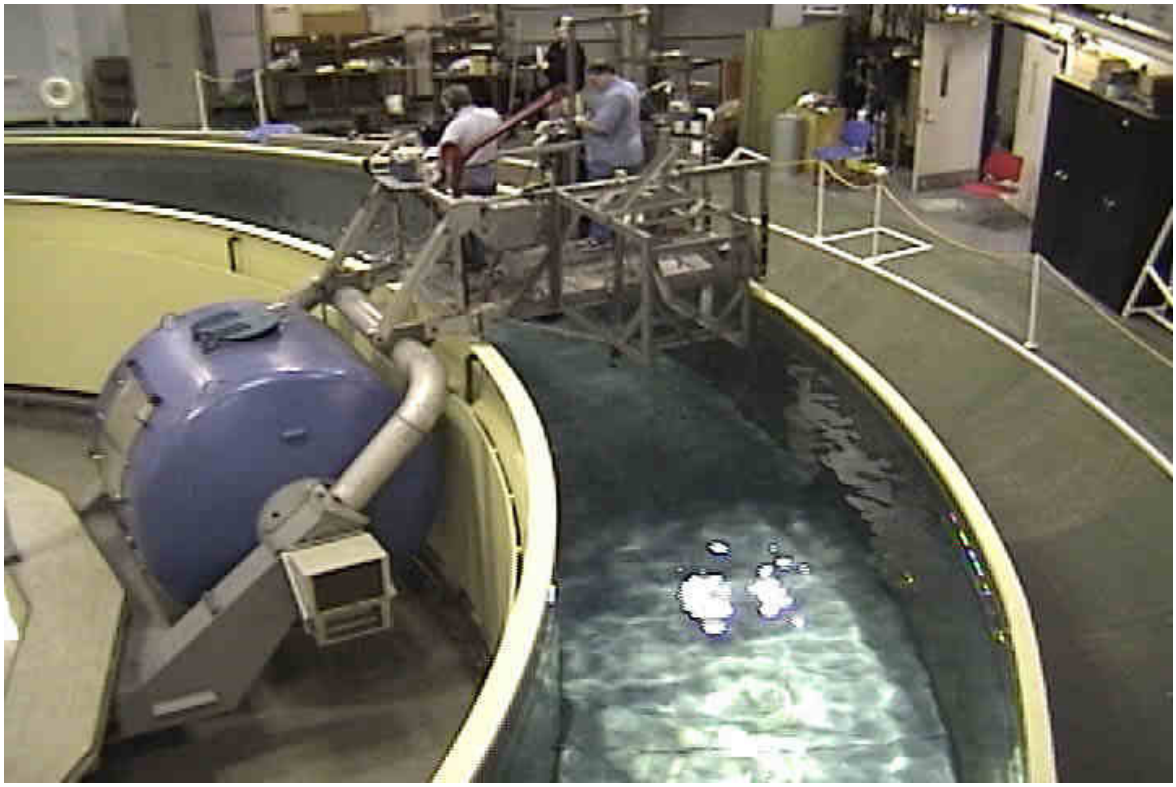

Figure 3.1 View of a portion of the torodial pool at the CRESE facility showing the centrifuge arm with motor attached.

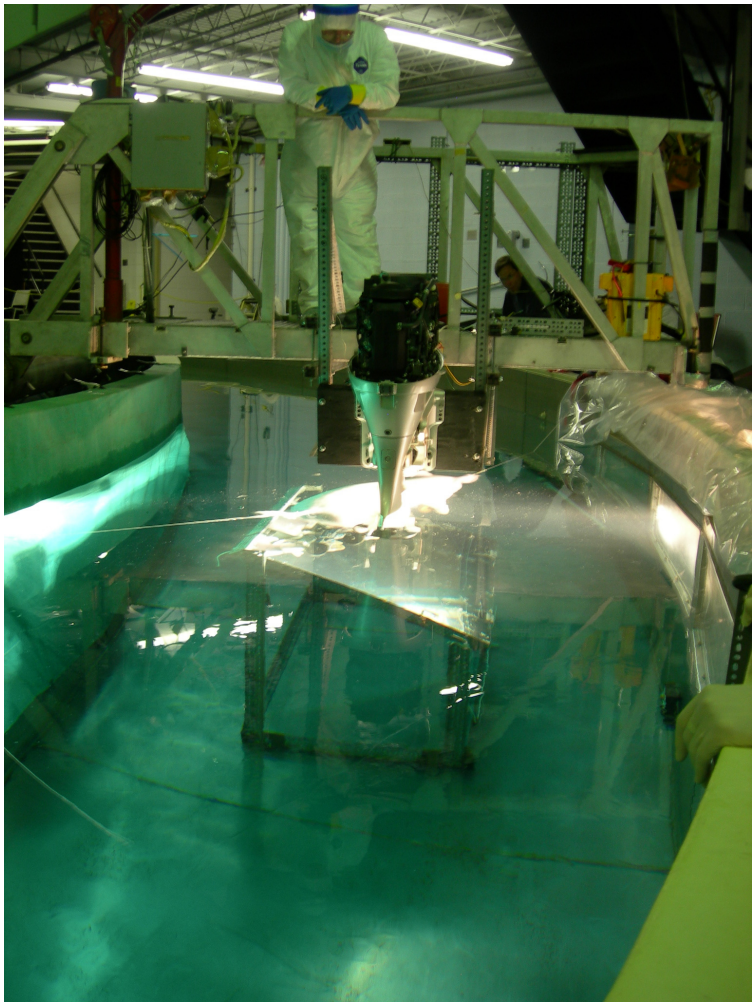

Figure 3.2 Outboard motor mounted to the platform over the water.

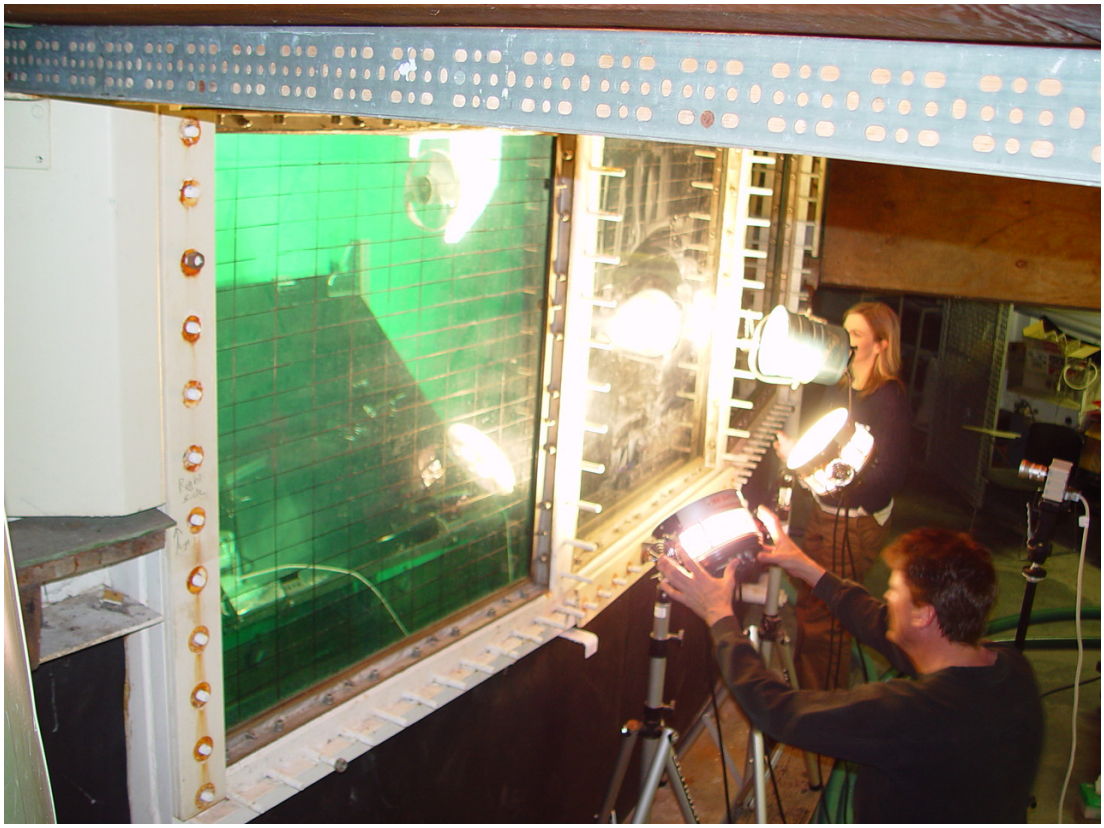

Figure 3.3 Underwater viewing windows and halogen lights for high speed filming.

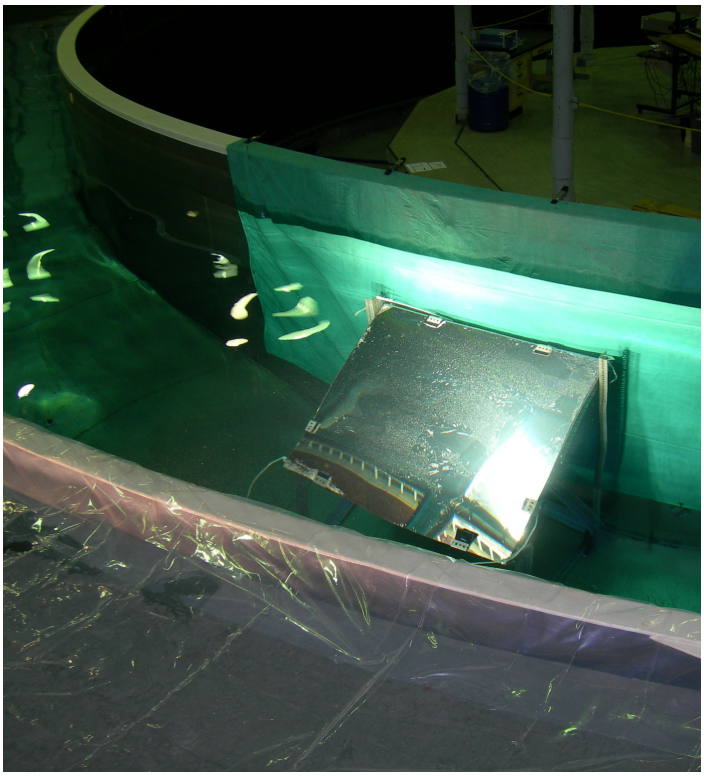

Figure 3.4 Mirror placed at a 45 degree angle to allow for lateral viewing of the specimen.

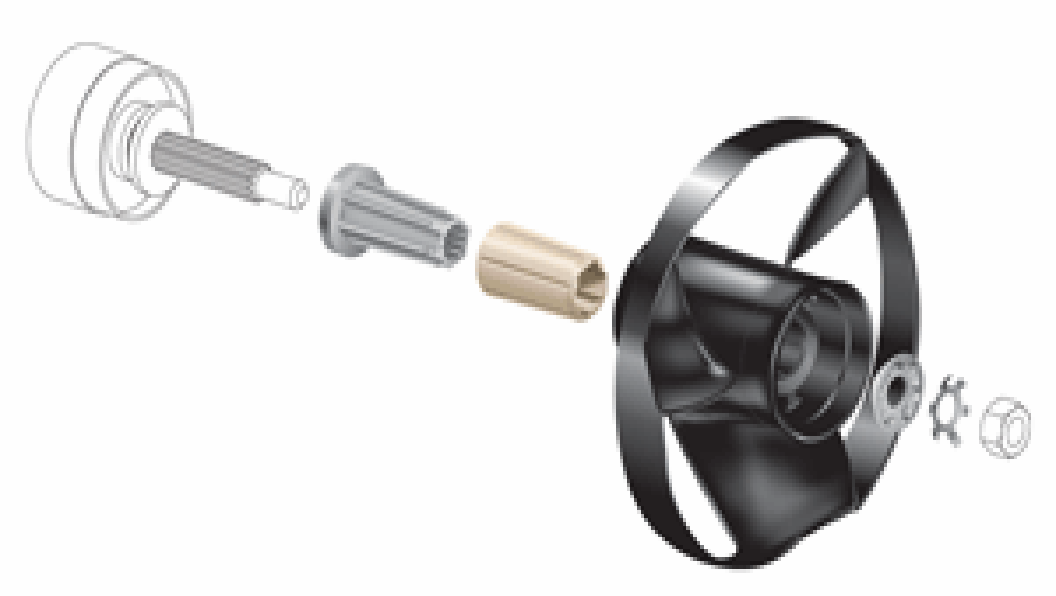

Figure 3.5 Schematic of RingProp propeller.

Figure 3.6 Schematic of standard propeller.

bequeathal program and ranged in age from 54 to 86 (Table 3.1). All had been deceased less than three weeks of the testing and had been stored in a low temperature cooler to prevent decomposition. The porcine specimens were obtained from a farmer and vet euthanized directly before testing.

The human cadavers were clothed in swim attire and placed into the pool via a crane. Weights were attached to the body in order for it to have slight negative buoyancy. The specimen was positioned directly over the mirror and held in place by strings, which were attached to the specimen by rubber bands, designed to break away during testing. The propeller and subject were positioned to obtain the desired impact scenario. A longitudinal line of impact was selected to maximize propeller engagement with the specimen.

A high speed color video camera captured the event through the underwater viewing window filming at 1,000 frames per sec. Halogen lights were positioned to achieve the lighting needed for maximum visibility for the high speed video. The high speed video was recorded on 8 mm tape. Several regular video cameras filmed alternate views of the impact event, including from above the water, and the view in the mirror. Each specimen was tested on both the right and left sides in a series of paired tests for comparisons between the two propeller designs. The velocity of the "boat" was set at 5, 7, and 10 mph, with motor RPMs of 2000, 3500, and 4000 respectively. Testing designations were allotted for each specimen in a consistent manner. The method for the testing designations is illustrated by the following sample: ***9.H1R5R.*** In this designation the first digit (***9***) represents the overall test number. The ***H1***

Table 3.1 Cadaver Data

# SUNY AB#	Age Sex	DOB DOD	Cause of Death	Condition
H1 2006-007	86yrs 11mos Female	2/4/1919 1/7/2006	Respiratory Arrest, Chronic Obstructive Pulmonary Disease	Obese, L Mastectomy
H2 2006-009	77yrs 8mos Male	4/30/1928 1/5/2006	Probable Cardiac Arrhythmia	Excellent! Midline Abdominal Surgical Scar
H3 2006-006	67yrs 2mos Female	11/1/1938 1/6/2006	Metastatic Breast Carcinoma	Very Good, Med-Large woman R Mastectomy
H4 2005-274	54yrs 2mos Male	11/2/1951 12/30/2005	Encephalopathy, Cerebral Concussion	Obese, Central line, Gastrostomy Tube

represents whether the test specimen is human (***H***) or porcine (***P***) and the specimen number. The ***R*** designates that the propeller being used in this test is a RingProp (***R***) or a standard propeller (***S***). The numeric value of ***5*** shows the approximate velocity of the test. The final notation (***R***) designated the side of the impact, right side (***R***) or left side (***L***). A test matrix was constructed for both the human (Table 3.2) and the porcine (Table 3.3) test specimens.

After testing, each specimen was photographed in their post-test position of rest. Following that documentation, the specimen was carefully removed from the water and transported to the designated autopsy area. Each specimen was given a through external examination. All of the external injuries were documented, measured, and photographed. Each specimen was also given a full dissection. Any suspect area was dissected to investigate if there was any underlying damage to the musculature of osseous tissue. All injuries were charted and photographed. After testing and dissection the specimens were returned to the University of Buffalo Department of Anatomy bequethal program.

Human Test Results

9.H1R5R

This test was conducted on human specimen 1, with the RingProp at an approximate velocity of 5 mph on the right side. The specimen was positioned in place for testing and secured using strings in four vectors. Approximately 3 -4 lbs of weight was attached to the neck in order to achieve negative buoyancy in

Table 3.2 Human Test Matrix

Test #	Specimen #	Sex	Age	Propeller Type	Approximate Impact Speed	Approximate RPM	Specimen Side	Impact Type
9	H1	F	86	RingProp	5	2000	Right	Longitudinal
10	H1	F	86	Standard	5	2000	Left	Longitudinal
11	H2	M	67	RingProp	5	2000	Left	Longitudinal
12	H2	M	67	Standard	5	2000	Right	Longitudinal
13	H3	F	77	RingProp	10	4000	Left	Longitudinal
14	H3	F	77	Standard	10	4000	Right	Longitudinal
15	H4	M	54	RingProp	7	3500	Right	Longitudinal
16	H4	M	54	Standard	7	3500	Left	Longitudinal

Table 3.3 Porcine Test Matrix

Test #	Specimen #	Propeller Type	Approximate Impact Speed	Approximate RPM	Specimen Side	Impact Type
1	P1	RingProp	5	2000	Right	Longitudinal
2	P1	Standard	5	2000	Left	Longitudinal
3	P2	RingProp	5	2000	Left	Longitudinal
4	P2	Standard	5	2000	Right	Longitudinal
5	P3	RingProp	15	3500	Left	Longitudinal
6	P3	Standard	15	3500	Right	Longitudinal
7	P4	RingProp	15	3500	Right	Longitudinal
8	P4	Standard	15	3500	Left	Longitudinal
17	P5	RingProp	1	-	Right	Reverse
18	P5	Standard	1	-	Left	Reverse
19	P6	RingProp	7.4	3500	Right	Perpendicular
20	P6	Standard	7.4	3500	Left	Perpendicular

the water. The specimen was clothed in shorts and a sports bra. During the test the propeller engaged with the specimen on the right lateral thigh. The sports bra became entangled with the propeller and drug the specimen with the motor.

During the external examination, numerous injuries were recorded. There was a cavitation/ laceration type injury to the lateral aspect of the right thigh and hip region (16 cm width X 16 cm length X 4 cm depth) (Figure 3.7). Deep dissection reveled that the osseous tissue in this location was undamaged. A laceration was also seen in the parietal region. The scalp was removed with exposed bone, but no fractures were seen (Figure 3.8).

10.H1S5L

This was the second test conducted on human specimen 1, this time using the standard propeller at a velocity of 5 mph on the left side of the body. The specimen was repositioned and secured in place for the appropriate impact location. The 3 -4 lbs of weight added for the previous test were left in place to maintain negative buoyancy. The specimen was clothed in a new sports bra. Due to the clockwise rotation of the propeller (when the propeller is being viewed from behind) the body rotated counter-clockwise during impact, causing the propeller to cross over the midline, impacting the thorax and head. The body almost appeared to be being pulled into the propeller impact instead of being pushed away.

The post-test examination of the body while still in the water showed clear propeller strike marks, evident by a series of parallel depressions in the body

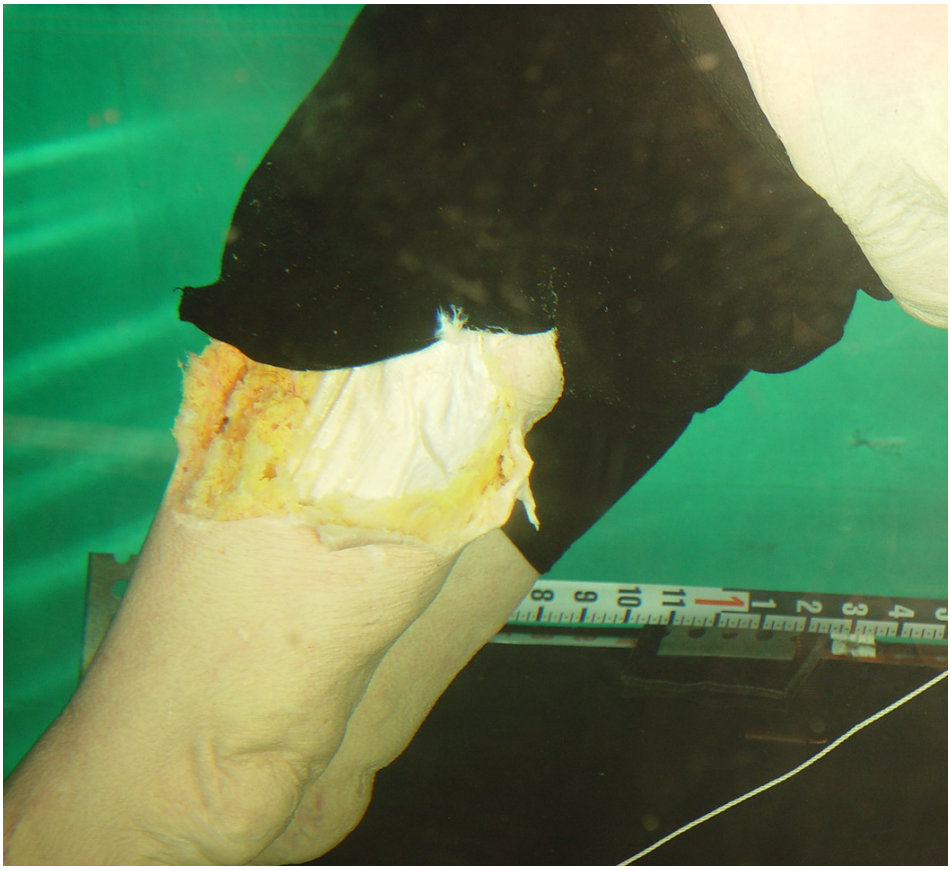

Figure 3.7 Cavitation/ Laceration type injury to the lateral aspect of the right thigh in human specimen 1 from test 9.H1R5R shown here in the post-test view.

Figure 3.8 Laceration injury to parietal scalp in human specimen 1 from test 9.H1R5R. No fractures were present.

(Figure 3.9). The dissection revealed that there were numerous rib and vertebra fractures. The spinous processes of vertebra 6 – 11 were fractures, along with ribs 4, and 7 – 9 (Figures 3.10 and 3.11).

11.H2R5L

This test was conducted on the second human specimen with the RingProp at an approximate velocity of 5 mph on the left side of the body. The male specimen was clad in cotton shorts. The specimen was positioned and secured using strings in four vectors, and weights at the neck for negative buoyancy. After contacting the body, the RingProp and the engine rose up and rolled along the top portion of the body and rotating the body in a counter-clockwise direction (when viewed from the back). The high speed video showed that the skin appeared to roll and the ring of the propeller passed over the body. This resulted in one long abrasion visible in the post-test view. Aside from the abrasion noted above, there was no other injury aside from a 3 cm by 3cm laceration near the left side of the rectum (Figure 3.12).

12.H2S5R

This was the second test on the second human specimen, this time using the standard propeller at an approximate velocity of 5 mph with an impact to the right side of the body. The standard propeller engaged with the specimen from the buttocks region all the way to the head. In there external examination there was clear patterned bruising along the right side of the body, along with a laceration of the right arm measuring 10.5 cm in length and 4.5 cm in width, and

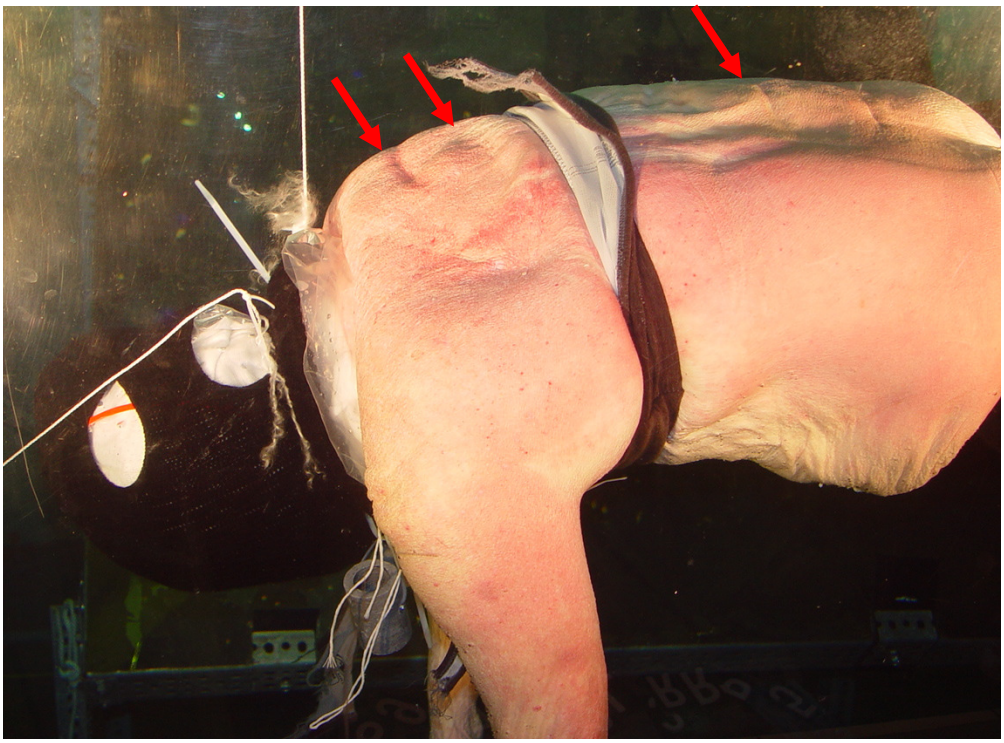

Figure 3.9 Parallel depressions (shown at red arrows) on the back of human specimen 1 from test 10.H1S5L from the blades of the propeller.

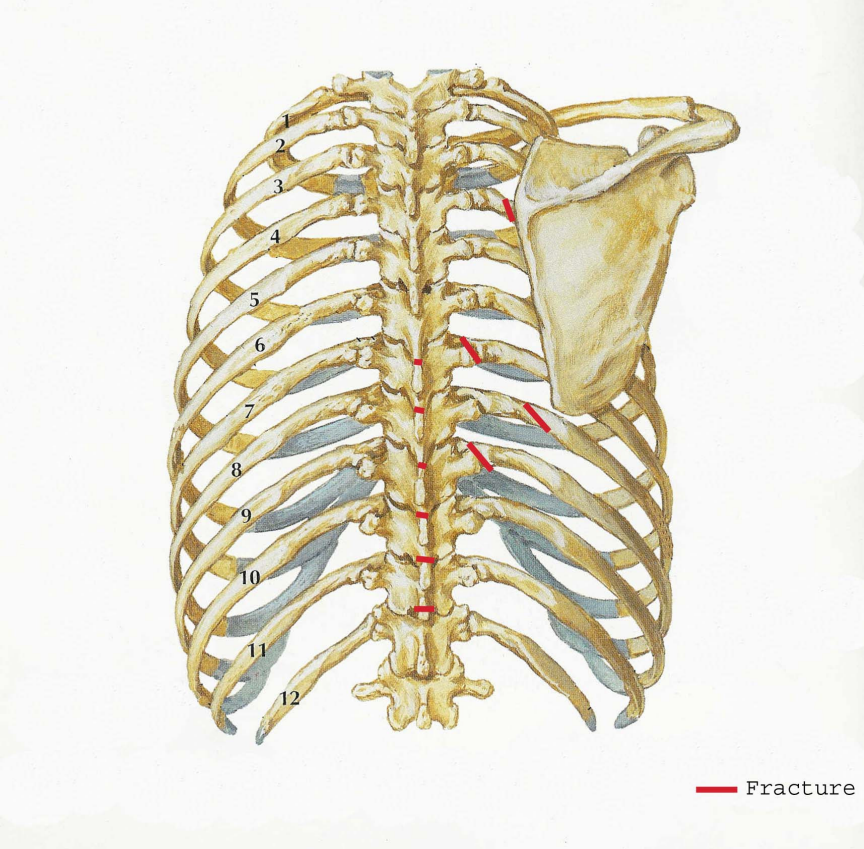

Figure 3.10 Diagram illustrating location of rib fractures in human specimen 1 from test 10.H1S5L.

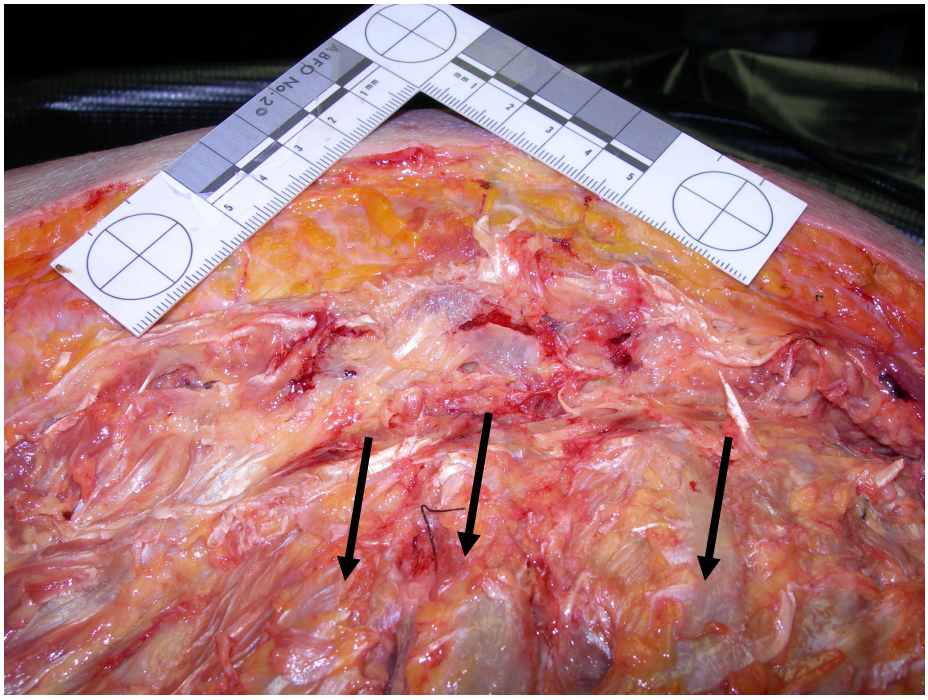

Figure 3.11 Location of rib fractures (black arrows) in human specimen 1 from test 10.H1S5L.

Figure 3.12 Laceration to the rectal region.

exposing the humerus (Figure 3.13). There were also fractures present at the posterior aspects of ribs 4 and 7 (Figure 3.14 and 3.15). There was also a 3 cm laceration to the temporal region with mild involvement of the temporalis muscle (Figure 3.16).

13.H3R7L

This test was preformed on the third human specimen with the RingProp at a velocity of 7.4 mph. The test number in the photos indicates 10, but the actual recorded velocity was 7.4 mph. The specimen was positioned with five strings in five vectors and weights were attached to the body at the ankles, thighs, neck, and wrists in order to achieve negative buoyancy and to keep the specimen in proper position for impact. Upon impact the RingProp and motor elevated in the water to essentially ride over the body. The post-test inspection of the body showed large wounds to the left side of the body. A large cavitation type wound was measured and documented in the region of the left buttocks and low back during the external examination (Figure 3.17). This area was thoroughly dissected. Dissection revealed that the laceration only involved the layers of skin and fat, and there was no damage to the underlying musculature. The deep nerve tissue of the area, including the sciatic nerve, was also intact with out injury. There was no damage to the osseous tissue, including the greater trochanter of the left femur.

Figure 3.13 Patterned brusing and exposure of the right humerus in human specimen 2 from test 12.H2S5R.

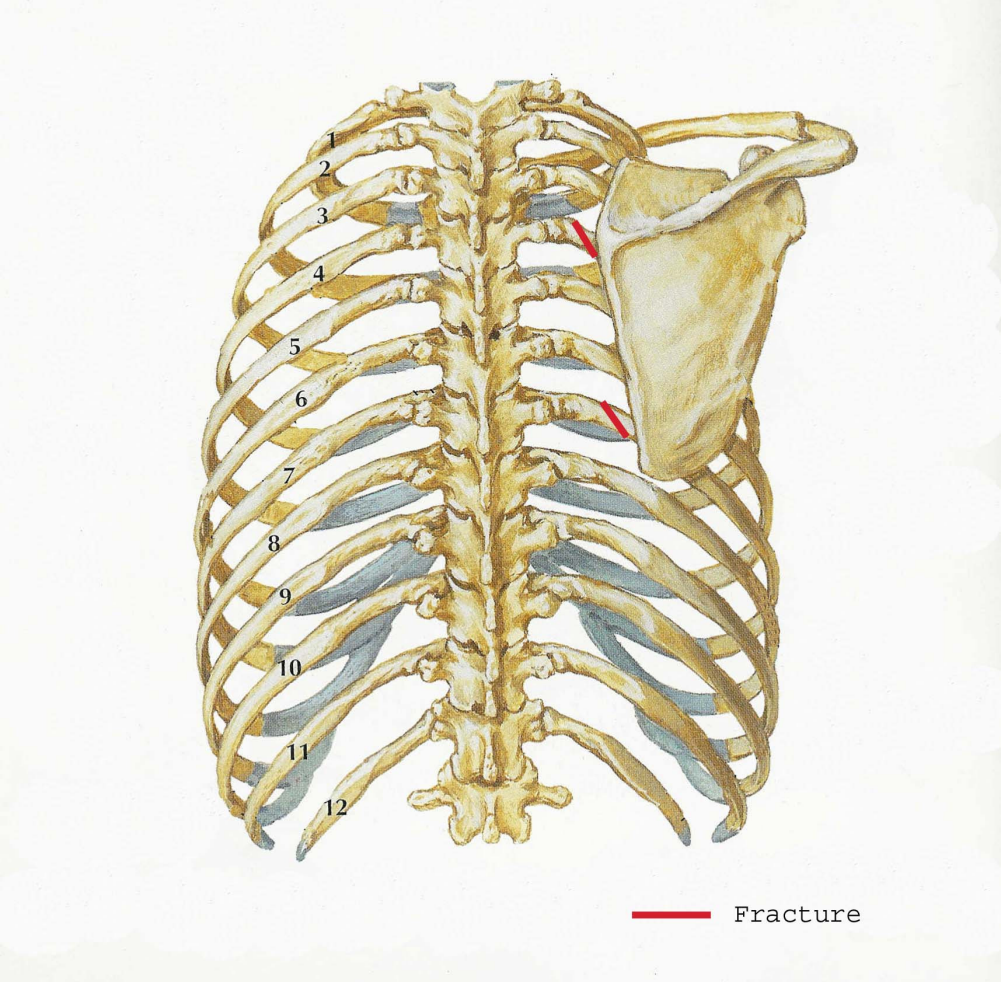

Figure 3.14 Diagram illustrating location of rib fractures in human specimen 2 from test 12.H2S5R.

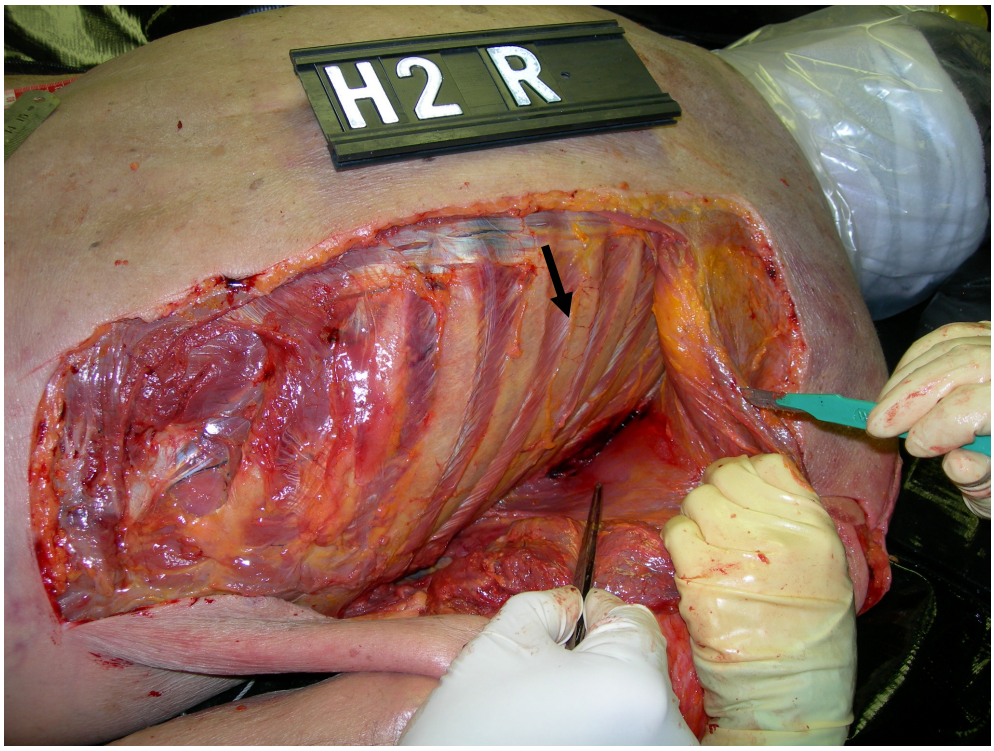

Figure 3.15 Dissection showing fracture of rib seven (black arrow) in human specimen 2 from test 12.H2S5R.

Figure 3.16 Laceration to temporal region with mild involvement of the temporalis muscle.

Figure 3.17 Large scooping laceration to left buttocks in human specimen 3 from test 13.H3R7L. There was no damage to the muscle, nerve, or bone tissue from the impact.

14.H3S7R

The third human specimen was used again for this test, this time with the standard propeller on the right side with an impact velocity of 7.4 mph. The specimen was positioned in place by strings, and negative buoyancy was achieved by adding weights to the cadaver. The impact with the standard propeller produced massive injuries to the specimen. The high speed video showed the standard propeller engaging the body and rotating the specimen into the blades, so there was a large amount of contact between the specimen and the propeller. Post test views of the specimen showed twelve distinct parallel lacerations and skin abrasions were seen on the right side of the body from the thigh region to the head (Figure 3.18). During the dissection and the external examination, all of the injuries were measured and charted and the region was dissected to reveal the full extent of the injury. The lacerations to the abdomen and shoulder were very deep. The dissection revealed that there were multiple fracture of ribs 2 – 10 on the right side (Figures 3.19 and 3.20). These fractures produced the classic “flail chest” in which there is a collapse of the structural integrity of the thoracic cavity (Knight 1996). In addition to the rib fractures, there was also a laceration of the right lung (Figure 3.21), and penetration of the pleural cavity (Figure 3.22). The lacerations to the head resulted in fractures to the zygoma, a comminuted skull fracture (Figure 3.23), and a laceration to the cerebral hemisphere (Figure 3.24).

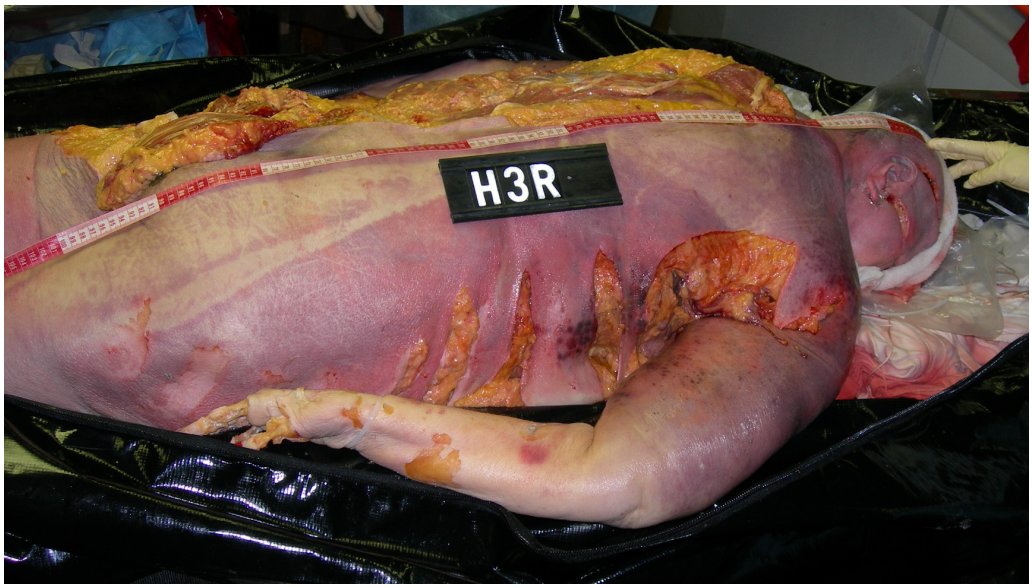

Figure 3.18 Twelve parallel lacerations on the right side of human specimen three from test 14.H3S7R.

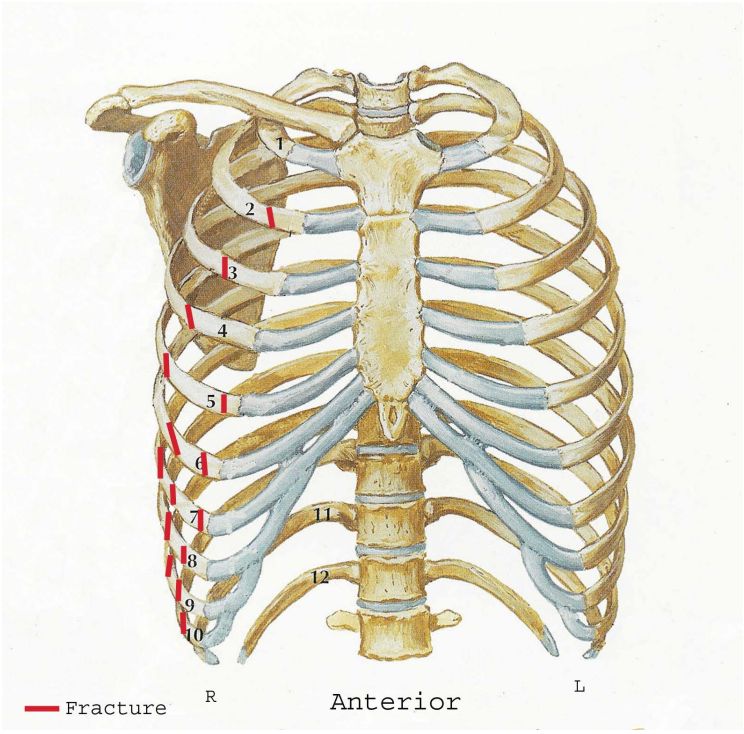

Figure 3.19 Diagram illustrating the location of rib fractures from the anterior view in human specimen three from test 14.H3S7R.

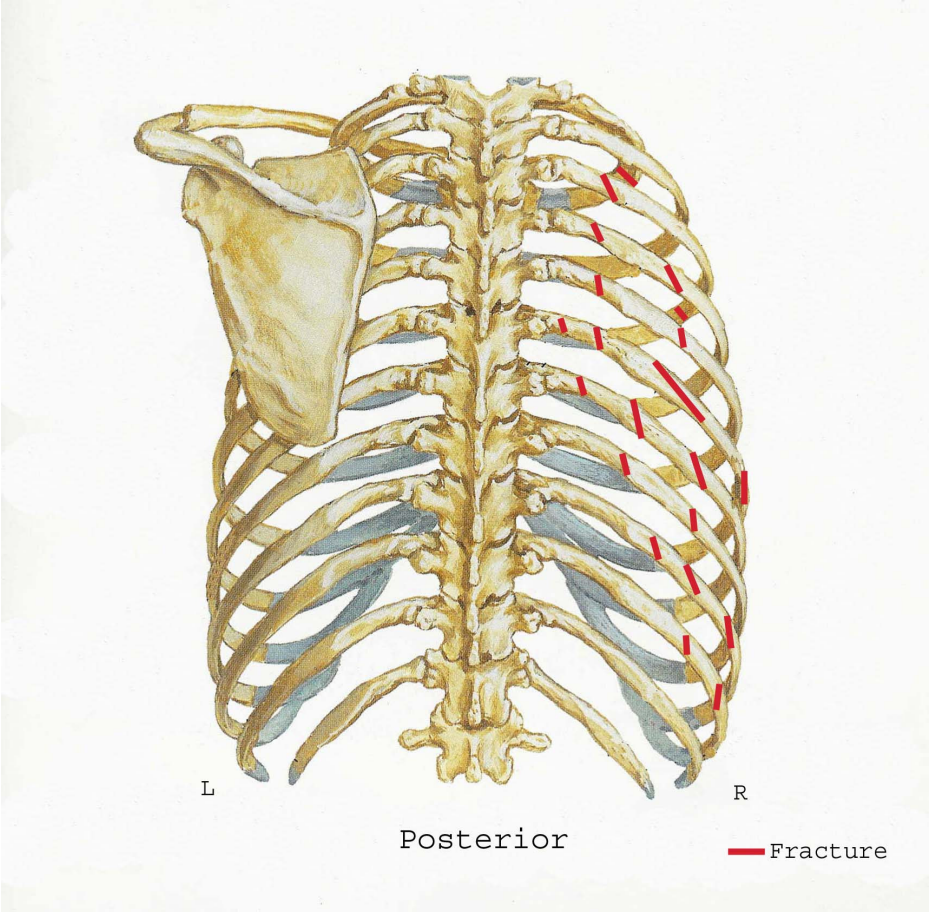

Figure 3.20 Diagram illustrating the location of rib fractures from the posterior view in human specimen 3 from test 14.H3S7R.

Figure 3.21 Multiple rib fractures and lacerated lung in human specimen 3 from test 14.H3S7R.

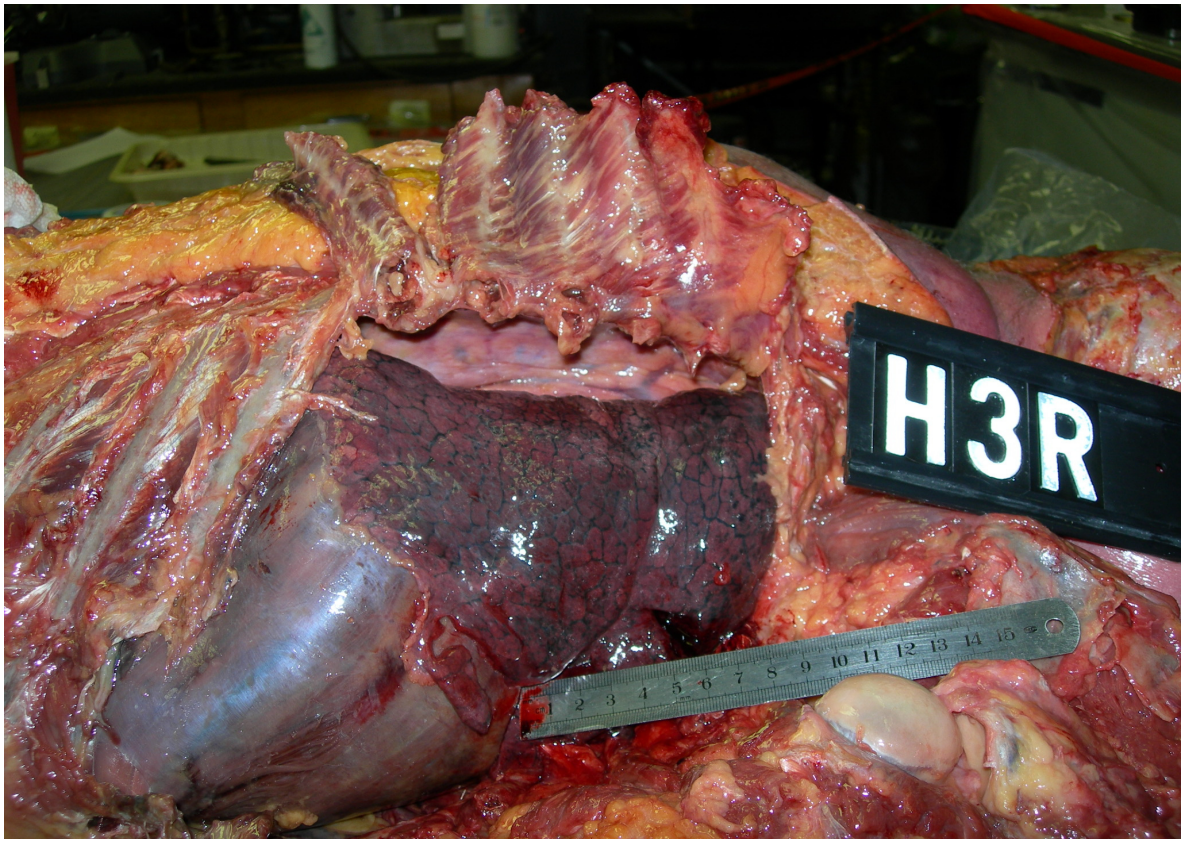

Figure 3.22 Reflection of the fractured ribs on the right side of human specimen 3 from test 14.H3S7R revealed a penetrated plural cavity.

Figure 3.23 Lacerations, fractured zygoma, and comminuted skull fracture from standard propeller blade impacts in human specimen 3 from test 14.H3S7R.

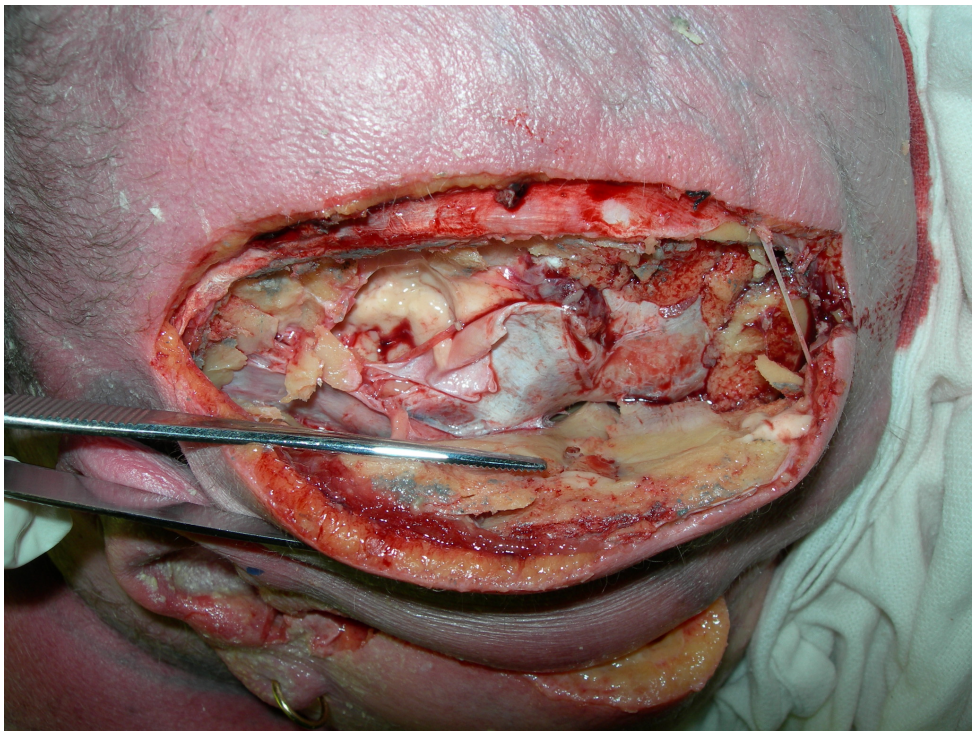

Figure 3.24 Laceration to right cerebral hemisphere in area of propeller blade impact in human specimen 3 from test 14.H3S7R.

15.H4R7R

This test was conducted on the fourth human specimen, using the RingProp at an approximate impact velocity of 7 mph on the right side. Weights and strings were used to position the specimen for the impact and achieve negative buoyancy. After testing, the specimen was removed from the water and examined for external injuries. The post-test examination only revealed an injury to the right thigh. This injury was a large cavitation wound on the lateral superior right thigh (Figure 3.25). While the skin, superficial fasica and fat layer was disrupted, dissection revealed that there was no damage to the femur or musculature.

Figure 3.25 Laceration to the lateral superior right thigh in human specimen 4 from test 15.H4R7R. Dissection reveled that there was no injury to the musculature or bone.

16.H4S7L

The final human test was using the fourth human specimen with the standard propeller at an approximate impact velocity of 7 mph on the left side of the body. The specimen was positioned in the water using a series of weights and strings. The post test examination of the body for external injuries showed injuries to the areas of the gluteal region as well as the posterior scalp. Dissection of these areas revealed a large laceration to the left buttocks region involving the fat and superficial layers, with no damage to the musculature or the osseous tissue. There was also an injury to the posterior scalp from the impact of a propeller blade (Figure 3.26). These impacts to the head resulted in a delamination fracture of the occipital bone.

Figure 3.26 Lacerations to the left buttock region and the posterior scalp in human specimen 4 from test 16.H4S7L.

Human Injury Summary

When comparing the soft tissue and osseous injuries from the RingProp propeller and the standard propeller there was a marked difference in injury severity, patterning, and ultimate survivability. Soft tissue injuries were seen from both types of propellers, however, the RingProp propeller impacts resulted in more superficial “scooping” type lacerations while the standard propeller caused deep, parallel cuts. A side by side comparison of the soft tissue injuries shows that there was no muscle damage cause by the RingProp, and significant muscle damage cause by the standard propeller (Table 3.4). A significant difference also existed between the osseous injuries caused by the RingProp and the standard propeller (Table 3.5). No fractures occurred from impacts with the RingProp, while the standard propeller created fractures in every test.

Porcine Test Results

Tests were conducted on porcine specimens in a manner identical to the human specimens, for the purpose of additional data and to try to understand propeller injuries to large underwater mammals, such as manatees. Large underwater mammals are also often the victim of propeller impacts from boats, especially in shallow waters. A total of twelve tests were completed using six recently euthanized porcine specimens. A summary of the complete porcine test series follows in Appendix B.

Table 3.4 Soft Tissue Injury Summary

Soft Tissue Injury Summary		
Specimen #	Standard Prop	Ring Prop
H-1	None Noted	16x16x4 cm Scooping/Laceration upper lateral R thigh, 7 cm Scalp Lac & 5 cm R Chest Lac, No muscle damage
H-2	3 small superficial Lac to abdomen, 10+ cm Lac to R arm thru muscle, 3 cm Lac to R Temple into muscle	Abrasion f L Buttock to R shoulder, 3x3 cm laceration to L Buttock, No muscle damage
H-3	4 Abrasions, 7 significant (>10cm) Deep Lacerations from Abdomen to the Head. Lacerated R lung from T-4 to T6. Lacerated R Cerebral Hemisphere	3 Large Scooping/Lacerations to L Buttock, No muscle damage
H-4	4 Abrasions to L shoulder, 3 Lacerations to L Buttock, 2 Lacerations (4 & 10 cm) to posterior head	25x20 cm Scooping/Laceration to R Thigh, 3 smaller but significant lac to abdomen, No Muscle Damage

Table 3.5 Osseous tissue injury summary

Osseous Injury Summary		
Specimen #	Standard Prop	Ring Prop
H-1	Spinous Process Fxs 6-11 plus 4 rib fractures	No Fractures
H-2	Fractures to Ribs 4 & 7	No Fractures
H-3	Multiple Fractures of Ribs 2 thru 10 (R Flail Chest), Massively comminuted R Scapula, Fx of Zygoma, Open Comminuted Depressed Skull Fx.	No Fractures
H-4	Delamination Fracture of Occipital Bone	No Fractures

Porcine Injury Summary

There was also a difference in the injury patterns and severity between the RingProp and standard propeller test in the porcine specimens, through not as marked of a difference compared to the humans. The soft tissue injuries from both propellers included lacerations and abrasions and shearing of the muscle tissue (Table 3.6). However, the osseous injuries were more severe from impacts from the standard propeller than the RingProp (Table 3.7). Only two minor fractures (fibula and zygoma) occurred from the RingProp, while numerous fractures to the head and thorax resulted from the standard propeller impacts.

Table 3.6 Soft tissue injury summary

Specimen #	Standard Prop	RingProp
P1	Skin abrasions	11 narrow cut abrasions
P2	No injuries	Laceration of the ear
P3	13 dents with muscle shearing and scoopings.	1 scooping injury, lacerations around head
P4	16 abrasions, lacerations, muscle shearing and scoopings.	6 areas of abrasions and muscle shearing.
P5	4 linear abrasions	Torn digit on left hoof
P6	No injuries	Minor abrasions

Table 3.7 Osseous tissue injury summary

Specimen #	Standard Prop	RingProp
P1	No Fractures	No Fractures
P2	No Fractures	No Fractures
P3	8 transverse rib fractures	Fractured zygomatic
P4	Numerous fractures, including super orbital rim	Fracture of the fibula
P5	No Fractures	No Fractures
P6	No Fractures	No Fractures

Discussion

The results from this series of tests provide important information regarding both the etiology of traumatic injury from boat propellers, but also how the thorax responds to force. The variables that had the most effect on the injuries created were the shape of the propeller and the speed. The impacting edge of the RingProp was a flat ring joining the blade tips. The ring created large scooping type lacerations, but was only able to penetrate the superficial fat layer and caused little damage to the underlying musculature or osseous tissue. The standard propeller had three rotating impacting blades. The standard propeller caused deep parallel lacerations that penetrated soft and hard tissue. The difference in the surface area and shape of the striking component of the

propeller made a great difference in the injury, with the RingProp creating a laceration that would be traditionally classified as a “blunt force trauma” injury, and the standard propeller creating a more classic “sharp force trauma” injury.

Speed also played a role in how the propeller interfaced with the specimen. The high speed video of the impact events reveals that at slow speed (approximately 5 mph) the standard propeller grips the body and rotates it back into the blade. At higher speed (approximately 15 mph) the standard propeller penetrates and lacerates that body with out the rotational movement.

The fractures to the ribs were most frequent in the posterior and lateral aspect of the ribs. The mechanism of fracture of the ribs was from the direct impact to the lateral and posterior aspect of the thorax from the blades of the standard propeller. The propeller strikes created fractures in the ribs and Spinous process of the vertebrae at the area of impact.

Conclusion

The experimental data from this study shows that when a human or marine life form is impacted at relatively slow speeds, the RingProp propeller causes significant less soft tissue and osseous tissue damage than a standard propeller. In some instances, the differences between the level of soft tissue and bone injuries resulting from an impact by a RingProp propeller versus a standard propeller may mean the difference in life and death, respectively.

CHAPTER 4: UPPER EXTREMITY TRAUMA

Relevance of Upper Extremity Trauma

Forensic and Physical Anthropology

Traumatic injuries to the arm are fairly common and seen frequently in skeletal samples in modern, historic, and prehistoric populations (Steele and Bramblett 1988). In historic and prehistoric populations, analysis of long bone fractures can assist in paleodemographic research and allow for comparison between samples (Burrell et al 1986). The correct analyses of these fractures, particularly in the upper extremity, lend important information to the rate of incidences such as falls or interpersonal violence in a community (Burrell et al 1986, Judd and Roberts 1999).

In a forensic context, fractures of the upper extremity can come into play when determining cause and manner of death. Fractures to the long bones of the arm can indicate a violent event such as a fall or a motor vehicle accident. Radial shaft fractures can also be created during attempts to ward off an attack (DiMaio and DiMaio 2001, Galloway 1999). Like wise a fracture of the distal aspect of the metacarpal (referred to as a "boxer's fracture") is often indicative of hitting someone or something with the hand in a fist position (Levine 1993). In addition to the traditional applications of trauma analysis, healed fractures of the extremities have also been used as potential identifying features of a skeleton (Komar 2003).

Impact Biomechanics

There is also concern for the tolerances of the upper extremity in many areas of engineering as well. A voluminous amount of research is devoted to musculoskeletal disorders of the shoulder, elbow, and wrist resulting from work place stress and repetitive motion. Acute trauma is also a concern in addition to cumulative trauma. The upper extremity, especially the shoulder girdle is especially vulnerable in side impact motor vehicle accidents, where the humerus is pushed laterally into the gleno-humeral joint (Levine 1993). While fractures of the upper extremity are rarely life endangering, they can have life altering consequences with a loss of movement and prehensile function (Gershuni 1985). One area of particular focus is fracture tolerances of the phalanges of the hand. Crushing injuries to the fingers are common in both adults and in children (Galloway 1999).

Experimental Testing of Phalanges

Introduction

In our current day, mechanized world hands and fingers are in danger of getting trapped in automatic car windows, car doors, escalators or numerous other devices. Numerous sources report that fractures to the hand phalanges and metacarpals occur with the highest frequency of all skeletal injuries (Emmett and Breck 1958, Jupiter and Belsky 1992, McNealy and Lichenstien 1940, Swanson 1970). These injuries can be dehabilitating and provide a large economic cost (Jupiter and Belsky 1992). In order to better understand the

fracture of human phalanges experimental testing and research is needed. The research presented here is part of an on-going effort to quantify the tolerance levels of adult and juvenile fingers.

Materials and Methods

The purpose of this study was to collect experimental data to increase the understanding of the compression tolerances of human fingers. Specifically, transverse forces were applied to the human phalanges until crush occurred utilizing three different test set-ups: 1) static testing (a common automobile window edge as the "impactor" in a compression testing machine with slow force application); 2) dynamic testing (a circular leading edge on the end of a cylindrical anvil as the "impactor" in a specially designed drop-test rig); and 3) field testing (a common product's hinge point as the "pinching mechanism" for the phalange, i.e. a wall-mounted baby changing table lifted up partially and then brought down).

Results and Discussion: Static Testing

For the static testing, four fresh human cadaver hands were utilized (ages 57 and 65 yr old males and a 72 yr old female). A crushing force was applied to each phalange by a PSB 5000 materials testing machine (Com-Ten Industries, Inc.). Figure 4.1 shows the testing set up. The anterior surface of each phalange was placed on the edge of a piece of tempered glass or plexiglass (3/16-inch thick). The flat surface of the testing machine then pinched the finger

Figure 4.1 Test set up for the static finger testing.

at a velocity of approximately 2.7 in/min. The forces were recorded and plotted against the elapsed test time.

The mean peak force applied to all 43 phalanges crushed in this study was 497 lbs (SD = 233). The phalanges of the third digit had the highest average peak force, 668 lbs (SD = 254), while those of the first digit were the lowest at 368 lbs (SD =192). The distal phalanges exhibited the lowest average peak force, 314 lbs (SD =115). The hands were radiographed but the medical images did not sufficiently demonstrate the fracture damage uncovered during dissection.

Results and Discussion: Dynamic Testing

For the dynamic testing, six fresh human cadaver hands were utilized. Anthropometric measurements were taken of each hand and each finger before testing. A crushing force was applied using the circular surface (3 in diameter) of the end of a cylindrical anvil/platen in a specially designed portable drop-test rig (approximate dimensions 2' x 2' x 2'). The hand was placed supine on a lower platen so that each phalange could be impacted individually anteriorly-to-posteriorly with the dropping anvil/platen (Figure 4.2). Force (using a load cell underneath the lower platen) and displacement (using a string potentiometer) were recorded with respect to time. After testing, each hand was examined and the fractures were charted and recorded.

Figure 4.2 Test set up for dynamic finger impact testing.

Hand One

Hand one was the right hand from a female cadaver. After testing, the hand showed soft tissue damage in the form of linear lacerations across the digits (Figure 4.3). All of the 14 phalanges fractured. All of the fractures were longitudinal to the phalange.

Hand Two

Hand two was the left hand from a female cadaver. After impacting, the hand was examined. There were numerous lacerations to the soft tissue. All 14 phalanges had fractures, which ran in the longitudinal direction (Figure 4.4).

Hand Three

Hand three was the right hand from a male cadaver. Again, there were numerous soft tissue lacerations and all 14 phalanges displayed longitudinal fractures. The fracture to the proximal phalanx of the thumb was particularly comminuted.

Hand Four

Hand four was the left hand from a male cadaver. All of the 14 phalanges were fractured in a longitudinal direction, with comminution of the middle phalanx of the second ray (index finger).

Figure 4.3 Soft tissue lacerations in hand one.

Figure 4.4 Longitudinal fractures of the phalanges in hand two.

Hand Five

Hand five was the right hand from a female cadaver. The only phalanges to fracture in hand five were the distal and proximal phalanx of the thumb. Both of these fractures were longitudinal.

Hand Six

Hand six was the left hand from a female cadaver. A longitudinal fracture was present in the intermediate phalanx of the fifth digit (Figure 4.5), as well as a comminuted fracture of the distal and proximal phalanx of the thumb. The fracture in the distal phalanx of the thumb transected the condyles of the phalanx (Figure 4.6).

Force Data

Forces exceeded the limits of the force transducer for many of the tests, but reliable data exists for at least n=30. The average force at impact was 1062 lbs (SD = 193) and average displacement was 0.43 inch (SD = 0.09).

Conclusions

The results from the testing indicate that the fracture behavior of phalanges is to fracture in a longitudinal direction, sometime accompanied by a transverse fracture transecting the condylar region of the phalange. All of the phalanges from the first two cadavers tested (hands one – four) fractures, whereas the phalanges from the third cadaver (hands five and six) appeared to be more resistant.

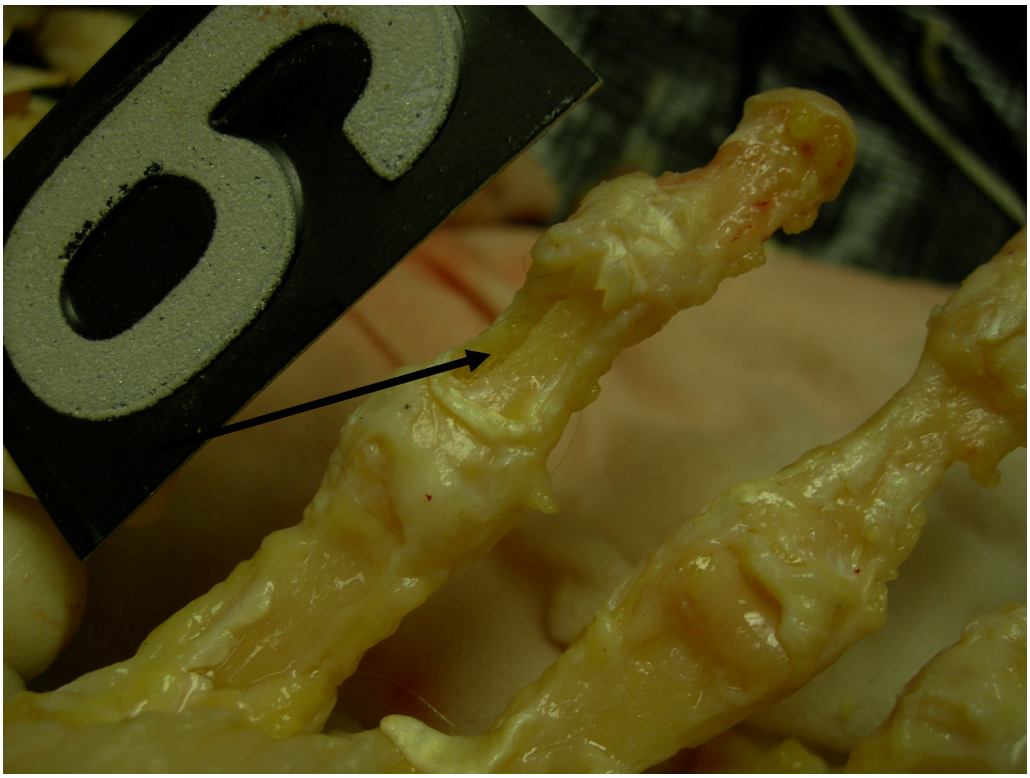

Figure 4.5 Longitudinal fracture to the intermediate phalanx of the fifth ray.

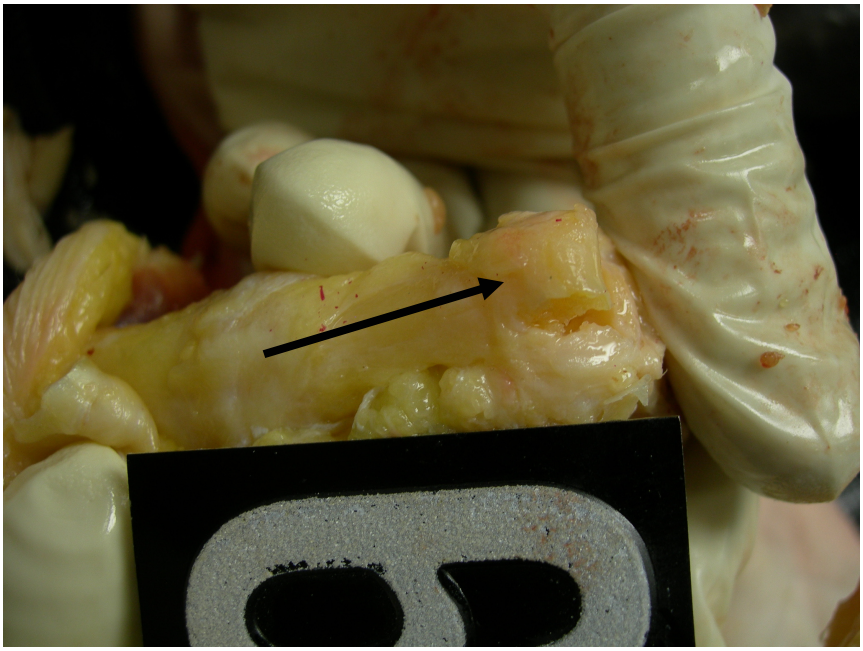

Figure 4.6 Fracture to the condyles of the proximal phalanx of the thumb.

Results and Discussion: Field Testing

For the field testing, six fresh adult human cadaver distal phalanges were utilized. A crushing force was applied using the hinge area of a baby changing table (commonly seen in public restrooms). The hand was placed supine on the partially lifted table in order to place the distal phalange in the hinge area. A weight of 25 pounds was placed on the changing table surface to simulate a baby's weight and the table was then lowered causing a crushing force to be applied to the phalange for approximately 2 to 3 seconds. Pre-test calculations allowed for the selection of the appropriate Fuji film and it was placed on the anterior surface of the phalange for each test. Analysis of the film yielded a pressure distribution across a contact surface area of each phalange (Figure 4.7). As a result, force levels could be determined yielding an average of 134.3 lbs (SD=78.2).

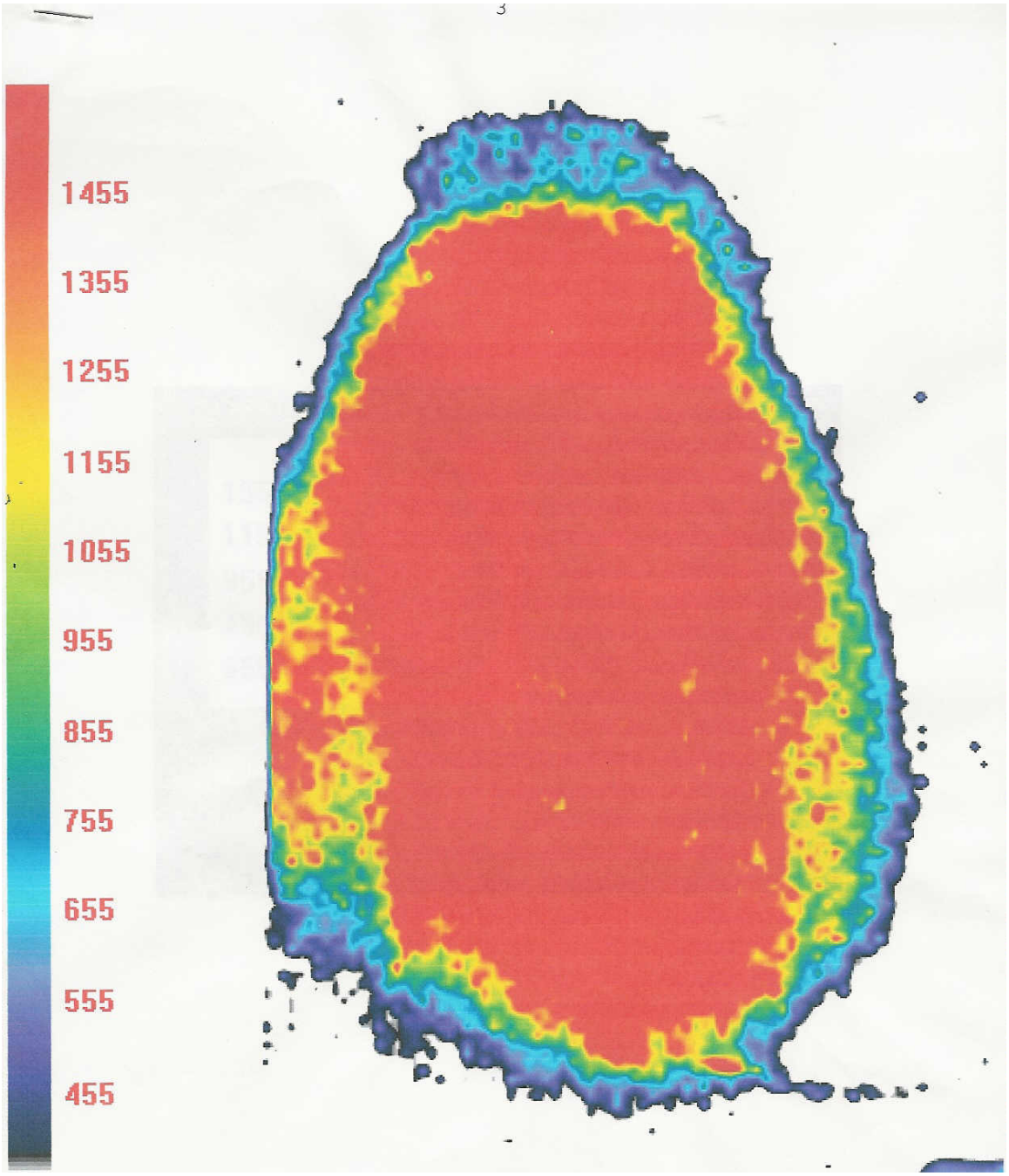

Figure 4.7 Fuji film reading with the pressure reported in psi.

CHAPTER 5: LOWER EXTREMITY TRAUMA

Relevance of Lower Extremity Trauma

Forensic and Physical Anthropology

Similar to trauma of the upper limb, the lower limb injuries are also of interest to physical and forensic anthropologists. As mentioned previously, studies of extremity fractures aid in the understanding of prehistoric populations (Ortner and Putschar 1981). In forensic cases, fractures of the lower leg are often seen from violent impact events such as plane crashes, motor vehicle accidents, or fall. They also can occur in impacts to pedestrians. In these instances, proper reconstruction of the bones and correct interpretation of the fractures can greatly aid in determining direction of force and positioning the victim in relation to the bumper of the car (DiMaio and DiMaio 2001). In addition to blunt force trauma, femoral fractures are also caused by firearm injury with increasing frequency (Ryan et al 1981).

Impact Biomechanics

The lower extremity is also susceptible to injury from motor vehicle accidents. The causes of these injuries have been an area of significant attention in the literature (see Hyde 1992 and Porta 1996 for review). Impact to the instrument panel is thought to be the cause of some of the most serious lower limb injuries (Huelke et al 1982). The intrusion of the foot well is also though to be a cause of leg fractures in accidents, particularly fractures of the distal tibia and fibula (Porta 1996). In fact, fractures to the malleolus are often

seen as the result of front end crashes (Madeley et al 2004). These types of fractures represent 24-56% of all the injuries below the knee in accidents (Lestina et al 1992, Sherwood et al 1999). In addition to motor vehicle accidents, injuries to the leg and the ankle are also common in sports related injuries (Porta 1996).

Relevant Anatomy of the Ankle

The ankle and foot are designed to be able to respond to a myriad of gait situations. The foot must be rigid enough to withstand the impact forces of walking or running, while still remaining pliable enough to conform to any type of terrain (Neumann 2002). Its proper function in gait and movement is significantly dependant of its precise structural integrity (Trafton et al 1992). To allow for this seemingly paradoxical situation, there is a large range of motion for the ankle and the foot. When categorizing motions for these joints, two sets of terminology are applied; fundamental terminology and applied terminology (Neumann 2002). The fundamental terminology describes the motions that occur at right angles to the three standard anatomical axes of rotation. *Dorsiflexion* and *plantar flexion* describes the movement around the medial axis and parallel to the sagittal plane (Neumann 2002). *Eversion* and *inversion* describe motion around the anterior-posterior axis and parallel to the frontal plane (Neumann 2002). *Abduction* and *adduction* describe movement around the vertical axis and parallel to the transverse plane (Neumann 2002). The applied terminology for the ankle incorporates all three motions. *Pronation* contains elements of eversion,

abduction, and dorsiflexion, while *supination* describes inversion, adduction, and plantar flexion (Neumann 2002).

The essential key to understanding injuries of the ankle is to understand the complex anatomy of the talocrural joint and the natural ranges of motion. The talocrural joint is also referred to as the ankle "mortise" after its similarities to a carpenter's mortise joint (Neumann 2002, Sarrafian 1983). The talocrural joint is formed by the articulation of the trochlear surface of the talus and the rectangular cavity formed by the tibial plafond and both malleoli (Hamilton 1984). In a complex hinge joint, such as the ankle the ligamentous anatomy also plays a vital role (Kelikian and Kelikian 1985, Trafton et al 1992). The medial collateral ligament (also referred to as the deltoid ligament) has both a superficial and a deep component. The superficial portion runs from the medial malleolus of the tibia to the calcaneus (tibiocalacaneal fibers) and to the navicular (tibionavicular fibers) (Neumann 2002, Trafton et al 1992). However, the superficial deltoid ligament does little to stabilize the ankle its self (Trafton et al 1992). The deep portion of the deltoid ligament run from the medial malleolus directly across to the talus (tibiotalar fibers) and provide stability for the medial aspect of the ankle (Hamilton 1984, Neumann 2002, Trafton et al 1992). Sprains and injury to the deltoid ligament are fairly uncommon, due to the strength of the ligament, along with the fact that the lateral malleolus blocks excessive eversion (Neumann 2002).

The lateral collateral ligaments of the ankle include the calconeofibular ligament, the anterior talofibular ligament, and the posterior talofibular ligament

(Hamilton 1984, Neumann 2002, Trafton et al 1992). The anterior talofibular ligament attaches to the lateral malleolus and runs medially to the neck of the talus (Trafton et al 1992). The posterior talofibular ligament runs from the lateral malleolus and attaches to the lateral tubercle of the talus (Neumann 2002). The calconeofibular ligament runs from the apex of the lateral malleolus to the lateral aspect of the calcaneus (Newman 2002). The majority of ankle sprains involve excessive inversion, and injury to the lateral collateral ligaments (Fallat et al 1998, Neumann 2002).

The most significant ligamentous complex of the ankle that is responsible for most of the structural integrity, are referred to as the inferior tibiofibular syndesmosis (Trafton et al 1992). The five components of the syndesmosis work to unite the distal tibia and fibula and prevent lateral displacement of the fibula (Trafton et al 1992).

The average axis of motion for the talocrural joint lies 8 degrees to the transverse plane, and 20 to 30 degrees from the frontal plane (Frankel and Nordin 1989, Inman 1976) This allows for a range of 10 to 20 degrees of dorsiflexion and 50 degrees of plantar flexion at the talocrural joint (Neumann 2002).

Lower Extremity and Ankle Injury Classifications

Malleolar fractures are the most common serious fracture of the lower extremity (Daly et al 1987, Trafton et al 1992). Malleolar fractures are most commonly produced by tensile and shearing forces transmitted through the talus

(Trafton et al 1992). Several systems have been devised in order to characterize ankle injury and to provide an understanding of injury patterns in regards to the mechanisms that caused them. Two of the most common systems used are the Lauge-Hansen and the Danis-Weber (AO) classifications.

Lauge-Hansen Classification System

The Lauge-Hansen system of ankle classifications was derived in the 1940's from cadaveric testing (Lauge-Hansen 1950). The studies produced injury through quasi-static mechanisms, instead of more dynamic impact testing (Lauge-Hansen 1950, Madeley et al 2004). The system categorizes ankle fractures based on the position of the foot and the forces acting on it at the time of injury. The position of the foot is noted first (i.e., supination or pronation) followed by a descriptor of the deforming force (i.e., abduction or external rotation). The severity of the resultant injury is governed by the amount of force applied. In its most widely used form there are four classes of fracture:

Supination-adduction class

Stage I - Transverse fracture of lateral malleolus

Stage II - Steep oblique fracture of medial malleolus

Supination-external rotation class

Stage I - Rupture of anterior tibiofibular ligaments

Stage II - Spiral fracture of distal fibula

Stage III - Disruption of posterior tibiofibular ligaments with or without avulsion of the posterior malleolus

Stage IV - Oblique fracture of medial malleolus

Pronation-abduction class

Stage I - Transverse fracture of medial malleolus or torn deltoid ligament

Stage II - Disruption of posterior and anterior tibiofibular ligaments with or without avulsion of posterior malleolus

Stage III - Oblique fracture of distal fibula

Pronation-external rotation class

Stage I - Transverse fracture of medial malleolus or torn deltoid ligament

Stage II - Disruption of anterior tibiofibular ligament complex and interosseous membrane

Stage III - High fracture of fibula (above the joint)

Stage IV - Disruption of posterior tibiofibular ligament with or without avulsion of posterior malleolus

Supination-Adduction Class

Adduction of a foot that is supinated (or inverted) causing weight on the lateral aspect is one of the most common mechanisms of injury to the ankle (Neumann 2002, Trafton et al 1992). The lateral side is in tension, and this is

usually where the failure occurs. The failure first occurs with the lateral collateral ligaments, but can lead into the avulsion of the lateral malleolus (Trafton et al 1992). The medial malleolus can also fracture if the talus is pushed medially into the malleolus (Trafton et al 1992) (Figure 5.1)

Supination-External Rotation Class

External rotation of a foot that is supinated is the cause of 40% to 75% of malleolar fractures (Hamilton 1984). Failure begins with a spiral oblique fracture of the lateral malleolus. If the force continues, the fibula is pushed medially into the tibia, creating failure at the distal end and possible avulsion of the medial malleolus (Trafton et al 1992) (Figure 5.2).

Pronation-Abduction Class

In the Pronation-abduction injury, the first area of failure is the deltoid ligament with possible avulsion of the medial malleolus. The tibia can then be pushed further to the lateral aspect and result in a bending fracture of the lateral malleolus (Trafton et al 1992) (Figure 5.3).

Pronation-External Rotation Class

The first stage of a pronation-external rotation injury is a failure on the medial aspect of the ankle of either the deltoid ligament or the malleolus. Following that, there can be a spiral fracture of the fibula, often followed by a fracture to the plafond (Trafton et al 1992) (Figure 5.4).

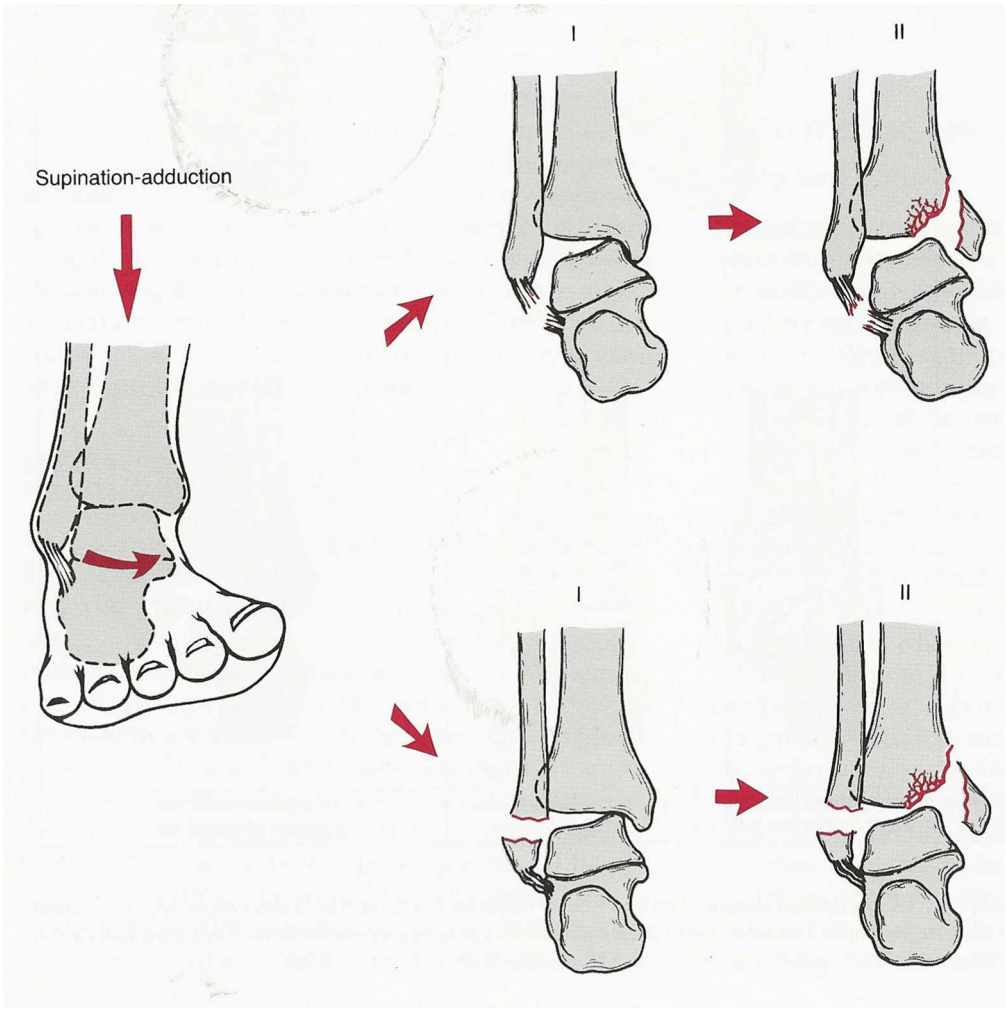

Figure 5.1 Injury mechanics for supination-adduction injury. From Trafton et al 1992.

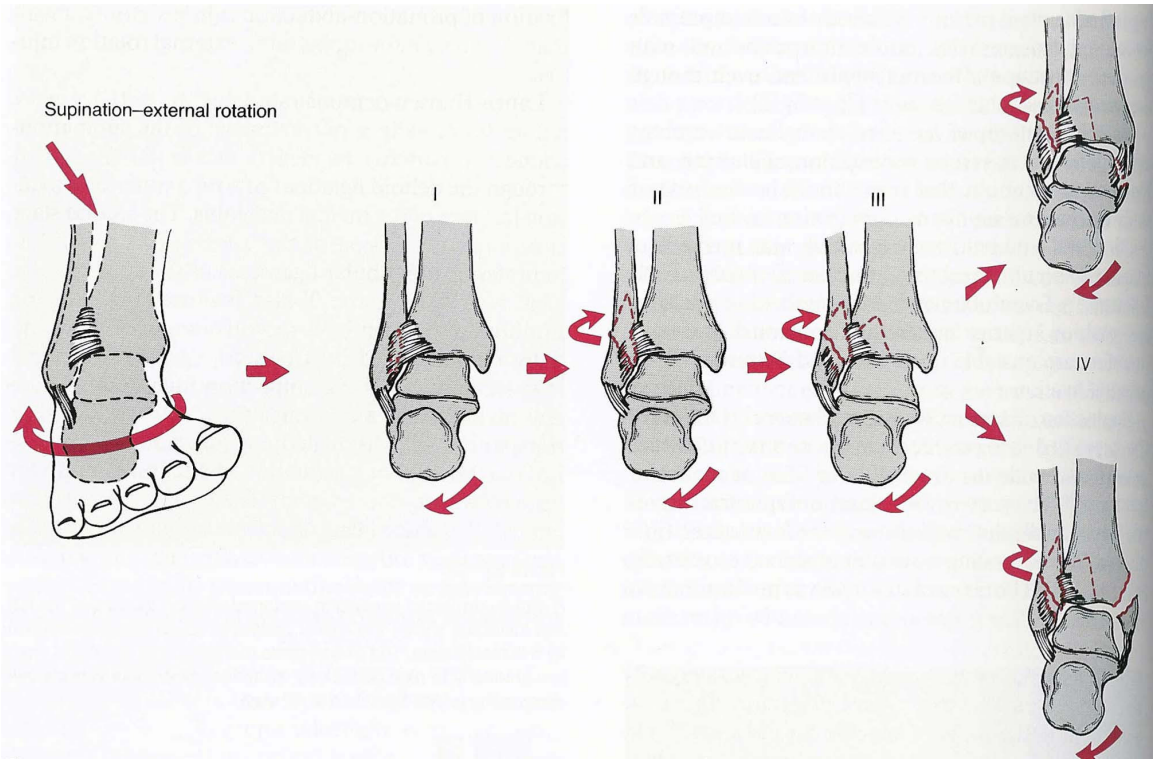

Figure 5.2 Injury mechanics behind supination-external rotation. From Trafton et al 1992.

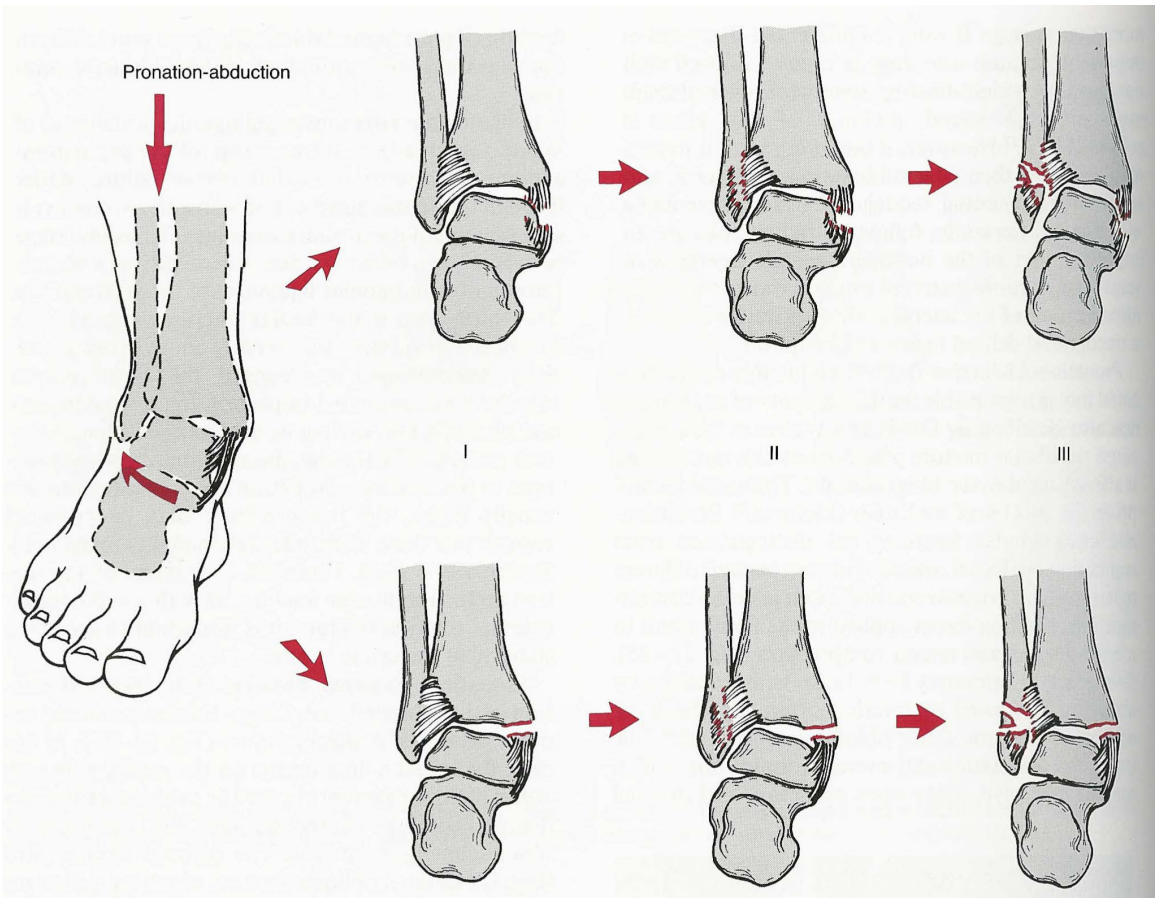

Figure 5.3 Injury mechanism for pronation-abduction. From Trafton et al 1992.

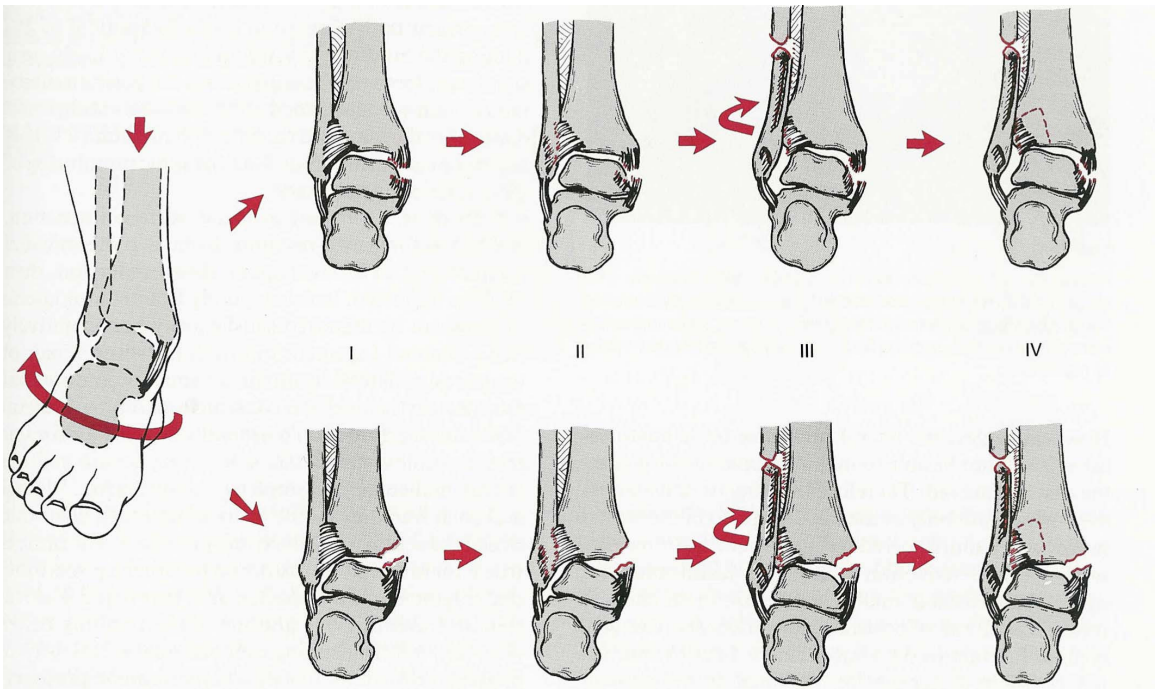

Figure 5.4 Injury mechanics for pronation-external rotation injury. From Trafton et al 1992.

Problems with Lauge-Hansen

However, some researchers have found several areas of weakness in dealing with the Lauge-Hansen system of ankle fracture classification. A study by Madeley et al in which ankles were experimentally fractured and then given to a group of Orthopedic specialists for analysis of injury mechanism, showed that their may not be one signature fracture pattern for every mechanism of injury (2004). This suggests that the Lauge-Hansen system of classification can not always accurately describe fractures resulting from impacts (Madeley et al 2004).

Danis Weber Classification System

Another classification system is the Danis-Weber system. This system is based on the level of the fracture of the fibula (Trafton et al 1992). There is a greater risk of injury to the syndesmosis the more proximal the fracture to the fibula, often making the joint unstable. In this classification system there are three types of fractures: A, B, or C.

Type A fractures consist of fracture of the fibula below the level of the tibial plafond. The foot supinates causing this avulsion fracture. It is also possible for there to be an oblique or vertical fracture of the medial malleolus if the force continues. In the Weber system, the type A fracture corresponds to the supination-adduction injury of the Lauge-Hansen system.

External rotation causes an oblique or spiral fracture, which is a type B injury. The fracture begins near or at the level of syndesmosis. It is possible to have an associated injury to the posterior malleolus and the medial side of the

ankle. In the Weber system, the type B fracture corresponds to the supination-eversion injury of the Lauge-Hansen system (Trafton et al 1992).

A fracture of the fibula above the syndesmosis is a type C fracture. There is a disruption of the syndesmosis, and usually there is an associated injury on the medial side of the ankle. Type C fractures in Weber's classification system are divided into two groups: fractures that involve the diaphysis of the fibula, and fractures that involve the proximal fibula (Maisonneuve type) (Trafton et al 1992). The Lauge-Hansen classification that corresponds to the Weber "C' is pronation eversion or pronation abduction.

The AO classification further divides the Danis-Weber system into three groups per type. The AO classification of malleolar fractures is described below:

Type A: Fibular Fracture Below Syndesmosis

A1 – isolated

A2 – with fracture of the medial malleolus

A3 – with postmedial fracture

Type B: Fibula Fracture at the Level of Syndesmosis

B1 – isolated

B2 – with medial lesion (malleolus or ligament)

B3 – with a medial lesion and fracture of the posterolateral tibia

Type C: Fibula Fracture Above Syndesmosis

C1 – diaphyseal fracture of the fibula simple

C2 – diaphyseal fracture of the fibula complex

C3 – proximal fracture of the fibula

Other relevant mechanisms of injury

Axial Loading

Axial loading is also a common injury mechanism to the lower leg (Trafton et al 1992). Axial loading of the ankle causes the talus to be forced upwards into the tibial plafond causing fracture. The tibial plafond can become comminuted from the force. In these instances, fractures of the fibula can often be secondary. Figure 5.5 demonstrates fractures resulting from axial load to the ankle in an individual who jumped from a trailer and landed on both feet. Axial loading can also be seen in the foot, when the calcanous is pushed in a superior direction causing fractures. Figure 5.6 demonstrates axial load fractures to the foot from a jump from a second story of a building. When an axial load is applied to the knee, fractures are common of the tibial plateau (Trafton et al 1992). Figure 5.7 shows a personal watercraft (PWC) operator with a depressed lateral tibial plateau fracture.

Figure 5.5 Fractures to the ankle from an axial load.

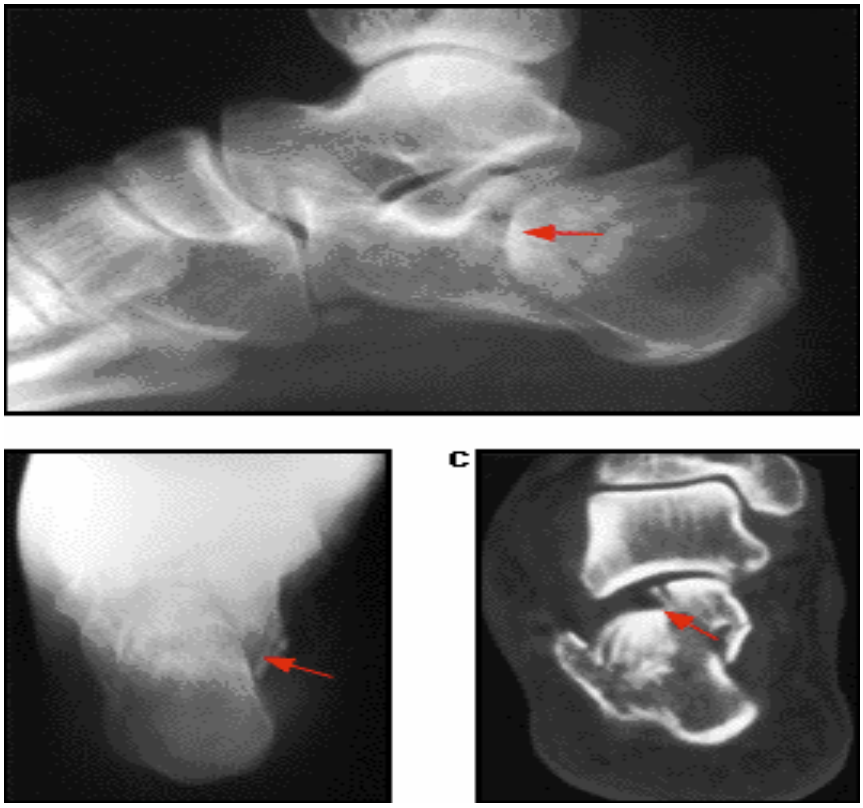

Figure 5.6 Fractures to the foot from an axial load.

Figure 5.7 Fractures to the knee from an axial load.

Torsional loading

Fracture from Torsional loading can occur from entrapment to the foot or distal portion of the leg. The most common fracture produced from Torsional loading is a spiral fracture, which can occur in either the tibia or fibula (Rockwood et al 1996). Figure 5.8 shows spiral fractures of both the tibia and fibula.

Bending Mechanism

Fracture from a bending mechanism can occur from inertial effects, or an impact with a structure (Kress 1996). An area of tension is created in the long bone on the side opposite from impact. Bone is much weaker in tension than in compression, so the first area of failure begins on the side of the tension (Porta 1996). The fracture then travels back towards the area of compression creating a wedge or "butterfly fracture". This fracture pattern can be used in forensic anthropology to determine the areas of tension and compression in a fractured bone, either from bending due to a direct impact, or bending of the overall bone. A common example is often seen in pedestrians impacted by motor vehicles. A wedge fracture often occurs in the tibia corresponding to the area of direct interface between the lower limb and the bumper, with the area of tension occurring on the side opposite from the impact (Kroman and Symes 2002).

However, the bone does not need to be weight bearing (i.e., standing on the leg) for a butterfly/wedge fracture to occur (Kroman and Symes 2002, Porta 1996). Wedge type fractures are common in ribs as well as the long bones of the upper extremity.

Figure 5.8 Sprial fracture from torsional loading.

Personal Watercraft Injury Study

Introduction

Personal watercraft (PWC) are populating the waterways of North America with increasing numbers. A "cross between a motorboat and a motorcycle", personal watercrafts are most commonly known by their trade names of Sea-Doo®, JET SKI®, WaveRunner®, and AquaTrax® (Tyler and Garrison 1997). The National Marine Manufactures Association calculated that there were 1.48 million PWCs in use in 2004 (NMMA Recreational Boating Statistical Abstract 2004). Part of the appeal of such crafts, is their low cost, with an average price of $9,226, and their ability to travel speeds up to 70 mph (NMMA Recreational Boating Statistical Abstract 2004). As one PWC retailer succinctly stated "You would have to spend at least $35,000 to $40,000 for a boat to go that fast. Personal watercraft is a cheap way to go fast" (Whitman 1996). As with any activity where speed is mixed with varying levels of operator experience, accidents and injuries are inevitable.

The use environment of PWC includes a wide range of variables. Operators are required to sit, stand, or kneel depending of make and model of the watercraft. They are also faced with a wide range of weather, water, visibility levels, and water traffic levels as well as many other obstacles. Also, similar to all watercraft there are no breaks on a PWC. Stopping is achieved by cutting the throttle and coasting to a stop. However, with out the propulsion from the jets, the operator has no steering mechanism to avoid an obstacle. All of these

factors hamper the ability to simply characterize all the possible accident scenarios and resulting injuries.

With the increased popularity of PWC, there has been a large amount of concern regarding the injury rates and severity (White and Cheatham 1999). A study by Branche et al found that rate of hospital treated injuries was 8.5 times higher for PWC riders and operators than for any injuries from a motorboat (1997). Unlike other watercraft and boats where the leading cause of fatalities is drowning, blunt trauma is responsible for most deaths related to PWC use (Committee on Injury and Poison Prevention 2000).

While attempts to assess the most common causes of injuries from PWC has lead to varied results (Haan et al 2002), the lower extremity appears to be one area that is commonly injured (Branche et al 1997, Jones 1997). These injuries can arise from falls from the craft, direct impact, or collision. Jones found that a common cause behind skeletal injury, especially the lower limb, was from a large axial load from inexperienced operators jumping wakes (Jones 1997). The National Electronic Injury Surveillance System (NEISS) was developed in 1971 by the Consumer Product Safety Commission (CPSC) to record product related injuries (Branche et al 1997). A query of PWC reported injuries from NEISS for the years 1989 – 1992 lists that 36.2% of the injuries involved the lower leg (Figure 5.9).

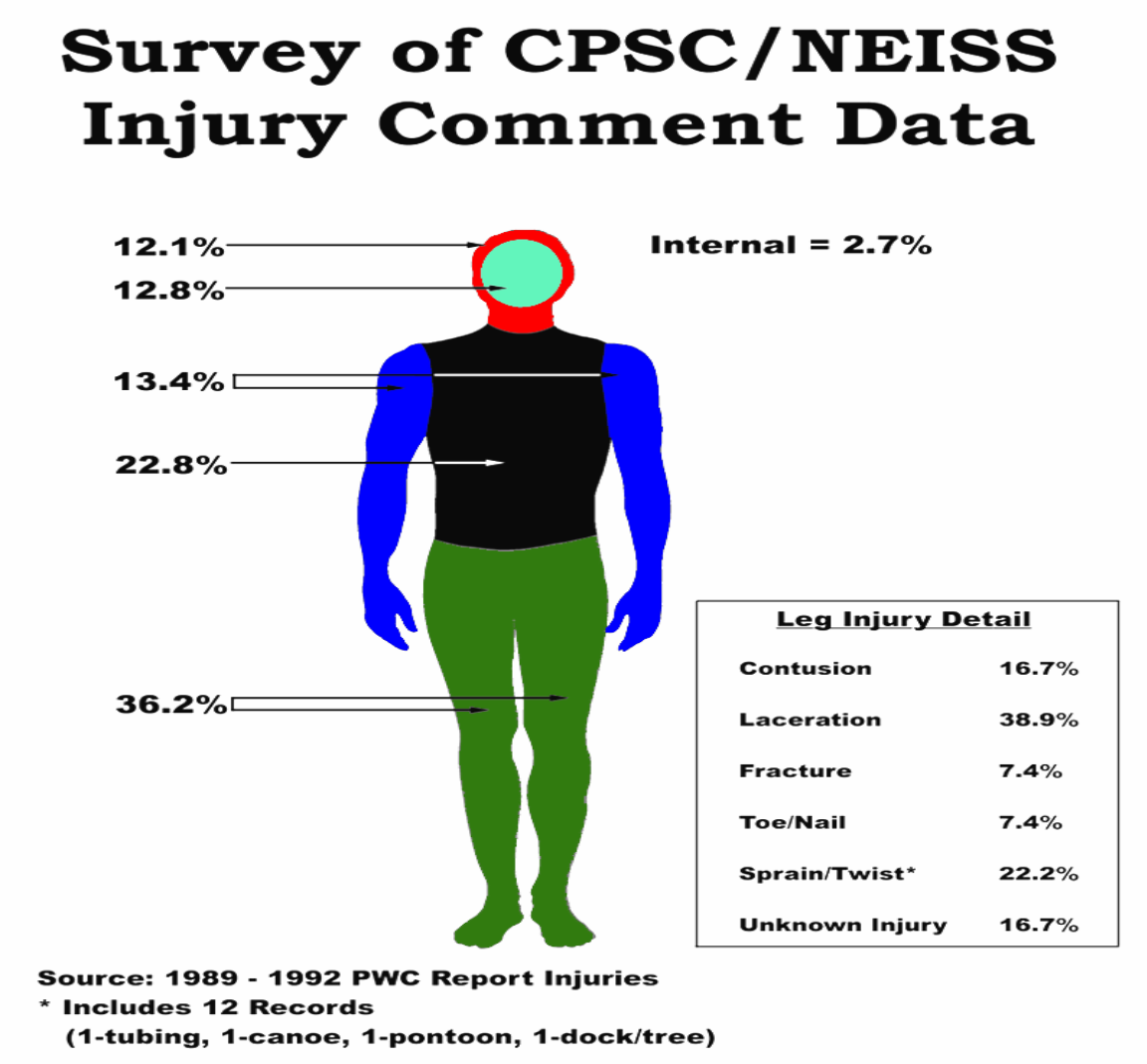

Figure 5.9 Injury data from PWC from 1989 to 1992.

PWC accident injuries and 38.1% non-collision PWC accident injuries involve the lower limb (Figure 5.10). A study conducted by the National Transportation Safety Board (NTSB) report states that approximately one-third of PWC injuries involve the lower leg, including the foot and ankle (Figure 5.11) (NTSB 1998). The results of these three studies indicate that the lower limb has a relatively high frequency of being injured in PWC accidents. Despite this fact, literature containing detailed reports of lower limb injury from PWC use is scarce.

The purpose of this study was two fold. The first goal was to examine accident and injury data from a series of PWC accidents to try and understand the mechanisms behind the lower limb injuries seen as the result of PWC related sports activities. The second component involved a comparison of the types of fractures, mechanisms, and frequencies of PWC lower limb injuries to other sports activities (skiing, skiboarding, soccer, etc.) to determine if the injuries seen were unique to PWC accidents.

Materials and Methods

Twenty eight real PWC cases involving the lower limb were included in this study. Case synopses were generated and can be read in Appendix C. Most of the case files contained medical records and X-rays of the injury (shown in Appendix C, Figures C.1 – C.27). From provided data an accident scenario was constructed. The nature and location of each injury was recorded, and all of the cases involving ankle fractures were characterized based on both the Lauge-Hansen and A-O systems of classifications discussed earlier.

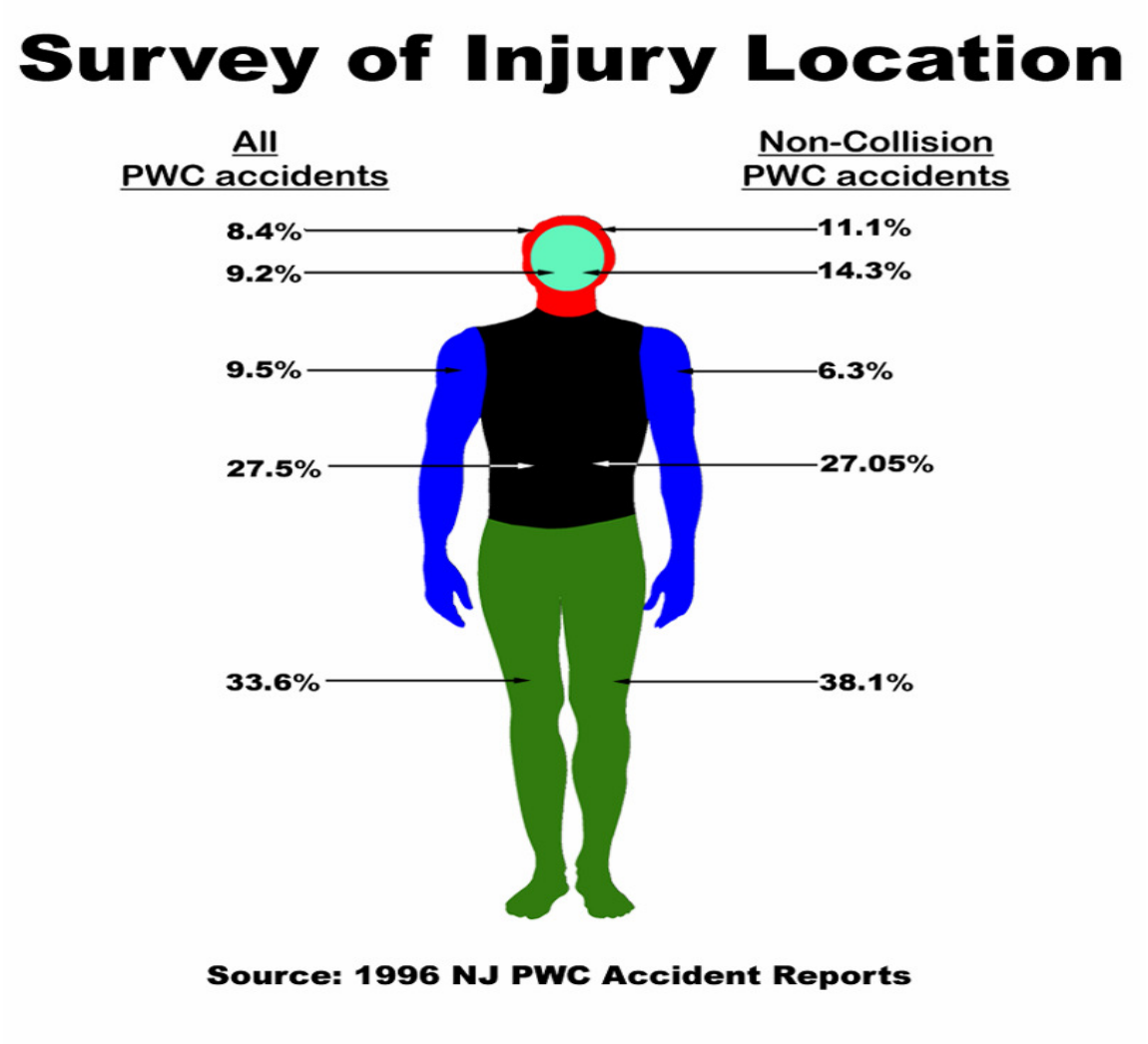

Figure 5.10 Breakdown of PWC injury location.

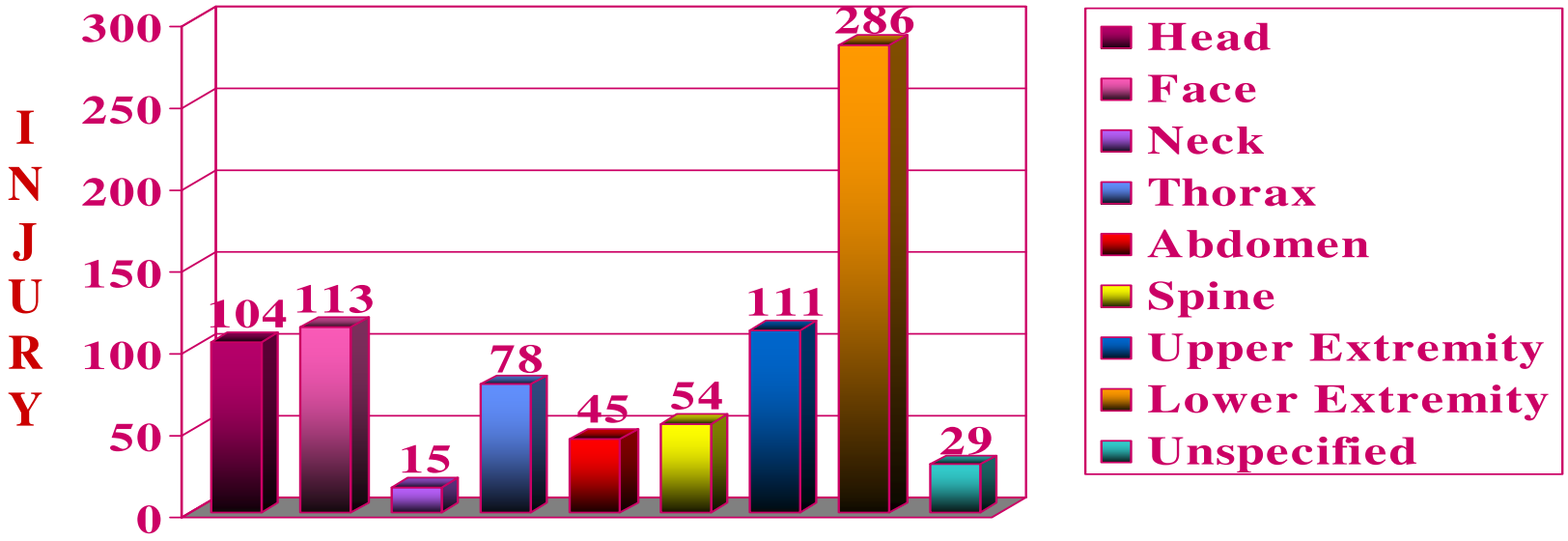

Figure 5.11 1998 NTSB Injury data for PWC accidents.

Fracture morphology was also examined to determine the mechanism of injury that caused the fracture.

In addition to the analysis of the twenty eight case studies, an extensive literature search was conducted to learn about patterns and mechanisms of injury to the lower limb in other sports activities. Sports included in the comparison were skiing, ski boarding, and soccer. Fracture patterns were compared by mechanism and location to try and understand if that fractures seen in the PWC case studies were a phenomenon unique to the sport, or were analogous to other sports and everyday activities.

Results

The medical records and radiographs were examined for each case to determine the type and location of the fracture (or fractures), the Lauge-Hansen (L-H) and Danis-Weber (A-O) classifications, and the mechanism of injury. Table 5.1 shows the abbreviations used in the following tables and analysis. Table 5.2 shows a summary of the case that were included in this study, along with their assigned classifications and mechanisms of injury.

Mechanisms of Injury

The mechanisms of injury that were found to have occurred in the cases were external rotation, bending and axial loading (Table 5.3). One of the files involved an impact of which two riders (cases 1 and 2) injury mechanisms were the same, therefore for the purposes of tallying injury mechanisms, these were only counted as one. Sixteen of the injuries were found to be the result of ankle

Table 5.1 Abbreviations used in the following tables.

Abreviations used in "Abbreviated Description of Fracture" section		
ABBREVIATIONS		MEANINGS
dist	=	distal
ER	=	emergency room
fib	=	fibula
frags	=	fragments
fx	=	fracture
L	=	left
lat	=	lateral
mall	=	malleolus
med	=	medial
post	=	posterior
prox	=	proximal
R	=	right
thru	=	through
tib	=	tibia
trans	=	transverse
w/	=	with

Abbreviations used under "Malleolus" descriptions in place of x's		
ABBREVIATIONS		MEANINGS
(bi)	=	bimalleolar
l	=	lateral
lat		lateral
m	=	medial
p	=	posterior
post		posterior
tri. X	=	trimalleolar

Abbreviations used in heading		
ABBREVIATIONS		MEANINGS
L-H	=	Lauge-Hansen
AO	=	Weber/AO classification

Table 5.2 Case Summaries

File	Age	Sex	Abbreviated Description of Fracture	Ankle Fx Classifications		Comments
				L-H	AO	
1	18	F	fx L prox tib, fx thru ant prox tib at level of tib tubercle, oblique fx.			impact
2	6	F	comminuted open fx L tib & fib w/ 10cm lacer of lat mall.			
3	34	F	obliquely-oriented fx of L lat mall, displaced 1-2 mm	S-ER	B1.1	external rotation
4	38	M	fx extending from L mediolateral tibial plateau extending inferiorly, multiple comminuted osseous frags present, fx extends thru all cortices, tibial spine depressed 1cm, multiple frags depressed on the medial, avulsion of the tib spine w/ fx's into the lat side, fib head avulsed off.			axial
5	32	M	small chip fx of the post mall, avulsed frag of med mall, anteromedial subluxationof R tibiotalar joint, R tib shaft fx, fx mid dist fib	S-ER	B2.2	external rotation
6	26	F	fx's of R med mall & distal fib, nondisplaced fx of post mall, slight lateral subluxation of the talus, avulsed frag from med mall, comminuted fx mid distal fib	S-ER	B2.3	external rotation
7	38	F	depressed, comminuted displaced lateral tib plateau fx L knee, torn lateral meniscus (valgus strain)			bending
8	40	M	Acute spiral fx thru distal shaft L tib, mild displacement of distal fx frag in relation to prox shaft frag, acute comminuted fx mid shaft L fib, 7mm displacement			external rotation
9	32	M	spiral fx distal shaft L tib w/ lat & post displacement of the distal fx frags, comminuted fx prox shaft fib			external rotation
10	57	M	open L tib plateau fx& testicular trauma w/ fx L testicle, Comminuted fx prox 1/3 at tib extending into tib plateau			axial
11	Unknown	Unknown	oblique distal L fib fx, spiral	S-ER	B1.1	external rotation
12	24	M	comminuted fx L lat mall, thin fairly large post medial butterfly frag, spiral fx fib	S-ER	B1.1	external rotation

Table 5.2 Continued

File	Age	Sex	Abbreviated Description of Fracture	Ankle Fx Classifications		Comments
				L-H	AO	
13	16	M	Salter IV fx R distal tib, fx extends obliquely thru lat aspect of distal tib metaphysis & thru physis & epiphysis, some post & lat disp of fx frag, associated oblique disp fx of dist fib diaphysis			inertial bending
14	37	M	L trimalleolar fx, distal fib fx w/ deltoid rupture, fx of post tibia: Non-displaced -posterior lip (malleolus)	S-ER	B3.1	external rotation
15	35	M	trimalleolus fx/dislocation w/ post displacement of talus, displaced oblique fx post mall, non-displaced transverse fx med mall, oblique fx distal fib w/ lat displacement distally, fx fib, rupt syndes lig, fx tib	P-AB	C1.3	inertial bending
16	27	M	R trimalleolar fx/subluxation, transverse fx med mall, comminuted spiral fx distal fib, small linear bone density adjacent to the dorsal aspect of the talus, which may represent a small avulsion fracture.	S-ER	B2.2	external rotation
17	Unknown	Unknown	comminuted, spiral fracture of the R dist tib w/ associated fx fib			external rotation
18	33	M	L ankle, trans fx med mall w/ 3mm separation of frag, fx of fib prox to tib-fib syndesmosis, an un-displaced fx of post mall, ankle mortise asymmetrical w/ lat disp of talus, L un-displaced transverse fractures of the base of the 2nd, 3rd & 4th metatarsals	P-AB	C1.3	inertial bending
19	47	M	oblique fx thru distal shaft L fib, calcification in distribution of the post tib artery.			external rotation
20	49	M	comminuted spiral variant fx distal tib shaft extending inferiorly thru metaphysis & post mall, marked post displacement of distal segment, diastasis of post mall frag, comminuted fib neck fx in the near anatomic position & alignment.			external rotation
21	47	M	open bi-malleolar fx: trans fx med mall, comminuted fx lat mall; post tibialis tendon rupture, R ankle, angular deformity from pronation-abduction	S-ER	B2.3	inversion, bending

Table 5.2 Continued

File	Age	Sex	Abbreviated Description of Fracture	Ankle Fx Classifications		Comments
				L-H	AO	
22	28	M	oblique fx L post mall, transverse fx base of third metatarsal			inertial bending
23	24	M	transverse fx from direct impact; R patella			impact
24	41	M	oblique spiral fx fib	S-ER	B1.2	external rotation
25	35	M	comminuted laterally and posteriorly displaced spiral fx of mid shaft of left femur			external rotation
26	37	M	spiral fx R distal fib (ER records only, no x-rays available)	S-ER	B1.2	external rotation
27	29	M	L displaced fx of lat & post mall (no x-rays available)	S-ER	B2.3	external rotation
28	29	F	complete trans fx mid shaft R femur, lat displacement fx frag, 1cm area apposition involving lat cortex prox femur & med cortex distal fx frag (no x-rays available)			bending

Table 5.3 Results Quantified

Bones	Quantity	% of total
med	0	-
lat	2	7.4
post	2	7.4
med & post	2	7.4
lat & post	1	3.7
med & lat	1	3.7
tri	4	14.8
tibia	11	40.7
fibula	15	55.6
femur	2	7.4

Movement / Mechanism	Quantity	% of total
external rotation	16.0	59.3
impact	2.0	7.4
pure bend	3.0	11.1
inert bend	4.0	14.8
axial	2.0	7.4

Malleolar fx's	Quantity	% type mall
singular mall	4	33.3
bi mall	4	33.3
tri mall	4	33.3
total mall	12	

Fx's of ankle	Quantity	% ankle fx
# external rotation	10.0	71.4
# inert bend	3.0	21.4
# pure bend (inversion)	1.0	7.1
total	14	

rotation (59.3%). In each of these cases, the dynamic force acting on the foot was external rotation. Case 16 is a good illustration of an external rotation injury (Figure 5.12). There is a right trimalleolar fracture, a transverse fracture of the medial malleolus, a comminuted spiral fracture of the distal fibula. A small linear bone density is also visible, adjacent to the dorsal aspect of the talus, which may represent a small avulsion fracture. The PWC operator reported that he had been having trouble making turns all day, and was practicing making sharp turns, when he flew off of the PWC. The fracture corresponds to the Lauge-Hansen classification of a Supination-external rotation injury, and an A-O classification of B2.2.

Nine of the injuries resulted from a bending mechanism, which also includes impact and inertial bending (33.3% of cases). Case 2 shows a fracture to the tibia and fibula caused by a bending moment resulting from an impact (Figure 5.13). This 6 year old female was a passenger on a PWC that was struck in the side by another PWC.

Two additional cases had an identified mechanism of axial loading (7.4% of cases). Case 10 shows an example of fractures resulting from axial loads (Figure 5.14). The operator of the PWC hit a wake and was thrown upwards as the PWC tilted vertical. He landed back down on the craft and had a fracture to the left tibial plateau, along with a loss of the left testicle.

In summary, of the twenty-seven files, sixteen are external rotation injuries. In other words, 59.26% of the injuries are the result of an external rotation movement of the foot. In other words, these were "rotational" injuries in

Figure 5.12 Radiographs from case 16 illustrating fractures from an external rotation injury.

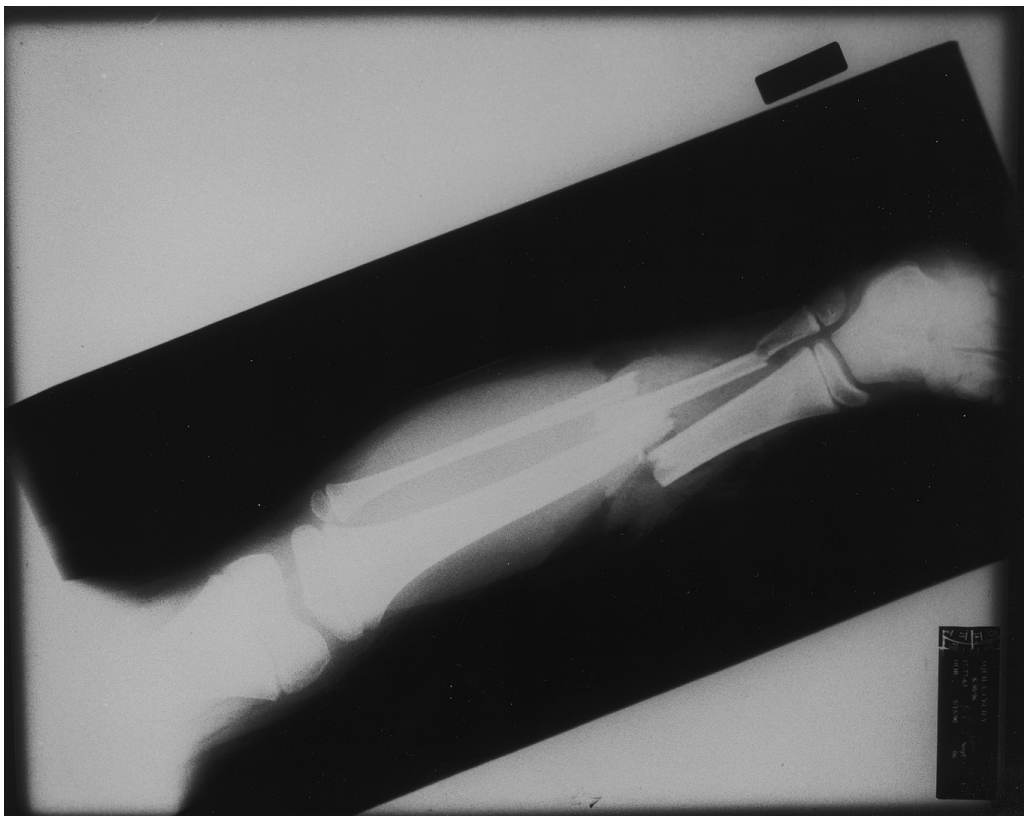

Figure 5.13 Radiograph showing fractures resulting from a bending mechanism.

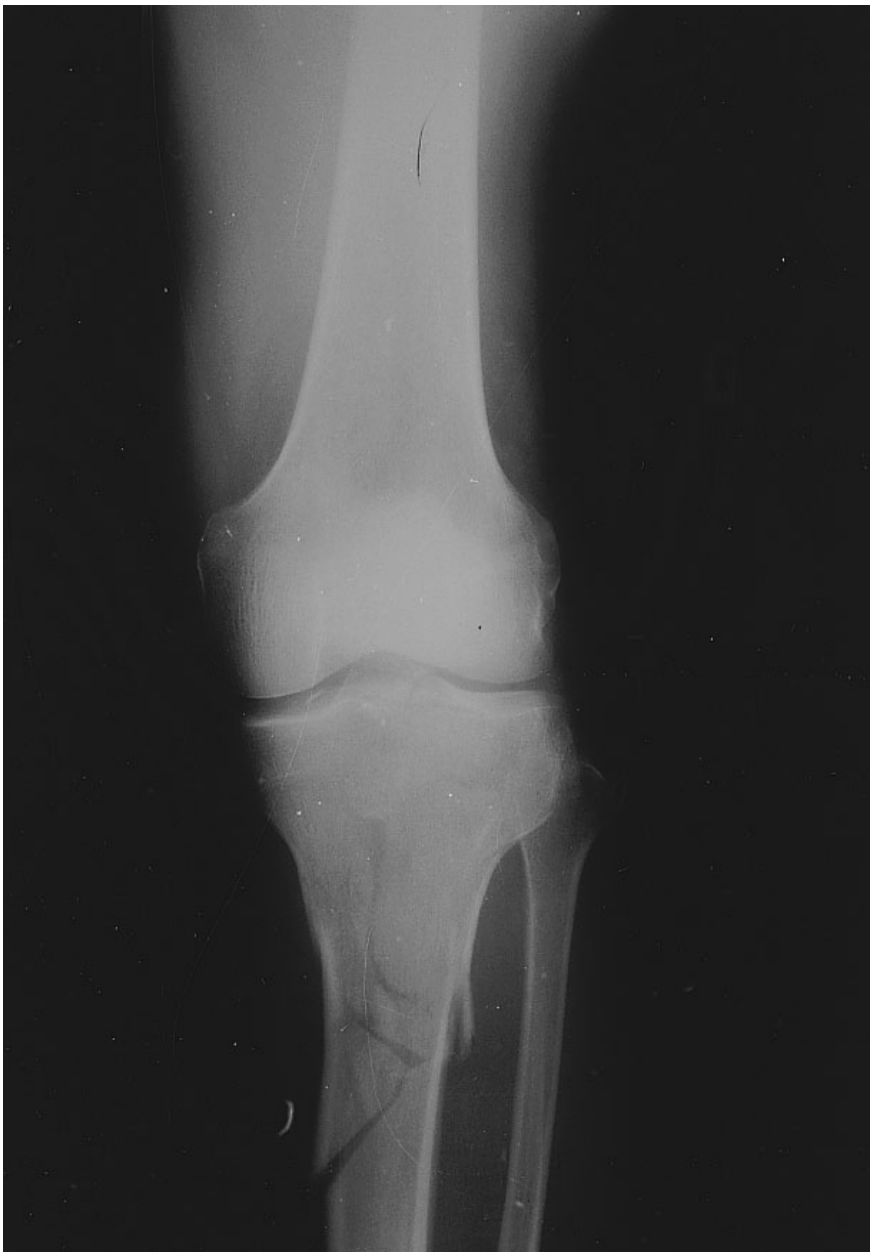

Figure 5.14 Radiograph showing
fracture from an axial load.

the sense that the foot rotated relative to the Tibia-fibula which is most commonly caused by the foot being out of the axial alignment at the time that the force was applied. These are classical injuries that occur in many sports, like tennis and basketball, or even stepping off a curb. These are not unique injuries and they are quite common in the American population. Also, nine out of twenty-seven, or 33.33% are due to one of the bending mechanisms including impact and inertial bending. The 33.33% of injuries due to a bending mechanism is broken up into 11.11% pure bending, 7.41% impact, and 14.81% inertial bending. There does not appear to be any association between the bending injuries and any particular size or shape of footwell. That leaves two of the twenty-seven, or 7.41% caused by an axial mechanism.

Location of injury

The fractures were all charted on diagrams in order to see if there was any pattern or consistency in the location of the trauma. The majority of the fractures involved the tibia and fibula. There were only two fractures of the femur and two fractures affecting the foot. The location of the fractures from each case were traced on a diagram in there anatomical location. This aided in visualization of the most common fracture patterns (Figures 5.15, 5.16, 5.17, 5.18, and 5.19). The most common skeletal element to be fractured was the fibula (55.6% of fractures), followed by the tibia (40.7%) of the fractures. Fractures to the femur and bones of the foot account for the other 7.4%. The results were also quantified by calculating the rate of fracture for the proximal end, the diaphysis,

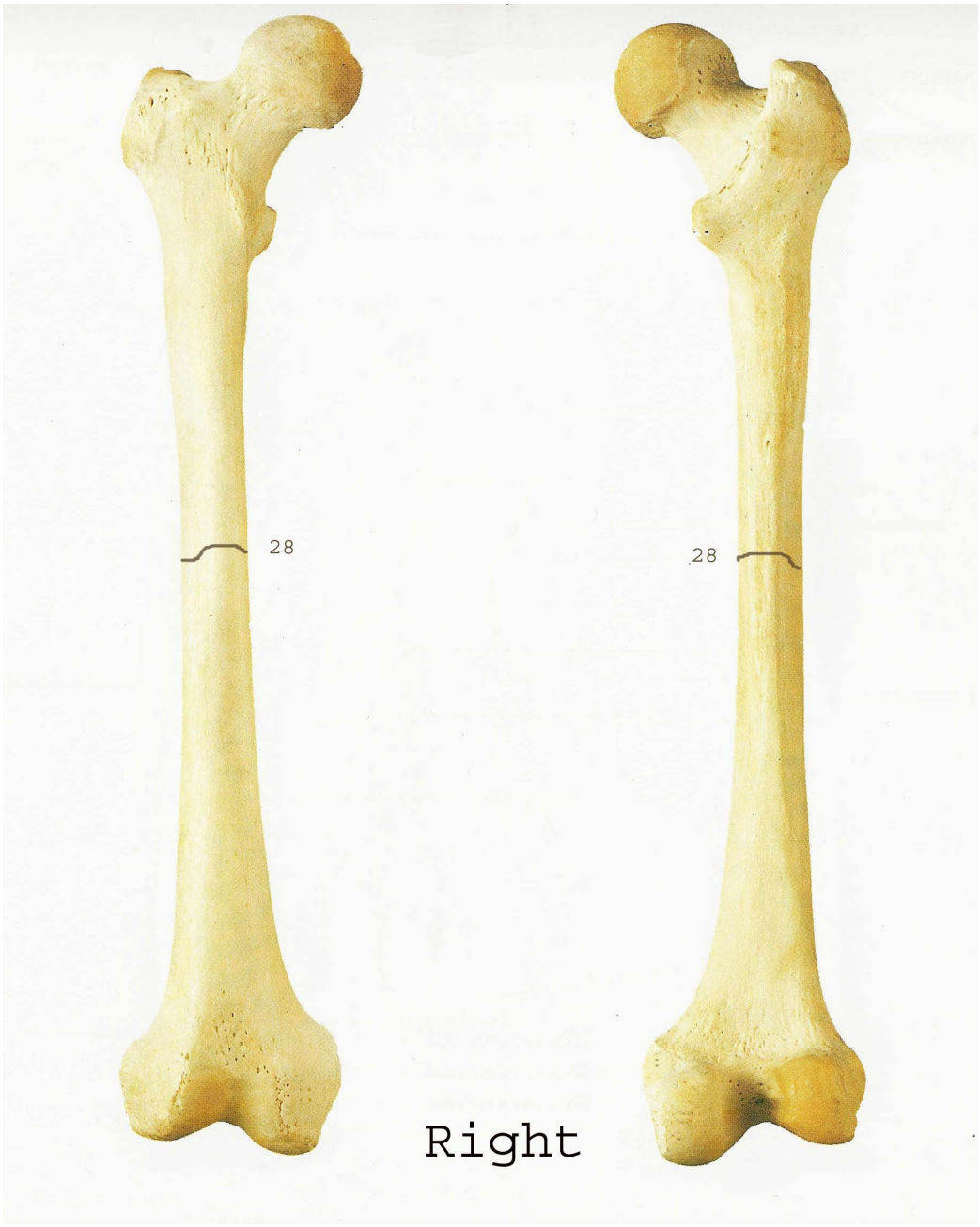

Figure 5.15 Locations of all PWC fractures involving the right femur.

Figure 5.16 Locations of all PWC fractures involving the left femur.

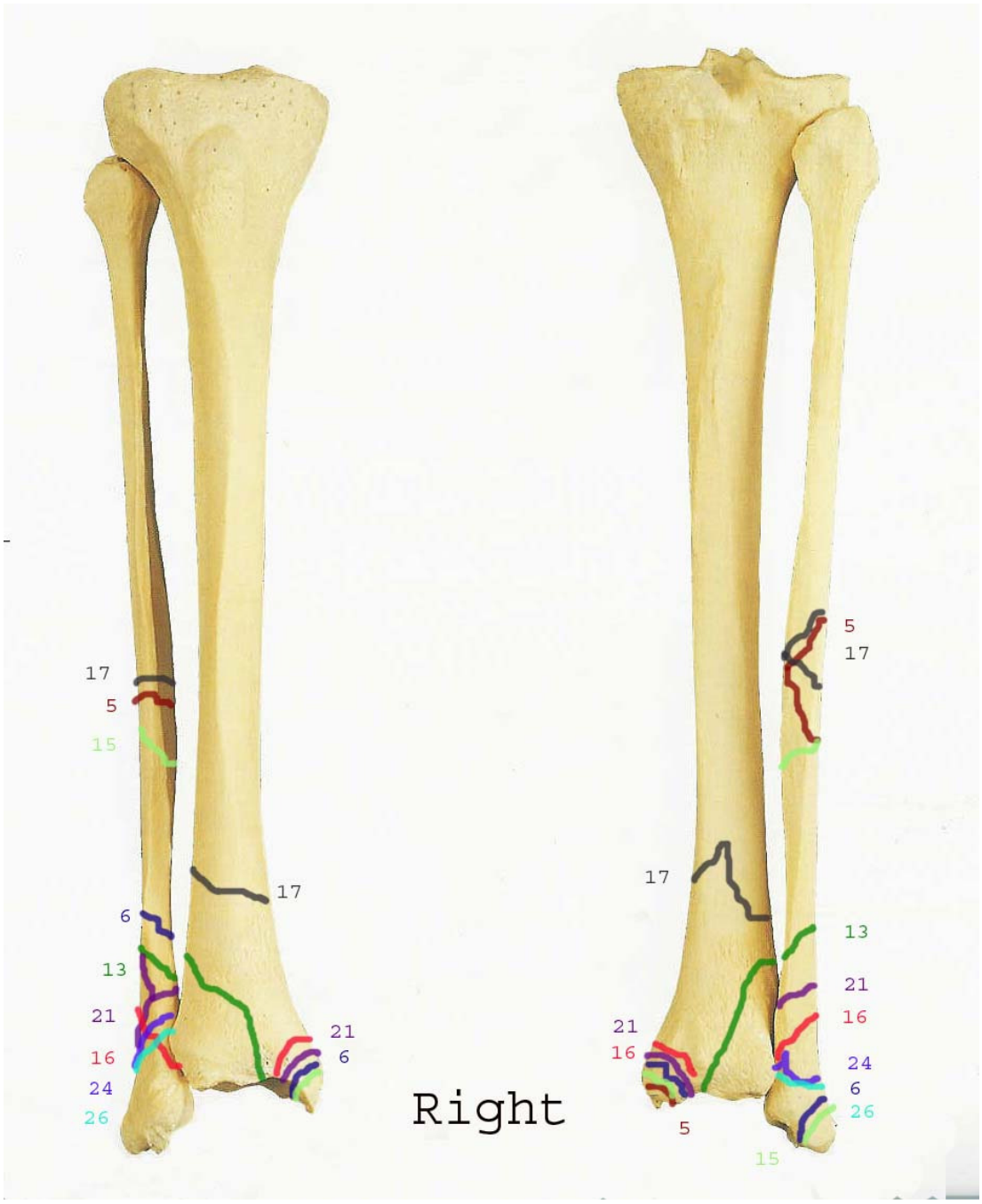

Figure 5.17 Locations of all PWC fractures involving the right tibia and fibula.

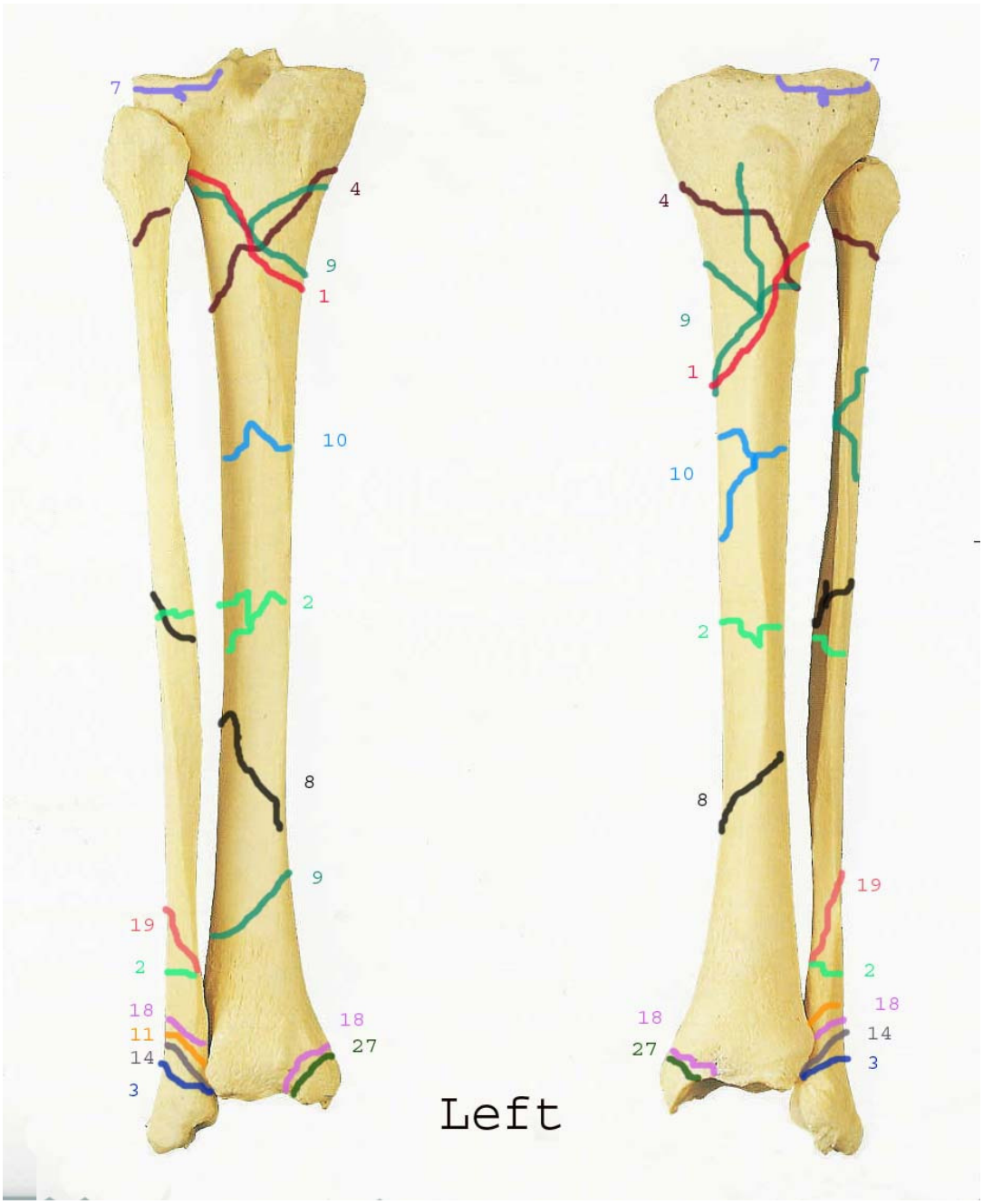

Figure 5.18 Locations of all PWC fractures involving the left tibia and fibula.

Figure 5.19 Location of all PWC fractures involving the left foot.

and the distal end for each long bone. Of the fractures affecting the tibia, 57.9% of the fractures occur at the distal end, 15.8% in the diaphysis, and 26.3% in the proximal end (Figure 5.20). In the fibula, 78.3% involve the distal end, 13.0% are located in the shaft, and 8.7% occur at the proximal end (Figure 5.20). 100% of the femur fractures occur in the midshaft region (Figure 5.21). Overall, the area to receive the most injury was the distal fibula, followed by the distal tibia. Of the twelve fractures to the ankle region involving the malleoli, four involved fracture to a single malleolus (33.3%), four involved a bi-malleolar fracture (33.3%), and four involved a tri-malleolar fracture (33.3%)

Comparison to other activities

Annually, it is estimated that seven million Americans receive medical attention for recreational or sports related injuries (Conn et al 2003). In the American public, males are also two times more likely to get injured than females (Conn et al 2003). Of the injuries surveyed, there were 464,000 lower limb fractures, which comprised 16% of all lower limb injury (Conn et al 2003). In a one year study of sports related fractures by Hon and Kock, 61% of fractures occurred in competitive sports and 39% occurred in recreational sporting activities (2001). Of the 61% of fractures from competitive sports, an overwhelming 98.6% of these fractures occurred in amateur players (Hon and Kock 2001). Of the activities, football had the highest percentage of injury (58.5%), and fractures from PWC use only contributed to 2% of the total (Hon and Kock 2001).

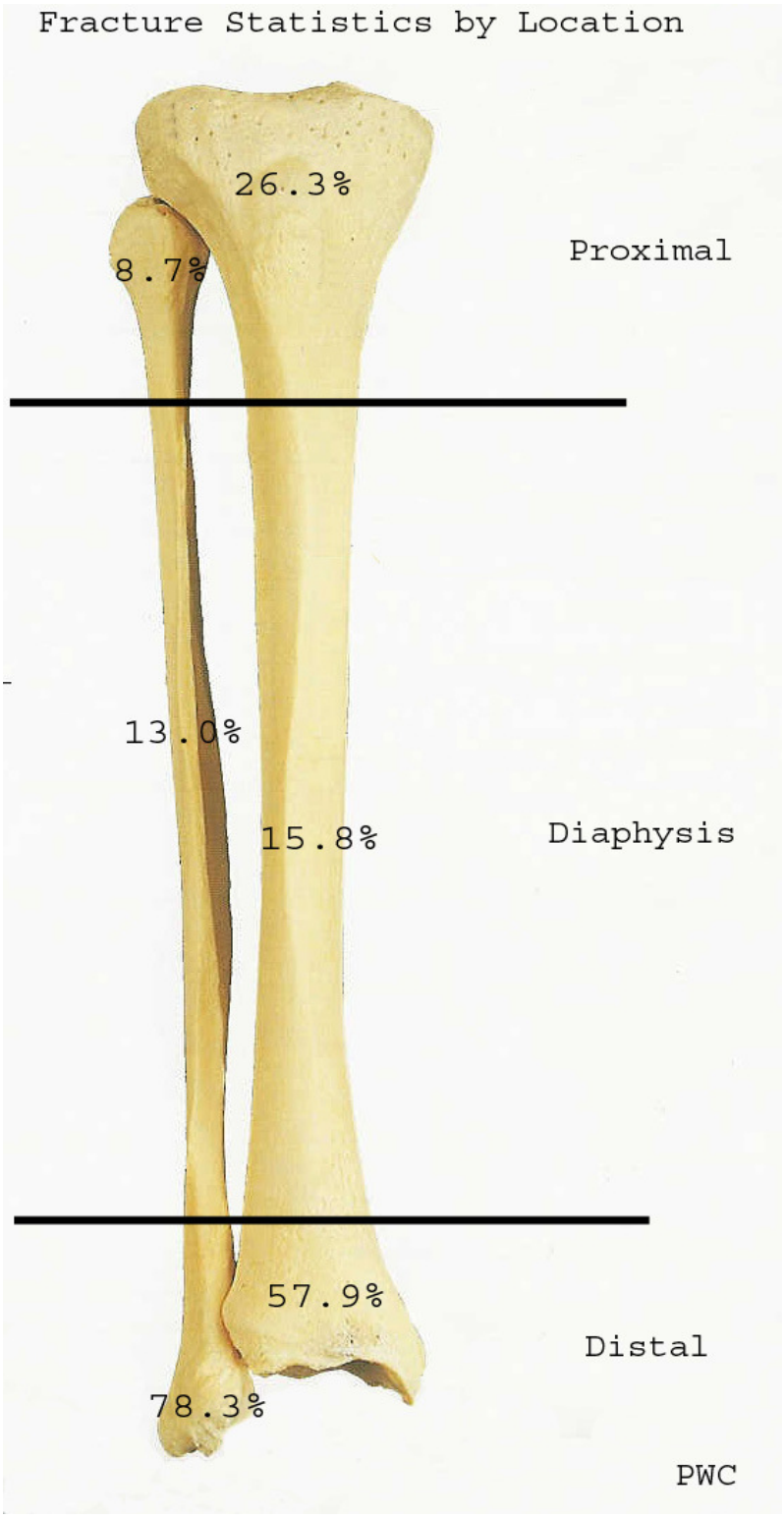

Figure 5.20 Locations of PWC fractures to the tibia and fibula.

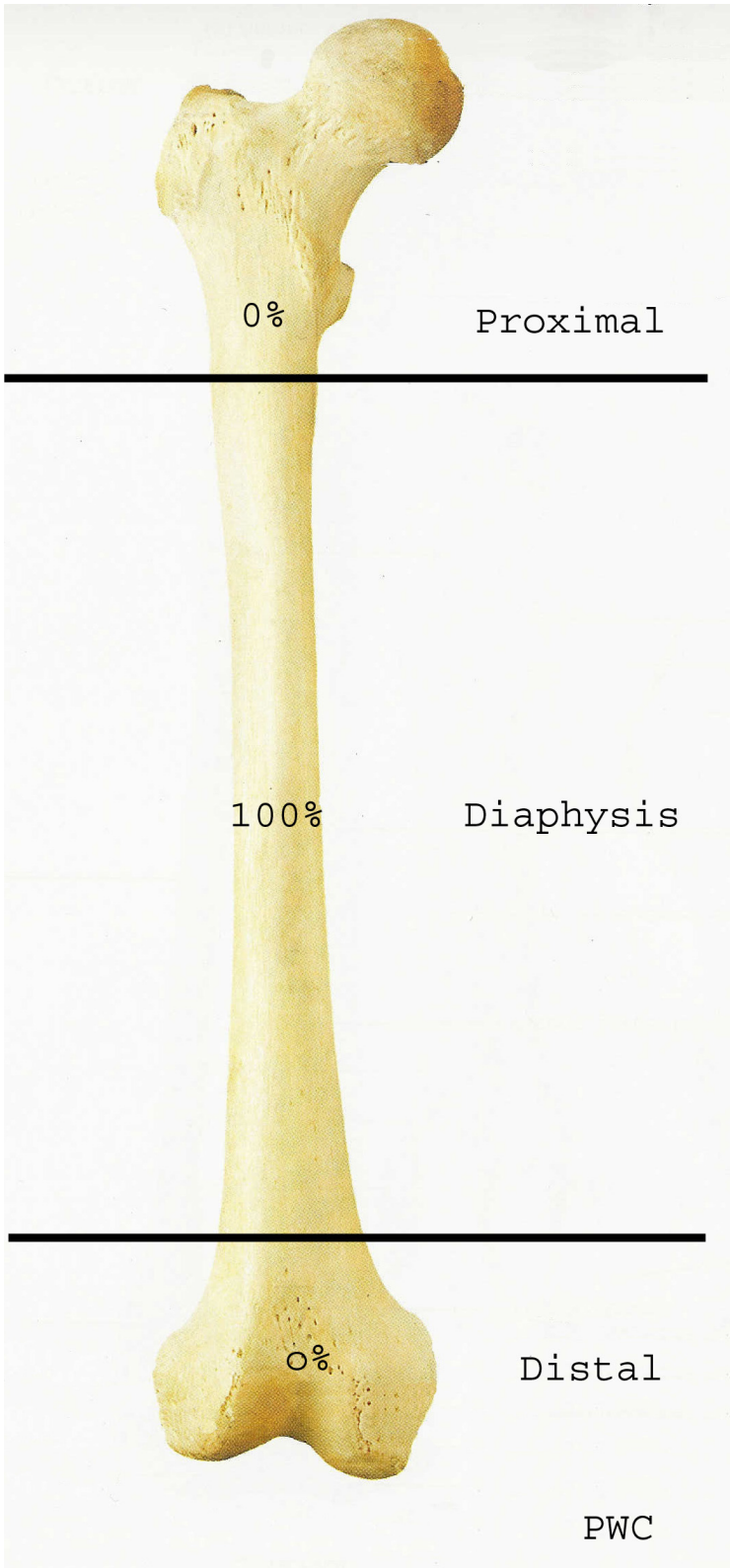

Figure 5.21 Locations of PWC fractures to the femur.

A comparison was made between sports in regards to the locations of injuries in the lower limb. As mentioned earlier, the majority of fractures to the tibia and fibula from PWC use occurred in the distal region (57.9% for the tibia and 78.3% for the fibula). Similar results were found in a study of fractures to the lower limb in soccer, with 74% of fracture occurring in the distal region (Boden et al 1999). Fractures of the distal tibia were also common among skiboarders, however with a slightly lower frequency than PWC use or soccer with 46.2% of skiboarding fractures occurring in the distal tibia and 53.8% occurring in the shaft or proximal region (Johnson et al 2003). Figures 5.22 and 5.23 show the side by side comparisons between these statistics.

In severe ankle injuries, it is common to see a fracture in both the tibia and the fibula, especially in injuries involving external rotation. In PWC cases, both the tibia and fibula were fractured 44% of the time. Fractures were isolated to the tibia 17% of the time. The fibula appeared to be more susceptible to fracture as compared to the tibia, with isolated fibular fractures were seen 39% of the time. The results from reported soccer injuries, showed that both the tibia and fibula were fractured together 48% of the time, similar to PWC use (Boden et al 1999). However, the soccer data showed that the isolated tibial fractures occurred at a higher rate (36%) than isolated fibular fracture (16%) (Boden et al 1999) (Figure 5.24).

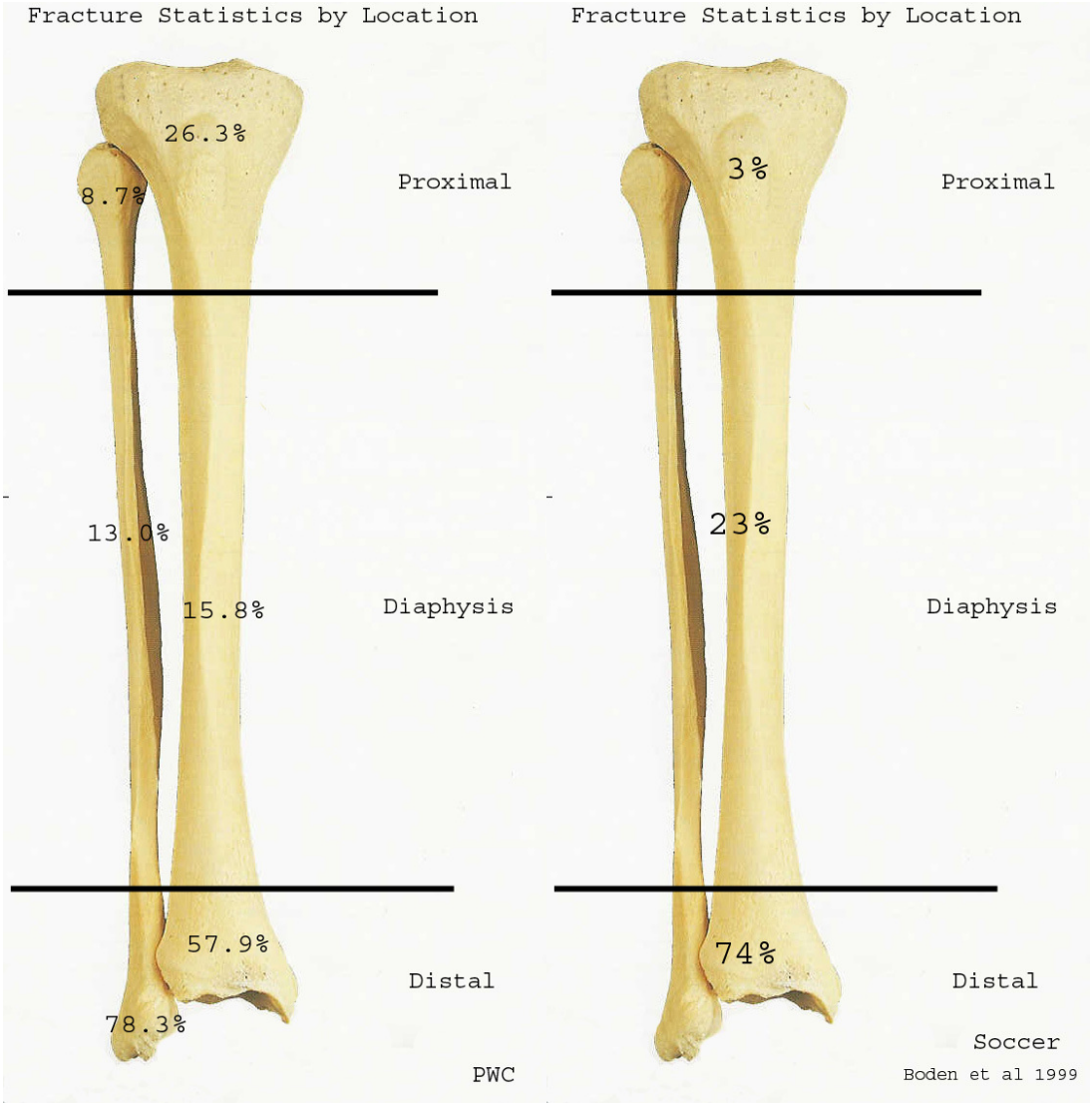

Figure 5.22 Comparison of location of fracture between soccer and PWC use.

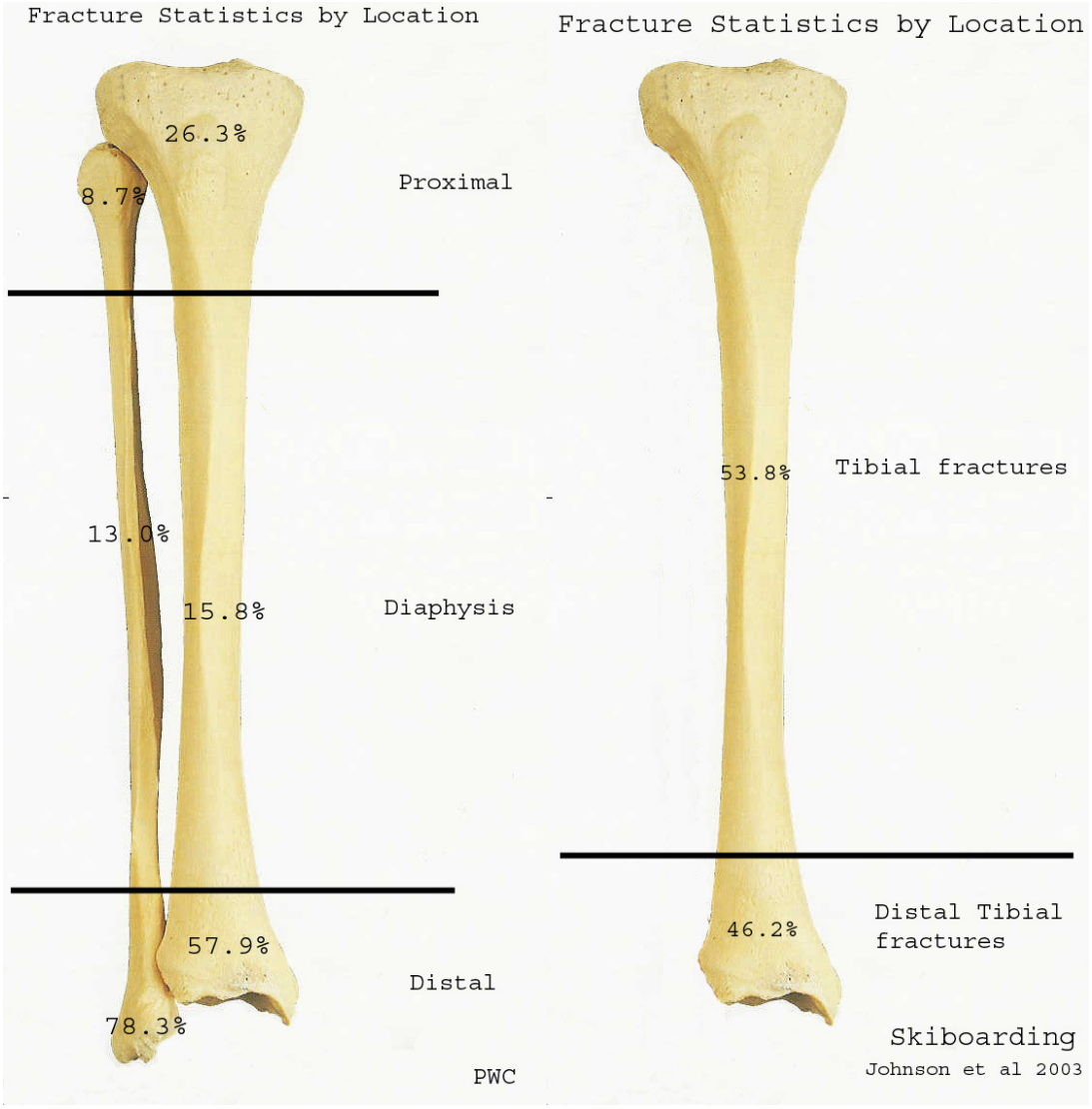

Figure 5.23 Comparison of fracture locations between skiboarding and PWC use.

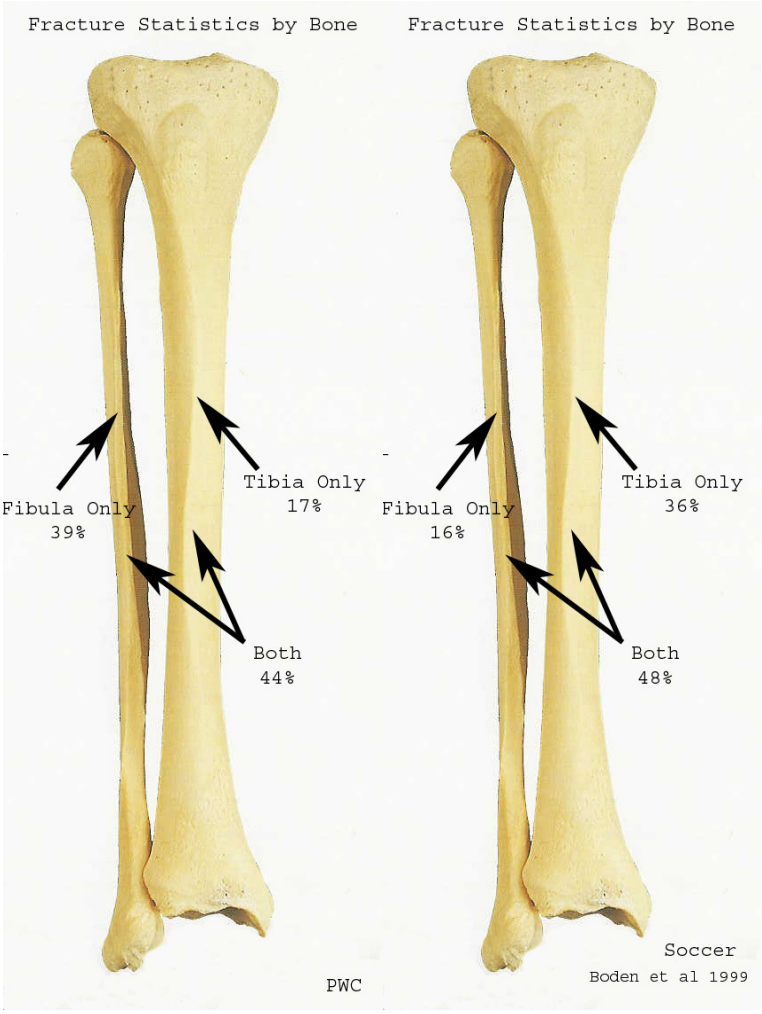

Figure 5.24 Comparison between fracture location between PWC use and soccer.

In order to tell if the fracture patterns from PWC use were unique to the sport, or were common among ankle injuries, radiographs from a variety of activities were examined and compared. Striking similarities existed between fractures from PWC related events, and everyday events such as motor vehicle accidents, sports, and slip and falls. PWC case 16 (shown on the left in Figure 5.25 below) shows a fracture to the medial and lateral malleoli. A radiograph from a motor vehicle accident (shown on the right Figure 5.25) has a very similar fracture pattern, with a fracture of the medial malleolus occurring in the same location. This indicates that this type of fracture pattern, caused here by the mechanism of external rotation, is not unique to the use of personal watercraft. The medial malleolus is a common fracture location in this type of injury.

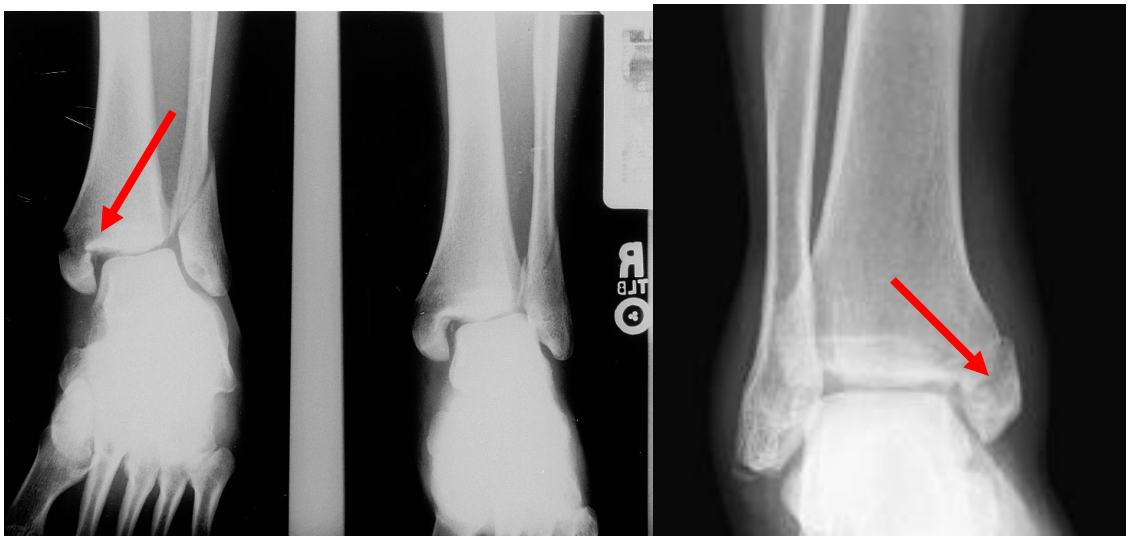

Figure 5.25 Comparison of fracture patterns between PWC case 16 (on left) to a MVA (on right).

The radiographs from PWC case 21 show a transverse fracture of the medial malleolus, and a comminuted fracture of the lateral malleolus (shown on the left in Figure 5.26 below). A radiograph from a football player clearly shows a very similar fracture pattern, with a fracture to the medial malleolus as well as a comminuted fracture of the lateral malleolus (shown on the right in Figure 5.26). Both of these fractures were created by a bending mechanism caused by inversion of the ankle. Comminution of the lateral malleolus, as well as fracture of the medial malleolus are common in this type of injury mechanism.

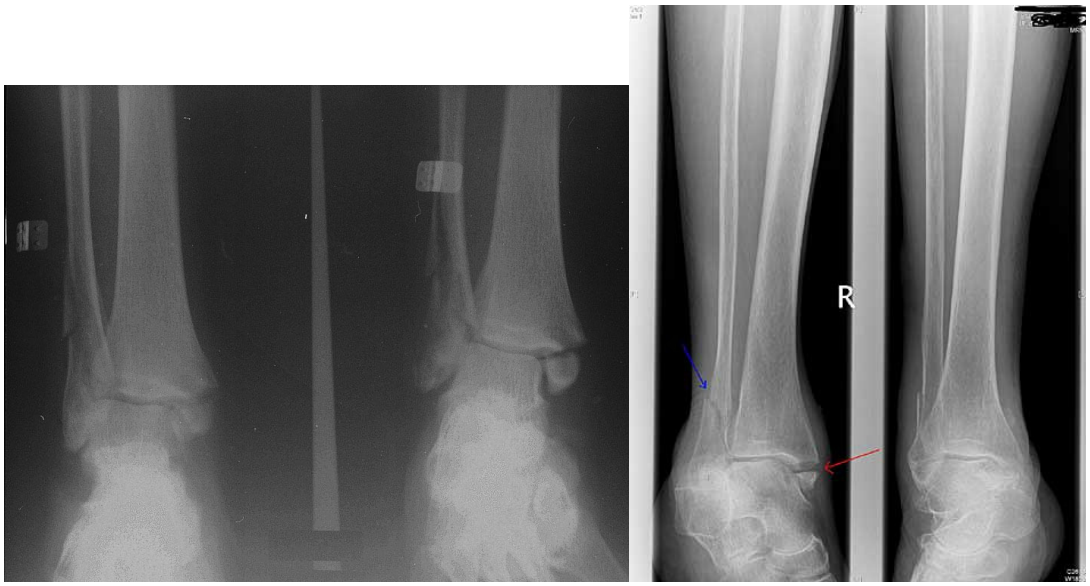

Figure 5.26 Comparison between fracture patterns in PWC case 21 (left) and a football player (right).

Radiographs for PWC case 15 show extensive fracturing, with a posterior displacement of the talus and anterior displacement of the tibia. Fractures are present on the lateral and medial malleolus, with displacement of the fibular shaft (shown on the left in Figure 5.27). The other radiograph picture in figure 5.27 (shown on the right) is from an individual who slipped on wet grass. The fracture pattern is very similar and there is a similar pattern of displacement. Both of these injuries has a mechanism of external rotation. Again, the similarities between the fracture patterns illustrate that the injuries seen are not unique to the use of personal watercraft and can occur from a variety of everyday activities.

Figure 5.27 Comparison of fracture patterns between PWC case 15 and a slip and fall.

Conclusions

After comparison to a variety of activities, there is nothing unique about the fracture frequency or patterning from PWC use. As with any sport or recreational activity, there is an inherent risk to the participant. Injury can be inevitable. When injuries from PWC use do occur, the bones fail in a predictable and normal manner. In other words, the fractures are not out of the ordinary nor distinguishably unique from other similar activities. The best recommendation for possible mitigation of the frequency of lower extremity injury from PWC use is not by altering the design of the craft,, but through operator training and proper use.

CHAPTER 6: CONCLUSION

Recommendations for physical and forensic anthropologists

As trauma analysis becomes a more vital component of forensic and physical anthropology, anthropologists are tasked with integrating trauma analysis into the traditional main stay of the laboratory based biological profile of age, ancestry, sex, stature, and pathology. Past approaches to trauma analysis have focused primarily on the identification of characteristics that indicate which category (i.e., blunt, sharp, ballistic) the specimen may fall into. This discrete category approach has the potential for confusion when there appears to be characteristics of multiple types of trauma, for example an incised wound (seen as an indicator of sharp trauma) coupled with a radiating fracture (seen as an indicator of blunt trauma).

The alternative mode of thinking about trauma, as proposed here, views trauma as a continuum rather than discrete categories. The fracture patterns and characteristics displayed by a specimen are influenced by three primary extrinsic variables of force, surface area of impacting interface, and acceleration/deceleration. When examining trauma, the anthropologists should think about the fractures in the context of how these three "engineering inputs" effect the seen "anatomical outputs."

Force

The variable of force proved to be very important through out the testing. The human body is subjected to a variety of forces in everyday activities; however, injury occurs when these forces exceed the tolerance levels for the tissues of the body. The amount of force influences the severity of the fractures

seen. For example, in the testing of the cranial base, the force of the impact determined the extend of fracturing. The impact at a force of 1,181 lbs in test one only produced a partial hinge fracture, while the force of 1,444 lbs in test two produced a complete hinge fracture that transected the entire cranial base. All other variables were constant between these two tests.

In forensic anthropology, clues to the amount of force may be seen in the extent of the fractures. For example, in the cranial vault, fracture patterns with numerous radiating and concentric fractures may be indicative of a higher force than a single linear fracture. However, anthropologists must keep in mind that the comparison of force is not always a one to one comparison. The intrinsic properties of the bone (such as geometry, location, quality of bone) also come into play and can explain differences in fracture patterns caused by the same amount of force.

Surface area of impacting interface

The variable of surface area between the impacting object and the bone is crucial to understand for forensic anthropologists. This variable explains the differences seen in trauma to bone between blunt and sharp trauma. An impact to the skull with the force of 12 lbs, but a large surface area may cause a typical blunt trauma fracture pattern with a point of impact, radiating, and concentric fractures. However, an impact to the skull with an identical force of 12 lbs, but a very small surface area (i.e., the edge of a knife or axe) will create an incising type wound with straight margins. While the force remains the same, a change

to the surface area of the impact interface alters the pounds per square inch (psi) influencing the bone. As frequently and aptly noted, sharp trauma is simply a beating with a sharp object (Symes et al 1989, Symes et al 2002b). The variable that dictates the difference between a sharp trauma wound and a blunt trauma wound is simply surface area. Because of this, it is possible to have sharp trauma wounds that also contain characteristics of blunt trauma.

In the experimental testing, this variable played an important role in understanding the mechanics of propeller impacts to the thorax. The ring style propeller, which had an impacting interface of a broad, flat ring, created markedly different injuries than the traditional blade style propeller. The ring propeller created more scooping lacerations, while the standard propeller incised into the body with each individual blade.

Acceleration/Deceleration

For forensic anthropologists the variables of acceleration or deceleration are important to grasp for understanding how a change in velocity over time can influence how bone responds to trauma. Since bone is a viscoelastic material, it has different mechanical properties dependant on the rate of loading (acceleration/deceleration). Forensic anthropologists are accustom to looking for the variable of plastic deformation to indicate blunt trauma, and an absence of deformation to indicate ballistic trauma. These differences are actually created by the differences in the acceleration/deceleration rates between the two types of trauma. Instead of viewing these categories as independent, they can be

visualized as a continuum influenced by how the deceleration of the impacting object (i.e., rifle bullet, pistol bullet, or baseball bat) influences the fracture mechanics of the bone. When conceptualized in this manner, it is easy to understand how a bullet can create plastic deformation and “blunt trauma” when it has slowed down (i.e., reached terminal velocity) to an acceleration/deceleration rate consistent with blunt trauma.

Final Recommendations

As the field of forensic anthropology grows trauma analysis has started to play a vital component. The intent of this dissertation is present some new ideas and ways of thinking about trauma analysis for forensic anthropologists. As a sub discipline of forensic anthropology, trauma analysis will continue to grow and evolve. There is a need for further research, both experimental and on existing cases. There are still numerous unanswered questions in the field of forensic trauma analysis. Continued research will work to increase our knowledge of the mechanisms behind bone fracture patterns and better apply them in medico-legal context.

BIBLIOGRAPHY

Adams JH, Doyle D, Graham DI, Lawrence AE, McLellan DR, Gennarelli TA, Pastuszko M, and Sakamoto T (1985) The contusion index: A reappraisal in human and experimental non-missle head injury. Neuropathology and Applied Neurobiology *11:*299-308.

Advani S, and Owings RP (1974) Evaluation of head injury criteria. Automotive Engineering Congress, pp. 1-11.

Allsop D (1993) Skull and facial bone trauma: Experimental aspects. In A Nahum and JW Melvin (eds.): Accidental Injury: Biomechanics and Prevention. New York: Springer-Verlag.

Alms M (1961) Fracture mechanics. The Journal of Bone and Joint Surgery *438:*162-166.

Antich P (1993) Ultrasound study of bone in vitro. Calcified Tissue International *53:*S157-S161.

Ashman R, Cowin S, VanBuskirk W, and Rice J (1984) A continuous wave technique for the measurment of the elastic properties of cortical bone. Journal of Biomechanics *17:*349-361.

Bartelink E, Wiserman J, and Demaree R (2001) Quantitative analysis of sharp-force trauma: an application of scanning electron microscopy in forensic anthropology. Journal of Forensic Science *46:*1288-93.

Beier G, Eisenmenger W, and Spann W (1983) Forensic medicine considerations of head and spine injuries. In C Ewing, D Thomas, A Sances and S Larson (eds.): Impact Injury of the Head and Spine. Springfeild, IL: Charles C Thomas.

Berryman H, and Symes S (1998) Recognizing gunshot and blunt cranial trauma through fracture interpretation. In K Reichs (ed.): Forensic Osteology: Advances in the Identification of Human Remains. Illinois: Charles C. Thomas, pp. 333-352.

Betz P, Stiefel D, and Eisenmenger W (1996) Cranial fractures and direction of fire in low velocity gunshots. International Journal of Legal Medicine *109:*58-61.

Betz P, Stiefel D, Hausmann R, and Eisenmenger W (1997) Fractures at the base of the skull in gunshot wounds to the head. Forensic Science International *86:*155-161.

Boden B, Lohnes J, Nunley J, and Garrett W (1999) Tibia and fibula fractures in soccer players. Knee Surgery, Sports Traumatology, and Arthropscopy *7:*262-266.

Bonfield W, JC B, and Charalambides C (1985) Orientation and age releated dependence of the fracture toughness of cortical bone. Biomechanics; current interdisciplinary research; selected proceedings of the Fourth Meeting of the European Society of Biomechanics*:*185-188.

Bonfield W, and Li C (1965) Deformation and fracture of bone. Journal of Applied Physics *37:*869-875.

Bouvier M (1989) The biology and composition of bone. In S Cowin (ed.): Bone Mechanics. Boca Raton: CRC Press, pp. 1-14.

Branche C, Conn J, and Annest J (1997) Personal watercraft-related injuries: a growing public health concern. The Jounral of the American Medical Association *278:*663-666.

Brinckmann P, Forbine W, and Leivseth G (2002) Musculoskeletal Biomechanics. New York: Thieme.

Brinn J, and Staffeld SE (1970) Evaluation of impact test accelerations: A damage index for the head and torso. Fourteenth Stapp Car Crash Conference, pp. 188-220.

Browner B, Jupiter J, Levine A, and Trafton P, eds. (1992) Skeletal Trauma. Philadelphi: W.B. Saunders Company.

Burrell L, Maas M, and Van Gerven D (1986) Patterns of long bone fractures in two nubian cementeries. Human Evolution *1:*495-506.

Byers S (2002) Introduction to Forensic Anthropology.

Calce S, and Roger T (2007) Taphonomic changes to blunt force trauma: A preliminary study. Journal of Forensic Science *52:*519-527.

Cavanaugh J (1993) The biomechanics of thoracic trauma. In A Nahum and JW Melvin (eds.): Accidental Injury: Biomechanics and Prevention. New York: Springer-Verlag, pp. 362-390.

Cesari D, and Ramet M (1979) Evaluation of human tolerance in frontal impacts. Twenty-Third Stapp Car Crash Conference, pp. 875-914.

Clarke TD, Smedley DC, Muzzy WH, Gragg CD, Schmidt RE, and Trout EM (1972) Impact tolerance and resulting injury patterns in the baboon: Air force shoulder harness-lap belt restraint. Sixteenth Stapp Car Crash Conference, pp. 365-411.

Committee on Injury and Poison Prevention (2000) Personal Watercraft Use by Children and Adolescents. Pediatrics *105:*452-453.

Conn J, Annest J, and Gilchrist J (2003) Sports and recreation related injury episodes in the US Population, 1997-99. Injury Prevention *9:*117-123.

Cowin S (1989) Mechanics of materials. In S Cowin (ed.): Bone Mechanics. Boca Raton: CRC Press, pp. 15-42.

Daly P, Fitzgerald R, Melton L, and Illstrup D (1987) Epidemiology of ankle fractures in Rochester, Minnesota. Acta Orthop Scand *58:*539-544.

DiMaio V, and DiMaio D (2001) Forensic Pathology. Boca Raton: CRC Press.

Emmett J, and Breck L (1958) A review and analysis of 11,000 fractures seen in a private practice of orthopaedic surgery. Journal of Bone and Joint Surgery *40A:*1169-1175.

Evans F (1970) Biochemical implications of anatomy. In J Cooper (ed.): Selected Topics of Biomechanics: Proceedings of the C.I.C. Symposium on Biomechanics: Indiana University.

Evans F (1973) Mechanical Properties of Bone. Springfield, IL: Charles C. Thomas.

Ewing C, Thomas D, Sances A, and Larson S, eds. (1983) Impact Injury of the Head and Spine. Springfield, Ill: Charles C Thomas.

Fallat L, Grimm D, and Saracco J (1998) Sprained ankle syndrome: Prevelance and analysis of 639 acute injuries. Journal of Foot and Ankle Surgery *37:*280-285.

Fan WRS (1971) Internal head injury assessment. Fifteenth Stapp Car Crash Conference, pp. 645-665.

Frankel V, and Nordin M (1989) Biomechanics of the ankle. In M Nordin and V Frankel (eds.): Basic Biomechanics of the Musculoskeletal System. Philadelphia: Lea and Febiger.

Frost H (1967) An Introduction to Biomechanics. Springfield, IL: Charles C. Thomas.

Galloway A (1999) Broken Bones: Anthropological Analysis of Blunt Force Trauma. Springfield, IL: Charles C Thomas.

Gershuni D (1985) Clinical aspects of extremity fractures. In A Nahum and JW Melvin (eds.): Biomechanics of Trauma. Norwalk, Connecticut: Appleton-Century-Crofts, pp. 414-446.

Gonza E (1982) Biomechanics of long bone injury.: Biomechanics of Trauma. Baltimore: Williams and Wilkins, pp. 1-24.

Gurdjian E, and Lissner H (1945) Deformation of the skull in head injury: a study with the "stresscoat" technique. Surgery, Gynecology, and Obstetrics *81:*679-687.

Gurdjian E, Lissner H, and Webster J (1947) The mechanism of production of linear skull fractures. Surgery, Gynecology, and Obstetrics *85:*195-210.

Gurdjian E, Webster J, and Lissner H (1949) Studies on skull fracture with particular reference to engineering factors. American Journal of Surgery *78:*736-742.

Gurdjian E, Webster J, and Lissner H (1950a) The mechanism of skull fracture. Journal of Neurosurgery*:*106-114.

Gurdjian E, Webster J, and Lissner H (1950b) The mechanism of skull fracture. Radiology *54:*313-338.

Haan J, Kramer M, and Scalea T (2002) Pattern of injury from personal watercraft. American Surgeon *68:*624-627.

Halstead D (2001) Preformance Testing Updates in Head, Face, and Eye Protection. Journal of Athletic Training *36:*322-327.

Hamilton W (1984) Traumatic Disorders of the Ankle. New York: Springer-Verlag.

Harkess J, Ramsey W, and Ahmadi B (1984) Principles of fractures and dislocations. In C Rockwood and D Green (eds.): Fractures in Adults. Philadelphia.

Harvey F, and Jones A (1980) "Typical" basal skull fracture of both petrous bones: an unreliable indicator of head impact site. Journal of Forensic Science *25:*280-6.

Hein P, and Schulz E (1990) Contrecoup fracture of the anterior cranial foss as a consequence of blunt force caused by a fall. Acta Neurochi *105*.

Hodgson VR, Thomas LM, and Brinn J (1973) Concussion levels determined by HPR windshield impacts. Seventeenth Stapp Car Crash Conference, pp. 171-190.

Hon W, and Kock S (2001) Sports related fractures: A review of 113 cases. Journal of Orthopaedic Surgery *9:*35-38.

Huelke D, O'Day J, and States J (1982) Lower extremity injuries in automobile crashes. Accident Analysis and Prevention *14*:95-106.

Hyde A (1992) Crash Injuries: How and why they happen. Key Biscayne, FL: Hyde Associates, Inc.

Inman V (1976) The Joints of the Ankle. Baltimore: Williams and Wilkins.

Johnson E (1985) Current developments in bone technology. In M Schiffer (ed.): Advances in Archaeological Method and Theory. Orlando: Academic Press.

Johnson R, Ettlinger C, and Shealy J (2003) Lower extremity injuries involving traditional alpine skis versus short skis with non-release binding. In R Johnson, M Lamont and J Shealy (eds.): Skiing Trauma and Saftey: Fourteenth Volume, ASTM STP 14400. West Conshohken, PA: American Society for Testing and Materials International, pp. 105-112.

Jones C (1997) Personal watercraft-related injuries in Arkansas: 1994-1996. Journal of the Arkansas Medical Society *94:*111 - 112.

Judd M, and Roberts C (1999) Fracture trauma in a medieval British farming village. American Journal of Physical Anthropology *109:*229-243.

Jupiter J, and Belsky M (1992) Fractures and dislocations of the hand. In B Browner, J Jupiter, A Levine and P Trafton (eds.): Skeletal Trauma. Philadelphia: W.B. Saunders Company, pp. 925-1024.

Keaveny T, and Hayes W (1993) Mechanical properties of of cortical and trabecular bone. In B Hall (ed.): Bone. Boca Raton: CRC Press, pp. 285-344.

Kelikian H, and Kielikian A (1985) Disorders of the Ankle. Philadelphia: W.B. Saunders.

Knight B (1996) Forensic Pathology. London: Arnold.

Komar D (2003) Lessons from Srebrenica: the contributions and limitations of physical anthropology in identifying victims of war crimes. Journal of Forensic Science *48*.

Kress T (1996) Impact Biomechanics of the Human Body, The University of Tennessee, Knoxville.

Kroman A (2003) Backwards and Forawards: The Gurdjian Theory and Blunt Force Trauma, University of Tennessee, Knoxville.

Kroman A (2004) Experimental study of fracture propigation in the human skull: A re-testing of popular theories. American Academy of Forensic Science.

Kroman A, Kress T, and Symes S (2005) Mandible and cranial base fractures in adults: Experimental testing. American Academy of Forensic Science.

Kroman A, and Symes S (2002) Butterfly fracture patterns. International Association of Forensic Science.

Lauge-Hansen N (1950) Fractures of the ankle. II Combines experimental-surgical and experimental-roentgenologic investigations. Arch Surg *60*:957-85.

Lestina DC, Kuhlmann TP, Keats TE, and Alley RM (1992) Mechanisms of injury in ankle and foot injuries to drivers in motor vehicle crashes. Proc 36th Stapp Car Crash Conference, pp. 59-68.

Levine R (1993) Injury to the extremities. In A Nahum and JW Melvin (eds.): Accidental Injury: Biomechanics and Prevention. New York: Springer-Verlag, pp. 460-491.

Low J, and Reed A (1996) Basic Biomechanics Explained. Oxford: Butterworth-Heinmann Ltd.

Madeley NJ, Srinivasan CMS, Crandall JR, Hurwitz S, and Funk JR (2004) Retrospective analysis of malleolar fractures in an impact enviornment. AAAM.

Marks M, and Mileusnic D (2007) Histopathy of antemortem infant bone fracture: Estimation of time since insult. American Academy of Forensic Science.

McNealy R, and Lichtenstein M (1940) Fractures of the bones of the hand. American Journal of Surgery *50:*563-570.

Melvin JW, Fuller PM, Daniel RP, and Pavliscak GM (1969) Human head and knee tolerance to localized impacts, pp. 1772-1782.

Mertz HJ (1972) Occupant injury tolerance factors. Williamsburg Conference on Highway Safety Research, pp. 35-41.

Mortiz A (1954) The Pathology of Trauma. Philadelphia: Lea and Febiger.

Myers JC, Okoye MI, Kiple D, Kimmerle EH, and Reinhard KJ (1999) Three-dimensional (3-D) imaging in post-mortem examinations: elucidation and identification of cranial and facial fractures in victims of homicide utilizing 3-D computerized imaging reconstructive techniques. International Journal of Legal Medicine *113*:33-37.

Nahum A, and Melvin JW (1993) Accidental Injury: Biomechanics and Prevention. New York: Spring-Verlag.

National Transportation Safety Board (1998) Personal Watercraft Safety. In National Transportation Safety Board (ed.): Washington, DC., pp. 98.

Neumann D (2002) Kinesiology of the Musculoskeletal System. St. Louis, Missouri: Mosby.

Nordin M, and Frankel V, eds. (1989) Basic Biomechanics of the Musculoskeletal System. Philadelphia: Lea and Febiger.

Ortner D, and Putschar W (1981) Identification of Pathological Conditions in Human Skeletal Remains. Washington, D.C.: Smithsonian Institution Press.

Patrick LM (1973) Human tolerance to impact and its application to safety design.: Biomechanics and Its Application to Automotive Design. New York, New York: Society of Automotive Engineers, pp. 1-15.

Petrucelli E (1984) Injury scaling and some considerations of disability consequences. In B Aldman and A Chapon (eds.): The Biomechanics of Impact Trauma: Elsvier Science Publishers, pp. 7-24.

Piekarski K (1970) Fracture of bone. Journal of Applied Physics *41:*215-223.

Porta D (1996) The Anatomy and Biomechanics of Experimentally Traumatized Human Cadaver Lower Extremity Components. Dissertation, University of Louisville, Louisville, KY.

Quatrehomme G, and Iscan MY (1997) Postmortem skeletal lesions. Forensic Science International *89:*155-165.

Roark R, and Young W (1975) Formulas for stress and strain. New York: McGraw Hill.

Rockwood C, Green D, Bucholz R, and Heckman J, eds. (1996) Rockwood and Green's Fractures in Adults. Phildelphia: Lippincott-Raven.

Rogers L (1992) Radiology of Skeletal Trauma. New York: Churchill Livingston.

Ryan J, Hensel R, Salciccioli G, and Pederson H (1981) Fracture os the femur secondary to low velocity gunshots. Journal of Trauma *21:*160-162.

Sances A, Thomas D, Ewing C, and Larson S, eds. (1986) Mechanisms of Head and Spine Trauma. Goshen, New York: Aloray.

Sarrafian S (1983) Anatomy of the Foot and Ankle. Philadelphia: J.B. Lippincott.

Schuknecht B, and Graetz K (2005) Radiologic assessment of maxillofacial, mandibular, and skull base trauma. European Radiology *15:*560-568.

Sherwood C, O'Neill B, and Hurwitz S (1999) Lower extremity causation in frontal crashes. IRCOBI, pp. 513-524.

Snyder RD (1973) Techniques for establishing tolerances to impact.: Biomechanics and Its Application to Automotive Design. New York, New York: Society of Automotive Engineers, pp. 1-19.

Spitz W, and Fisher R (1980) Medicolegal Investigations of Death. Springfield: Charles C. Thomas.

Steele D, and Bramblett C (1988) The Anatomy and Biology of the Human Skeleton. College Station, TX: Texas A&M University Press.

Swanson A (1970) Fractures involving the digits of the hand. Orthopedic Clinical North America *1:*261-274.

Symes S, Berryman H, and Smith O (1989) The changing role of the forensic anthropologist: Pattern and mechanism of fracture propigation. Mountain, Swamp, and Beach Forensic Anthropology Meetings.

Symes S, Ferraro C, Patton S, Smith O, and Kroman A (2002a) From Caffey (1946) to Kempe (1962): Historical perspectives on the recognition of child abuse. American Academy of Forensic Science.

Symes S, Patton S, Campbell T, Gardner C, Smith O, Sutton T, Mallak C, and Kroman A (2002b) Child abuse: It's all in the recognition. American Academy of Forensic Science.

Trafton P, Bray T, and Simpson L (1992) Fractures and soft tissue injures of the ankle. In B Browner, J Jupiter, A Levine and P Trafton (eds.): Skeletal Trauma. Philadelphia: W.B. Saunders Company.

Turner C, and Burr D (1993) Basic biomechanical measurments of bone: a tutorial. Bone *14:*595-608.

Tyler B, and Garrison H (1997) Injuries associated with personal watercraft. An emerging epidemic in need of legislative action. N C Medical Journal *58:*284-287.

White M, and Cheatham M (1999) The underestimated impact of personal watercraft injuries. The American Surgeon *65:*865-869.

Whitman R (1996) Personal watercraft get bigger.: The Kansas City Star. Kansas City, pp. 8.

APPENDIX

Appendix A : Fracture Propagation in the Cranial Vault

Test One

Test specimen 1 is a female age 89, with head weight of 3.6 killograms (kg). The left parietal was impacted from a drop height of 77 in (1.96 m) and a weight of 23 lbs (8.58 kg). The impact caused two radiating fractures. The main radiating fracture traveled from the point of impact to terminate into the squamosal suture, a total distance of 2.5 inches (6.35 cm). A secondary fracture radiated laterally a distance of 1.25 inches (3.175 cm) (Figure A.1). All fractures recorded were radiating from the impact site. No fractures were noted to radiate back towards the impact site.

Data from load cells was analyzed. The axial load reached a force of 817 lbs (Figure A.2). The first peak of the curve represents the initial bone failure and the creation of the radiating fracture. This event occurred .966 seconds after impact. There are two secondary peaks present in the data that represent further release of energy. These may represent the creation of secondary radiating fractures. Both occur around at a force level of around 650 lbs. The sharp decline in the energy shows that the skull has been fractured. A comparison of the high speed video of the event demonstrates that at energy decline the skull was freely moving away from the impactor.

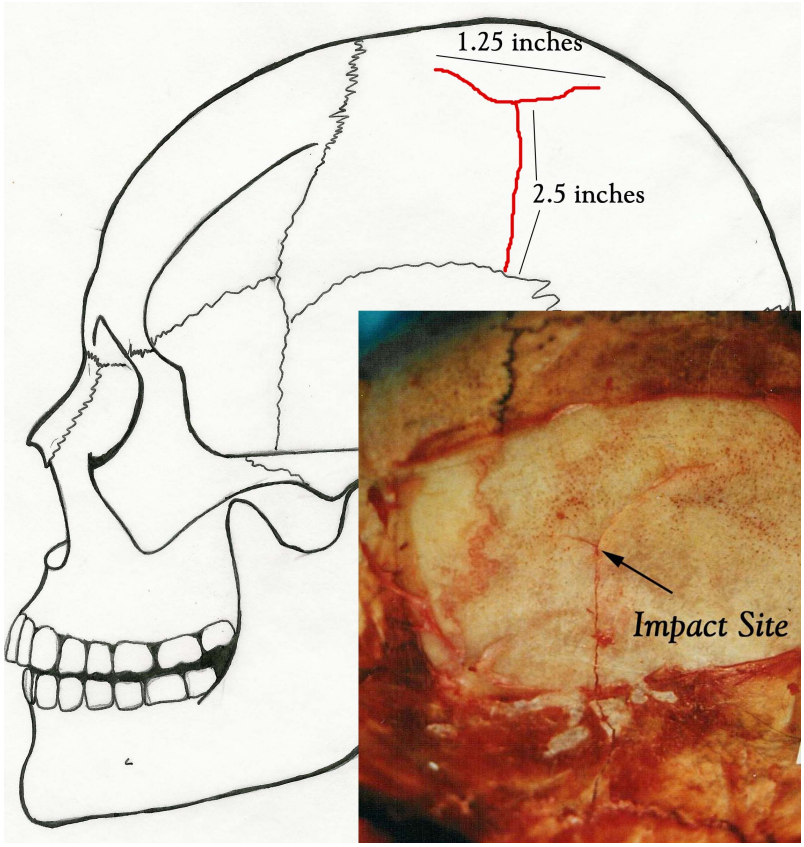

Figure A.1. Fracture pattern in test one in the left parietal, with impact site 2 in (5.08 cm) from sagittal suture .6 in (1.52 cm) from coronal suture, and 2.5 in (6.35 cm) from the sqaumosal suture.

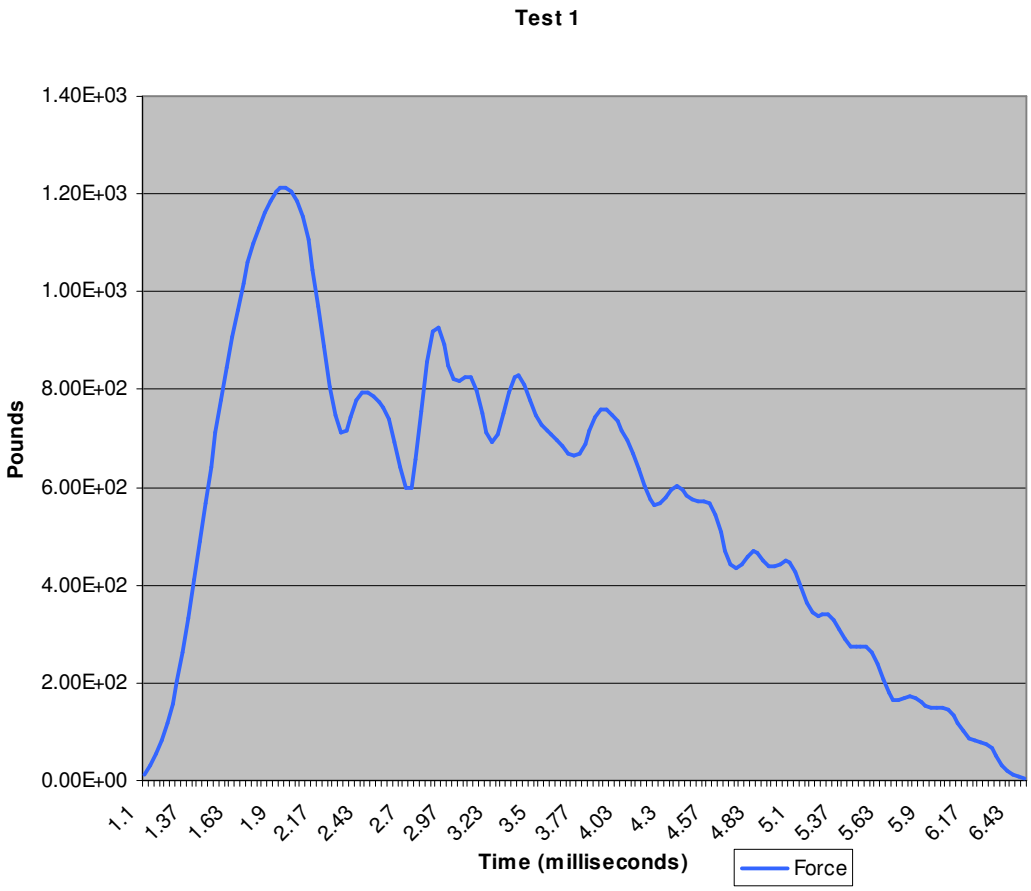

Figure A.2 Load cell data from Test 1.

Test Two

Test specimen 2 is a 61 year old female with a head weight of 8.84 lbs (3.3 kg). The left parietal was impacted from a drop height of 111 in (2.82 m) with a drop mass of 23 lbs (8.58 kg). Fractures were formed at the point of impact and radiated into the sqaumosal suture traveling a total distance of 3.5 inches (Figure A.3). Additional small fractures in the outer cortex were noted in a circular concentric pattern around the point of impact. No additional fractures radiating from locations other than the impact site were noted.

The load cell reported a maximum axial load of 1140 lbs (Figure A.4). This major peak represents the main failure point for the bone and fracture initiation. The earlier secondary peak may represent a microfracture, or failure of the outer or inner cortex. The major failure occurred at 1.1 seconds into the event. From a comparison of the fracture patterns and timed sequence of the data it is probable that the main radiating fracture was created at the force peak of 1140 lbs, with secondary fractures occurring at 800 lbs of force.

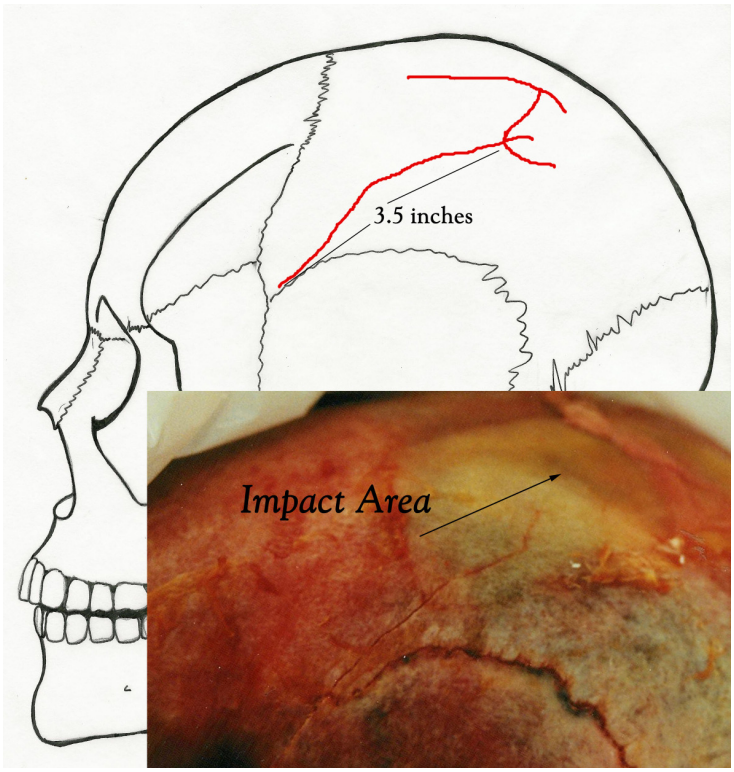

Figure A.3 Fracture pattern in the left parietal for test two with an impact site 2 in (5.08 cm) from the sagittal suture, .75 in (1.91 cm) from the coronal suture, and 2 in (5.08 cm) from the sqaumosal suture.

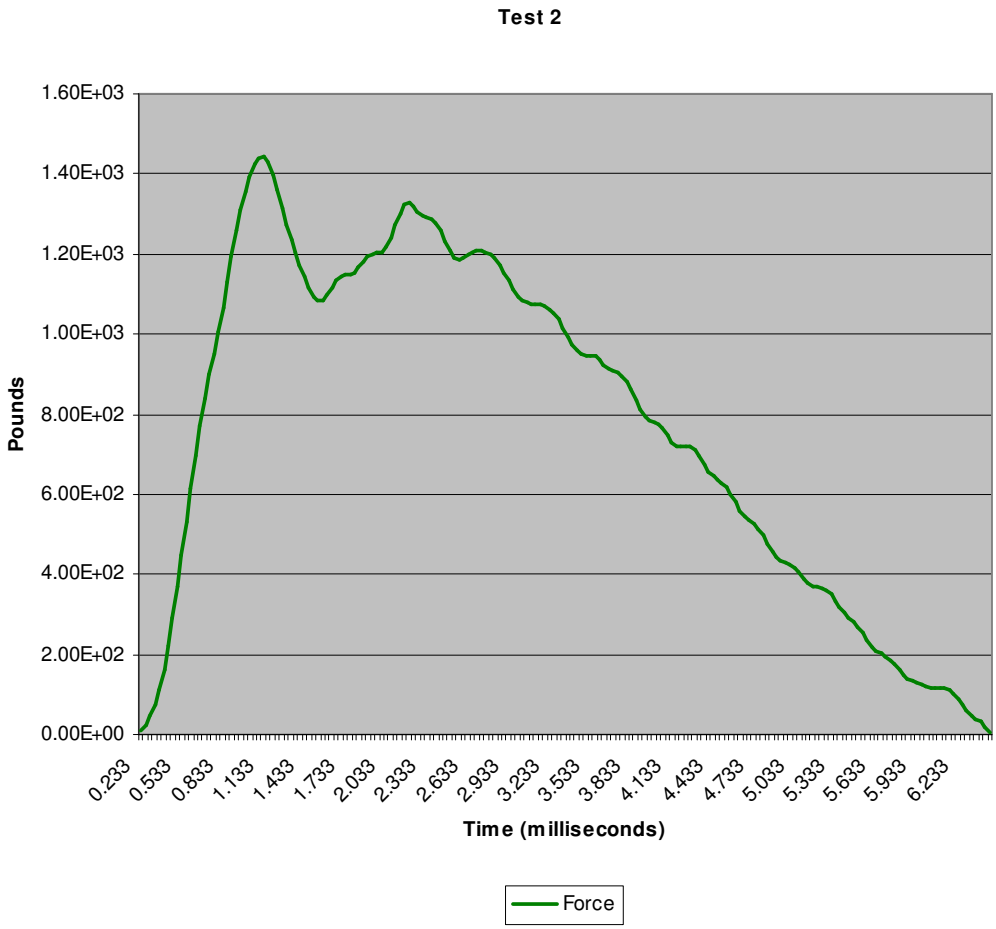

Figure A.4 Load cell data from Test 2.

Test Three

Test specimen 3 is a 61 year old male with a head weight of 5.3 kg. The cranium was impacted on the right parietal from a drop height of 111 inches with a drop mass of 23 lbs. The right parietal was used to avoid an area of soft tissue damage directly over the potential impact site on the left parietal. The only resulting fracture was a very small fracture affecting the outer table in a small stellate pattern directly under the main impact site (Figure A.5). No radiating or concentric fractures occurred at the impact site and no other fractures were notes radiating from any locations remote to impact.

While all impact variables were constant between test two and test three, vault thickness might explain the differential fracturing. Furthermore, specimen three is a large male with a skull weight of 14.20 lbs (5.3 kg).

The main fracture occurred after an applied force of 1400 lbs (Figure A.6). This occurred 3.01 seconds into the event. There is an earlier peak in the data which could signal a microfracture or failure of the outer or inner cortex. This peak occurs around 875 lbs of force. After the main failure there was a swift loss of energy and analysis of the high speed video show that the skull was moving away from the impactor at this time.

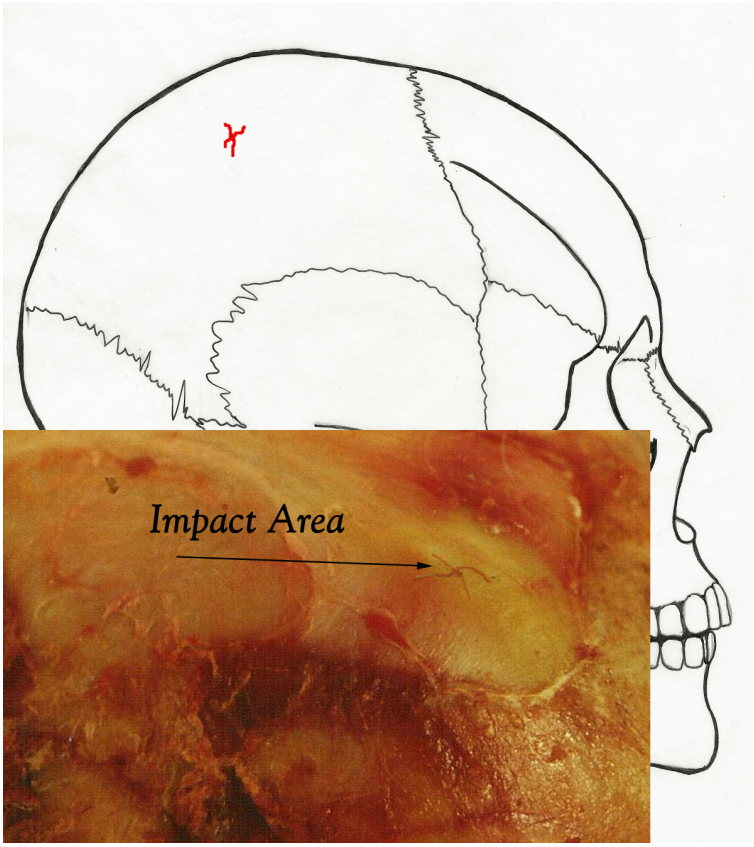

Figure A.5 Fracture pattern in test three in the right parietal, with impact site 2 in (5.08 cm) from sagittal suture .75 in (1.91 cm) from coronal suture, and 3.5 in (8.89 cm) from the sqaumosal suture.

Figure A.6 Load cell data from Test 3.

Test 4

Test four involved a 71 year old male with a total head weight of 4.4 kg. The drop height was 111 inches with a drop mass of 23 lbs. The left parietal was impacted with no visible fractures.

The data shows a peak at 1400 lbs of force. However no fracture resulted. There is a smaller peak at around 600 lbs of force, and it is possible that damage did occur but was contained within the inner cortex or hidden by soft tissue. The drop in energy is sharp and the high speed video shows that the skull moved from the impactor almost immediately.

Test 5

Test five tested the difference in fracture patterns between un-constrained impacted crania and those with semi rigid boundary. This test was conducted to see if the constraint of the skull would produce the fracture patterns similar to Gurdjian's findings. The board that stabilized the other four test subjects until impact was not scored in this test. The board doesn't completely constrain the skull but provided enough resistance to measure the differences. The semi rigid boundary was the only variable altered in the test. The drop height and drop mass remained constant.

At impact, the board failed allowing the skull to move in the direction of the impact. However, the presence of the semi rigid boundary drastically changed the results of the test. The fracture pattern was different with two main areas of fractures occurring on the left parietal (site of impact) and the right parietal. Fractures are more complex with many radiating and concentric fractures present (Figure A.7, A.8). Bilateral fractures were also present through the frontozygomatic sutures (Figure A.9). The complex fracture patterns failed to occur at remote locations and travel back towards the impact site. Damage to the left side of the cranium results from direct impact and damage to the right results from the semi rigid boundary provided by the board.

There was a noticeable difference between the data collected by the load cell data between the unconstrained and constrained tests. The event for the constrained test lasted considerable longer with several fracture events visible in the graph (Figure A.10). The main peak occurs at 840 lbs of force but there are

other major failures. Analysis of the high speed video show that the first peak indicates the failure in the area of the impact site with radiating fractures creating the release in pressure as indicated by the sharp drop after peak one. The semi rigid boundary created additional peaks in energy, indicating failure of the right parietal (side opposite from impact), and failure of the facial skeleton.

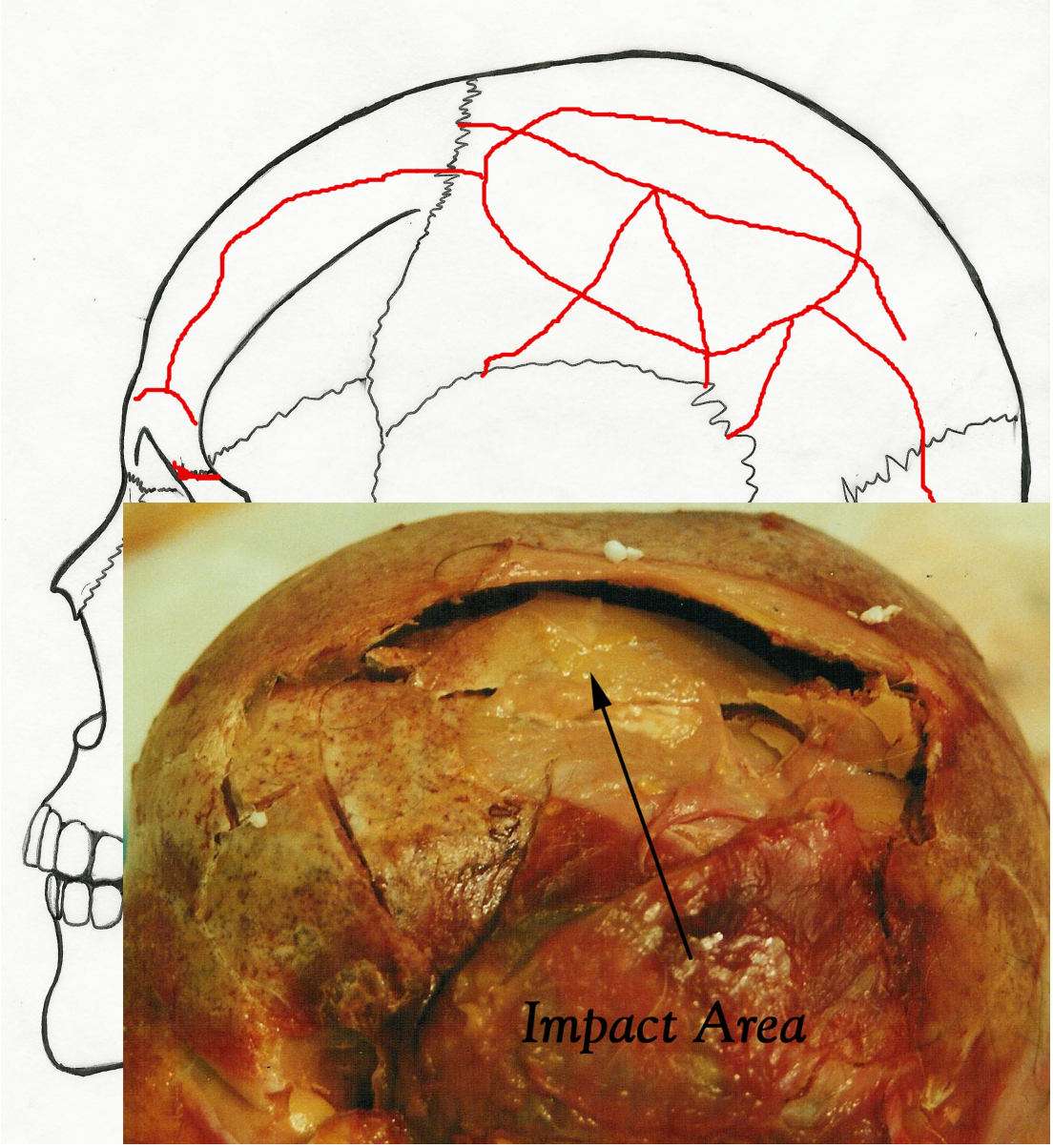

Figure A.7 Fracture pattern in test three in the right parietal, with impact site 2.5 in (6.35 cm) from sagittal suture .75 in (1.91 cm) from coronal suture, and 3.5 in (8.89 cm) from the sqaumosal suture. Extensive fracture are present at the area of impact.

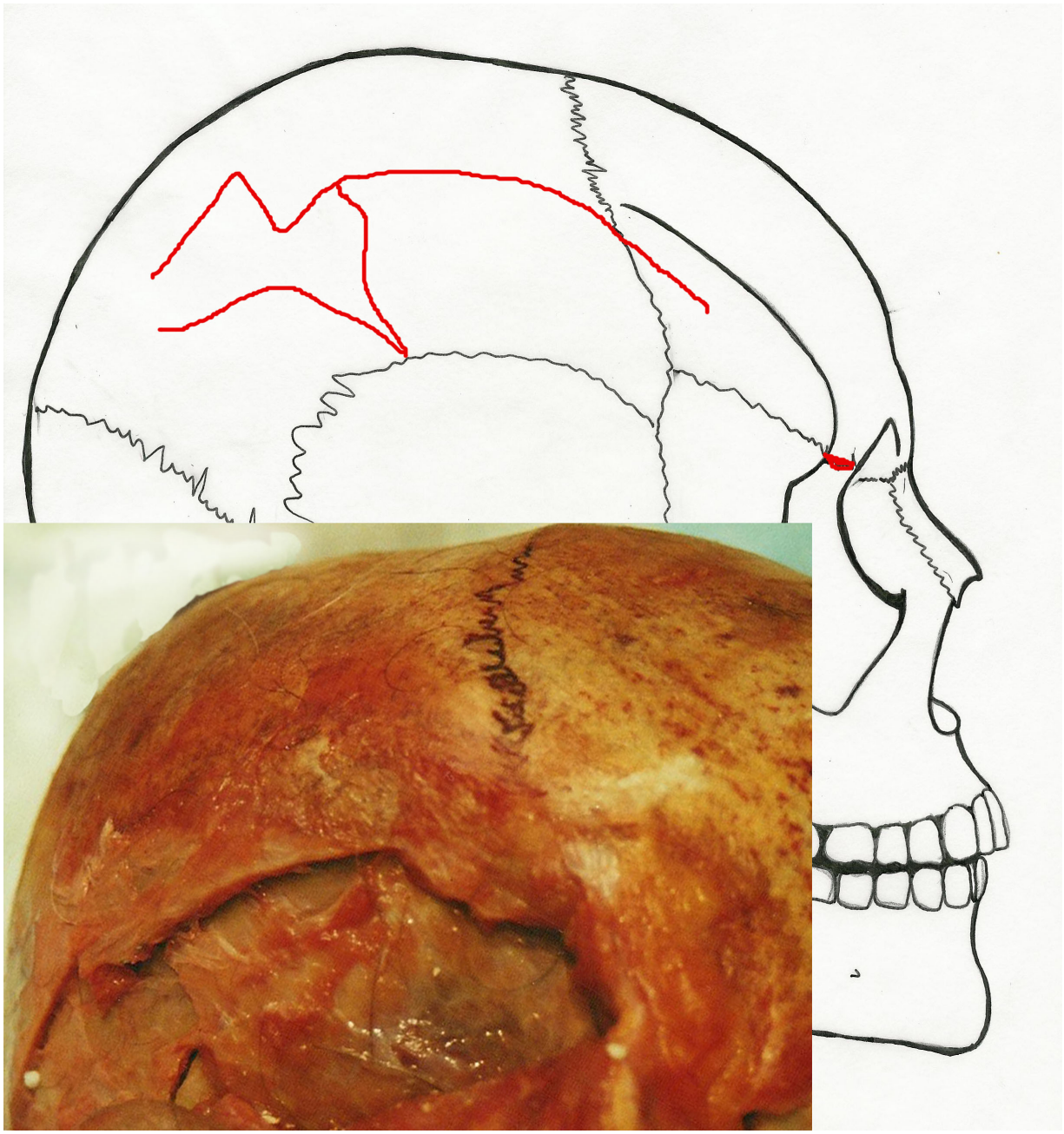

Figure A.8 Right parietal, area on the opposite side from impact.

Figure A.9 The frontal view of the skull used in test five and resulting fractures. There were bilateral fracture of both fronto-zygomatic sutures (insert).

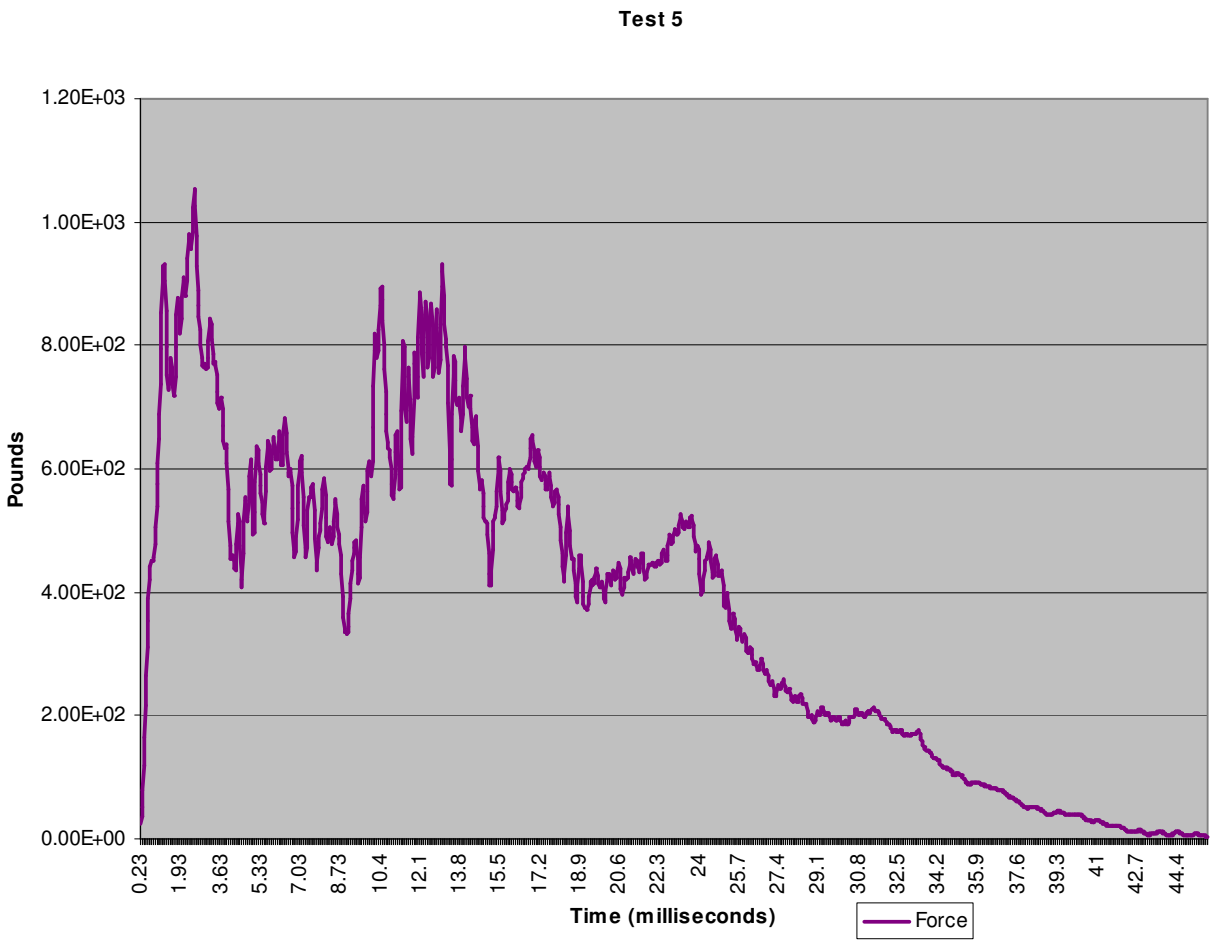

Figure A.10 Load cell data from Test 5.

Appendix B: Propeller Impact Testing

1.P1R5R

Test 1 was conducted on the right side of porcine specimen one using the RingProp at an approximate velocity of 5 mph. The impact was oriented so that the pig was at a 40 degree angle in the water (Figure B.1). The pig was positioned using three strings with rubber bands – one from the tail, one from the right ear, and one from the left ear. Weights were attached at the ankles to achieve negative buoyancy. The front portion of the motor impacted the pig, and the pig was rotated slightly to the left. The only damage was a small abrasion to the right flank region (Figure B.2). There was no damage to the musculature or osseous tissue.

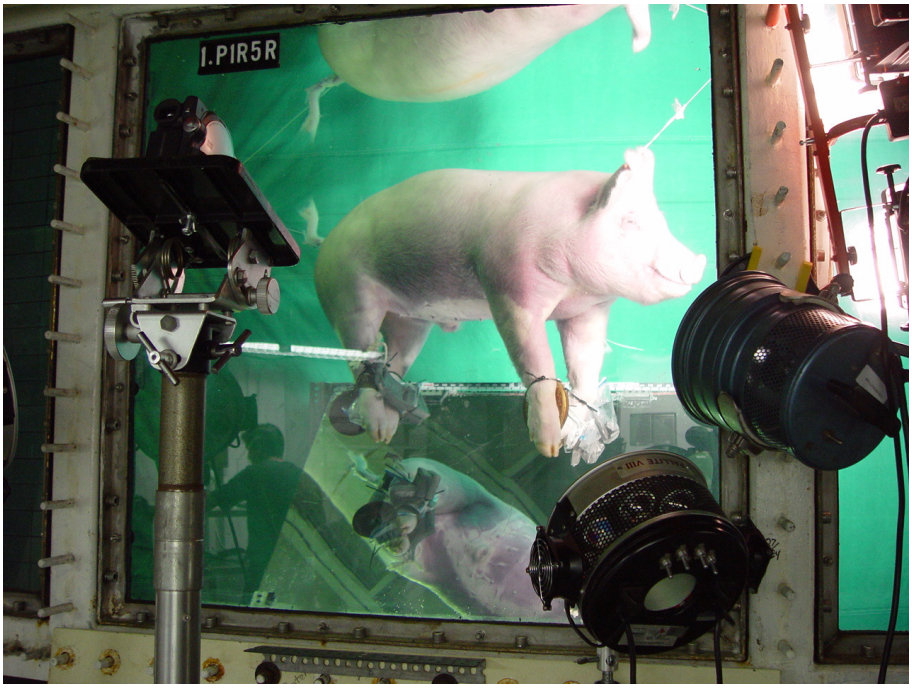

Figure B.1 Position of pig prior to test one.

Figure B.2 Small abrasion from test one.

2.P1S5L

Porcine test specimen one was also tested in test two, this time on the left side using the standard propeller at an approximate impact velocity of 5 mph. Again, the pig was oriented at a 40 degree angle and positioned using strings and weights. The impact pushed the pig down and to the right. There were eleven dermal abrasions and lacerations due to the propeller blades (Figure B.3). Dissection showed that there was no damage to the musculature or skeleton.

Figure B.3 Dermal abrasions from the propeller blades.

3.P2R5L

After tests one and two, the pigs were oriented longitudinally instead of at a 40 degree angle in order to achieve more engagement between the propeller and the specimen. Porcine specimen two was impacted on the left side by the RingProp at an approximate velocity of 5 mph. The only injury from test three was a small laceration to the left ear (Figure B.4).

Figure B.4 Laceration to the left ear from test three.

4.P2S5R

Porcine specimen two was impacted on the right side for test four with the standard propeller at an approximate velocity of 5 mph. The pig was secured in place for the longitudinal hit using three strings and weights for negative buoyancy. No injuries were seen in the external examination or the dissection.

5.P3R15L

In this test, pig three was impacted on the left at an approximate velocity of 15 mph using the RingProp. During the impact, the RingProp broke, with the ring portion coming completely off the three blades (Figure B.5). There was a large laceration to the hindquarters of the pig (Figure B.6), along with a laceration near the orbit. There was an accompanying fracture to the left zygoma (Figure B.7).

Figure B.5 Broken ring from test five.

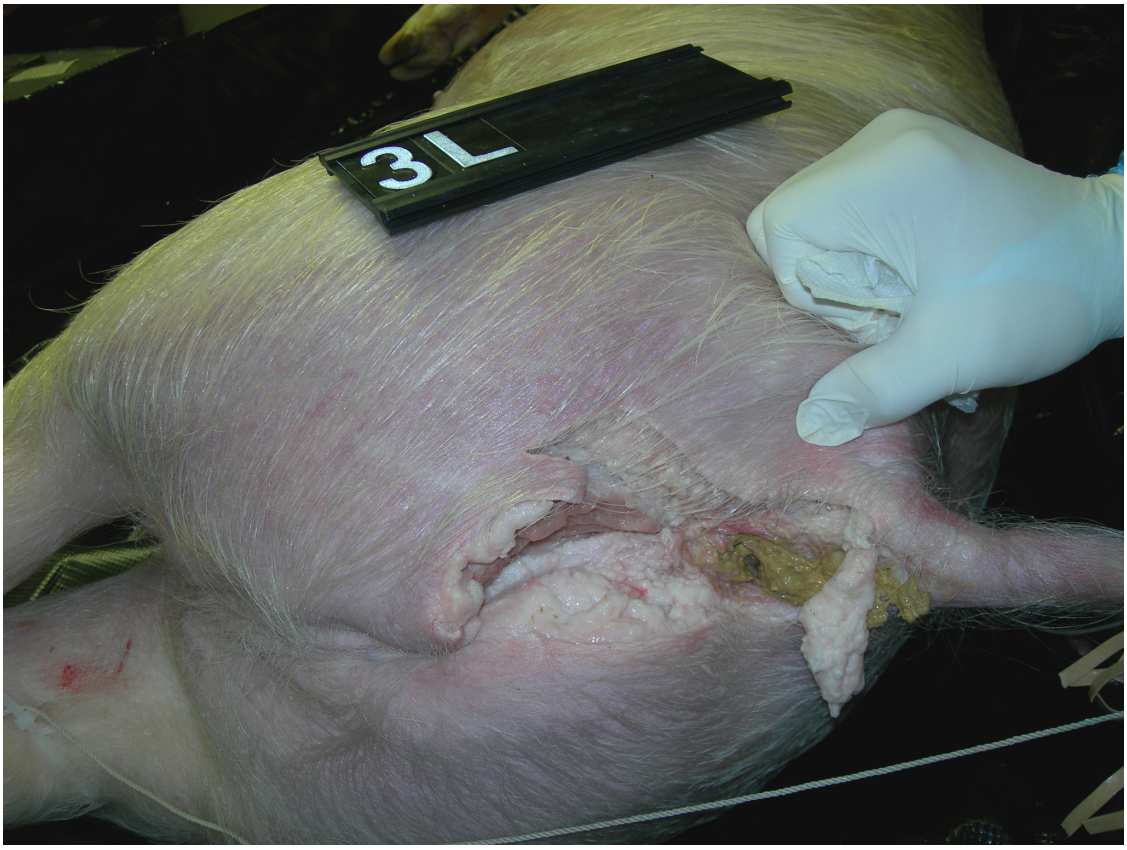

Figure B.6 Large laceration to left flank from test five.

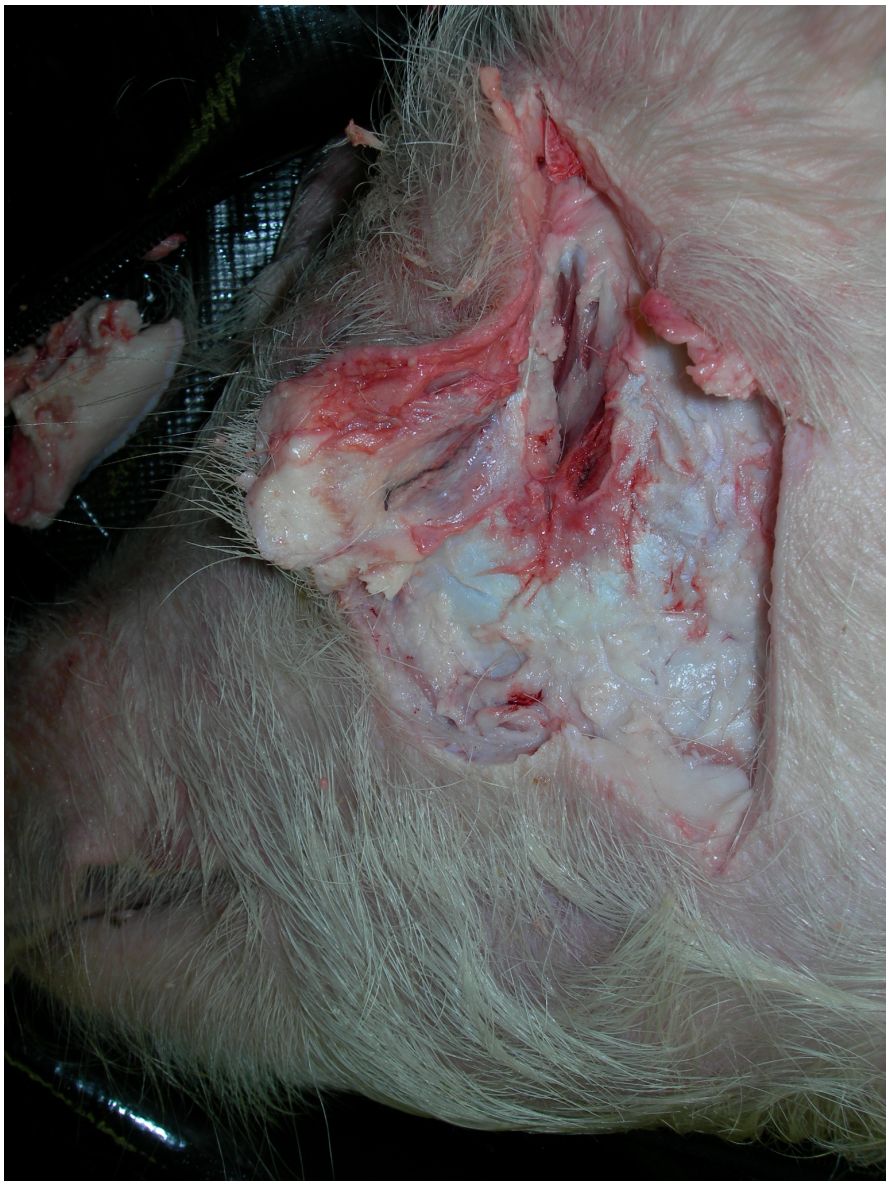

Figure B.7 Small fracture to zygoma.

6.P3S15R

This test was conducted at 15 mph using porcine specimen three, this time on the right side and with the standard propeller. While there were no open wounds from the impact, there were approximately 13 linear indentations in the right side (Figures B.8 and B.9). Upon dissection, there were eight rib fractures associated with the linear indentations (Figure B.10) and areas of muscle shearing (Figure B.11).

Figure B.8 Linear creases from standard propeller impact.

Figure B.9 Linear creases from standard propeller impact.

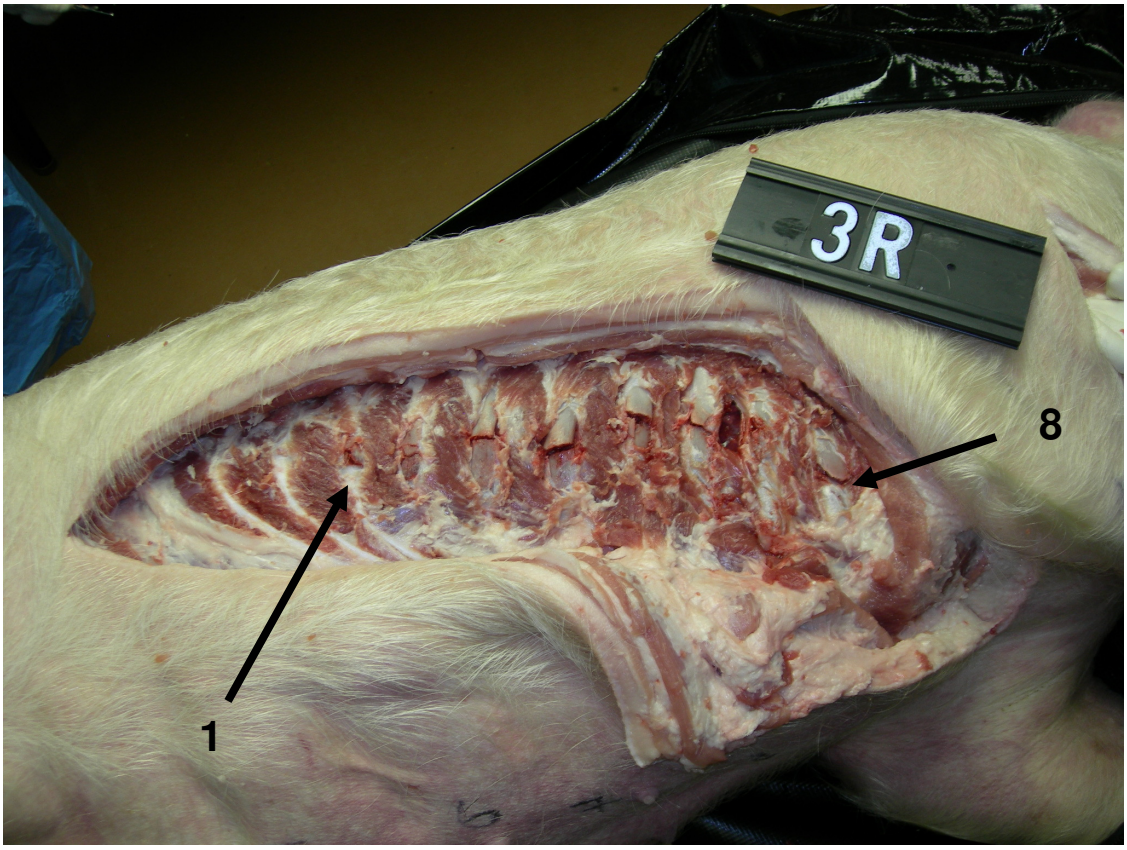

Figure B.10 Eight associated rib fractures.

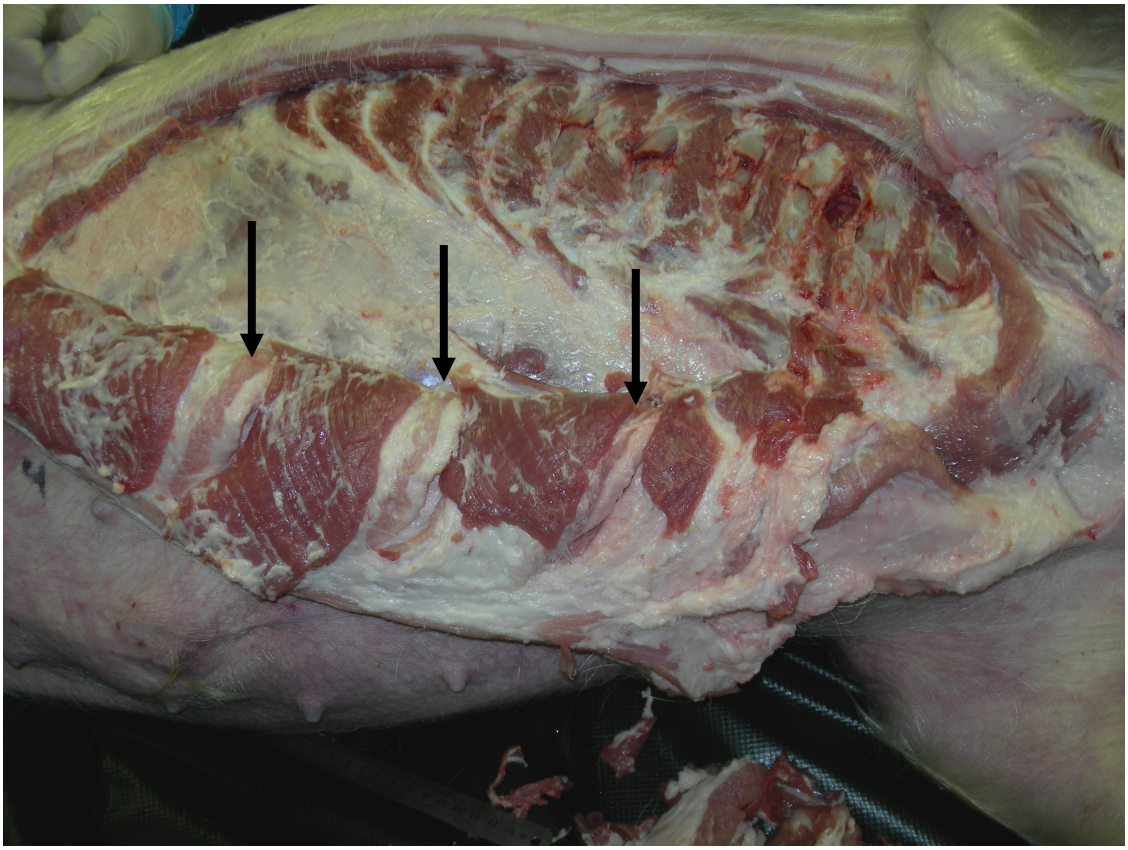

Figure B.11 Shearing of the abdominal muscles.

7.P4R15R

Test seven used porcine specimen four and the RingProp, impacting the pig on the right side at an approximate velocity of 15 mph. The RingProp was replaced after being damaged during test five. The pig was held in position using strings attached to the tail, right ear, and left ear. The injuries to the pig were a very large laceration of the right flank with avulsed muscle tissue (Figure B.11) and a large laceration to the right abdominal area (Figure B.12). A fracture of the right ulna was also present (Figures B.13 and B.14).

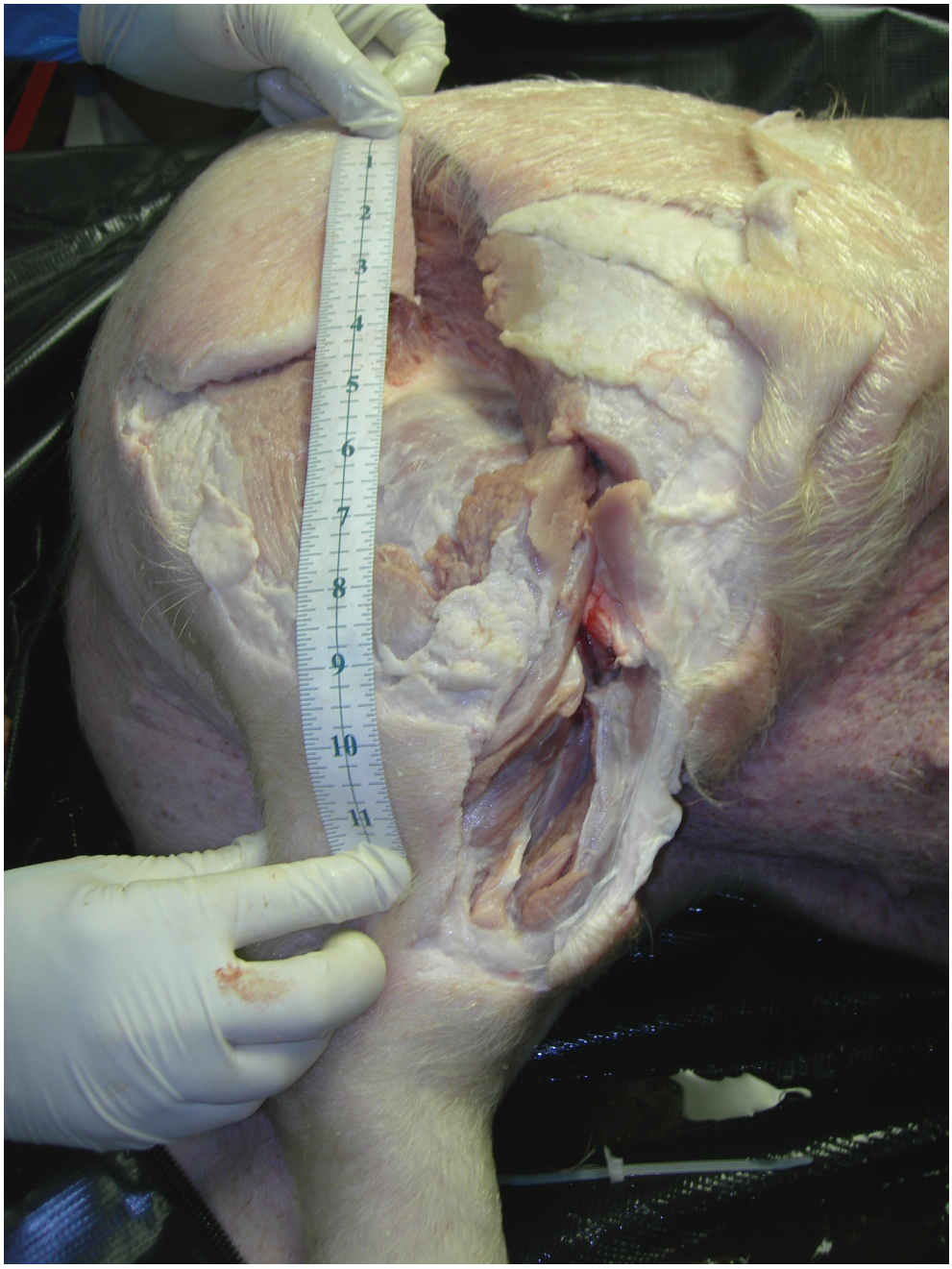

Figure B.11 Large laceration to soft tissue from test seven.

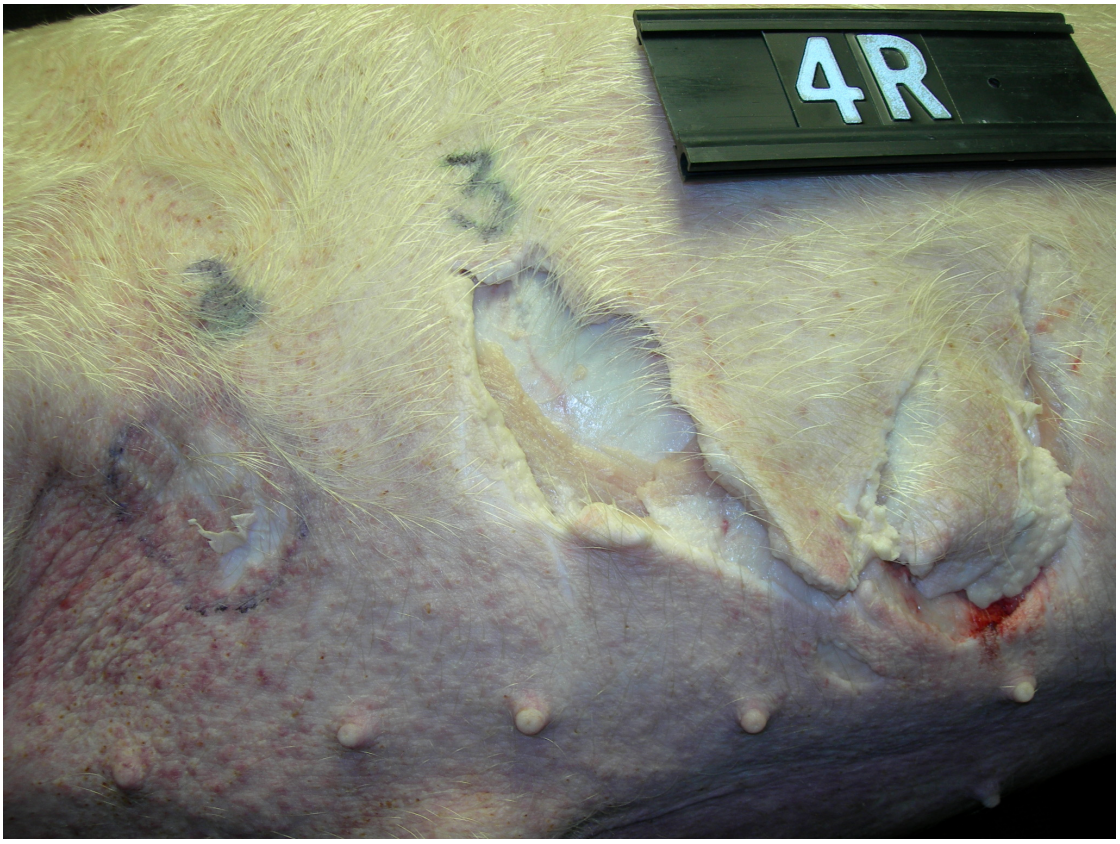

Figure B.12 Laceration and abrasions to the abdominal region.

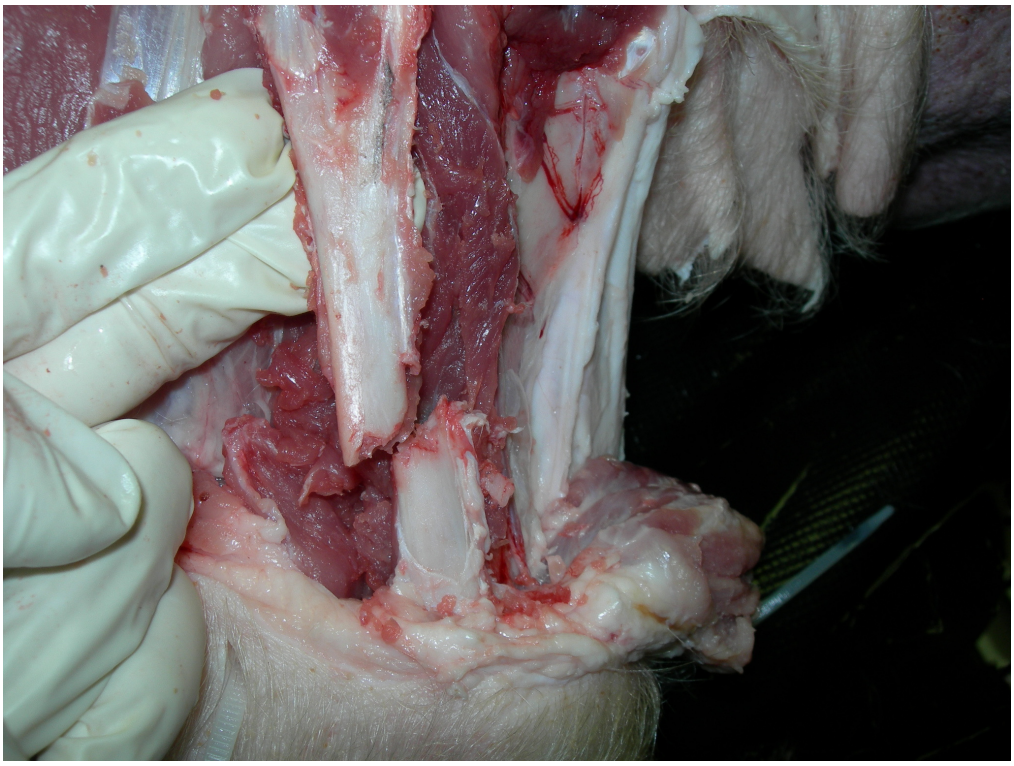

Figure B.13 Fracture of right ulna.

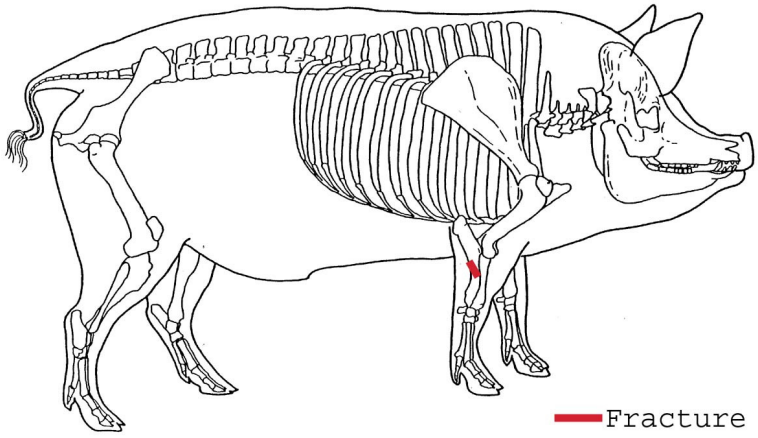

Figure B.14 Location of right ulnar fracture.

8.P4S15L

Porcine specimen four was tested on the left side with the standard propeller at an approximate velocity of 15 mph. The propeller had good engagement of the specimen. The injuries to the pig were numerous parallel lacerations to the left side (Figure B.15). Table B.1 describes each laceration. Many of the lacerations were very deep and cut down to the level of the bone.

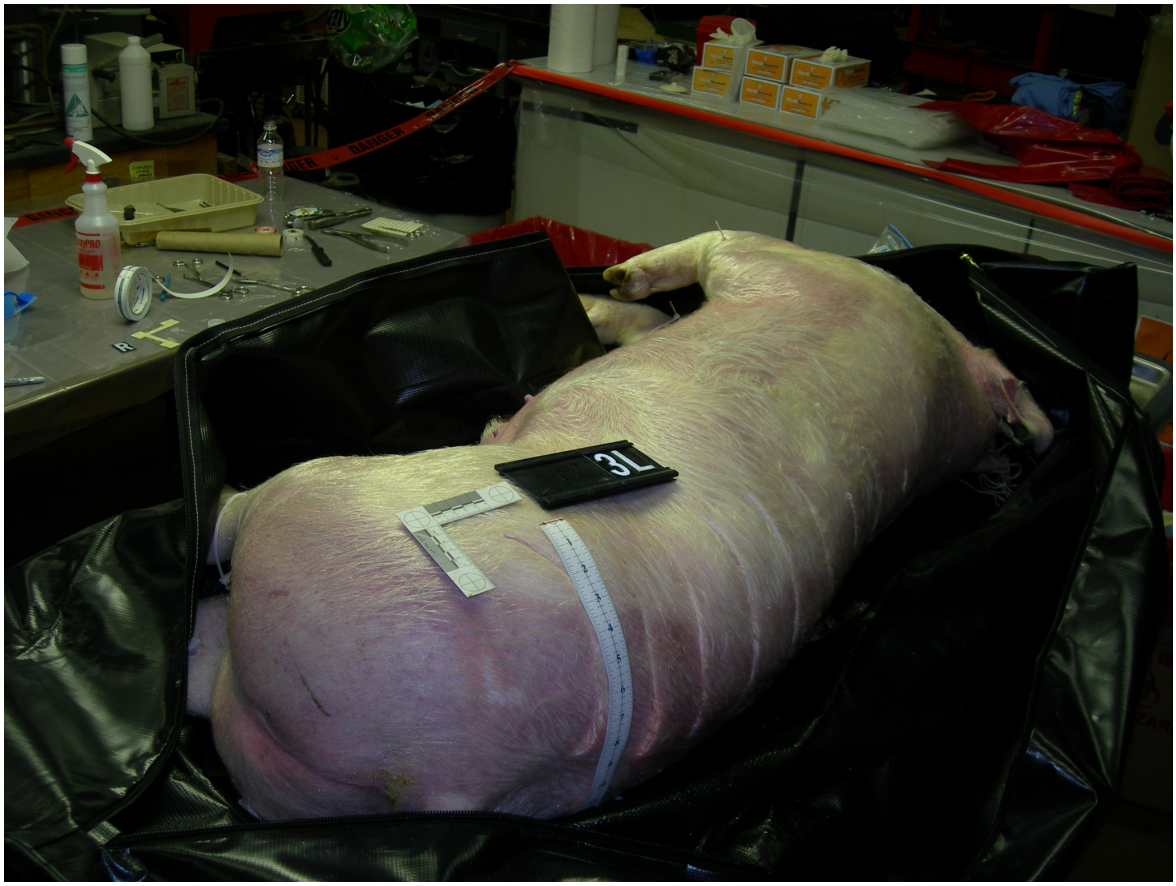

Figure B.15 Parallel lacerations from the propeller impact.

Table B.1 Laceration injuries from test eight.

Number	Type	Measure Anterior from Tail	Measure lateral of spine	Length	Depth	Notes
1	Abrasion	3cm	10cm	4cm	3cm	
2	Laceration	9cm	2cm	22cm	7-8cm	Cut to bone
3	Laceration	14.5cm	2.5cm	22.5cm	6.5-8.5cm	Cut to bone
4	Laceration	22cm	2.5cm	23cm	9.5cm	Cut to joint
5	Laceration	29cm	2.5cm	21cm	8.5cm	Cut to bone
6	Laceration	36cm	3cm	20.5cm	7cm	Cut to bone
7	Laceration	44.5cm	2.5cm	18.5cm	6.5cm	Cut to bone
8	Laceration	52.5cm	3cm	17cm	5cm	Cut to bone
9	Laceration	61cm	4cm	11cm	3.5cm	Cut to bone
10	Abrasion	70cm	3cm	9.5cm	1cm	
11	Abrasion	79cm	3.5cm	12cm	0.5cm	
12	Abrasion	88cm	2cm	15cm	2cm	
13	Abrasion/Laceration	102cm	3.5cm	9cm	0.25cm	
14	Laceration	~117cm	n/a – on ear	9cm	4cm	
15	Laceration	120cm	6cm	10cm	1.5cm	
16	Abrasion	131cm	2cm	7cm	1cm	

17.P5R1R

For this impact, pig five was impacted in the side by a reverse hit at 1 mph by the RingProp. The pig was positioned at a 40 degree angle in the water and held in place by three strings attached to the tail, the left ear, and the right ear. The motor was backed into the specimen at a slow speed with the motor running. There was no soft tissue or osseous damage to the pig.

18.P5S1L

This impact was also a rear hit at 1 mph. Porcine specimen five was also used, but this time the left side was impacted using the standard propeller. The pig was positioned under the water at a 40 degree angle, and held in place by the three strings. This test resulted in 4 abrasions to the epidermis in the abdominal region (Figure B.15). Even though the dermis was intact there were lacerations of the underlying soft tissue (Figure B.16).

Figure B.15 Four linear abrasions from rear impact.

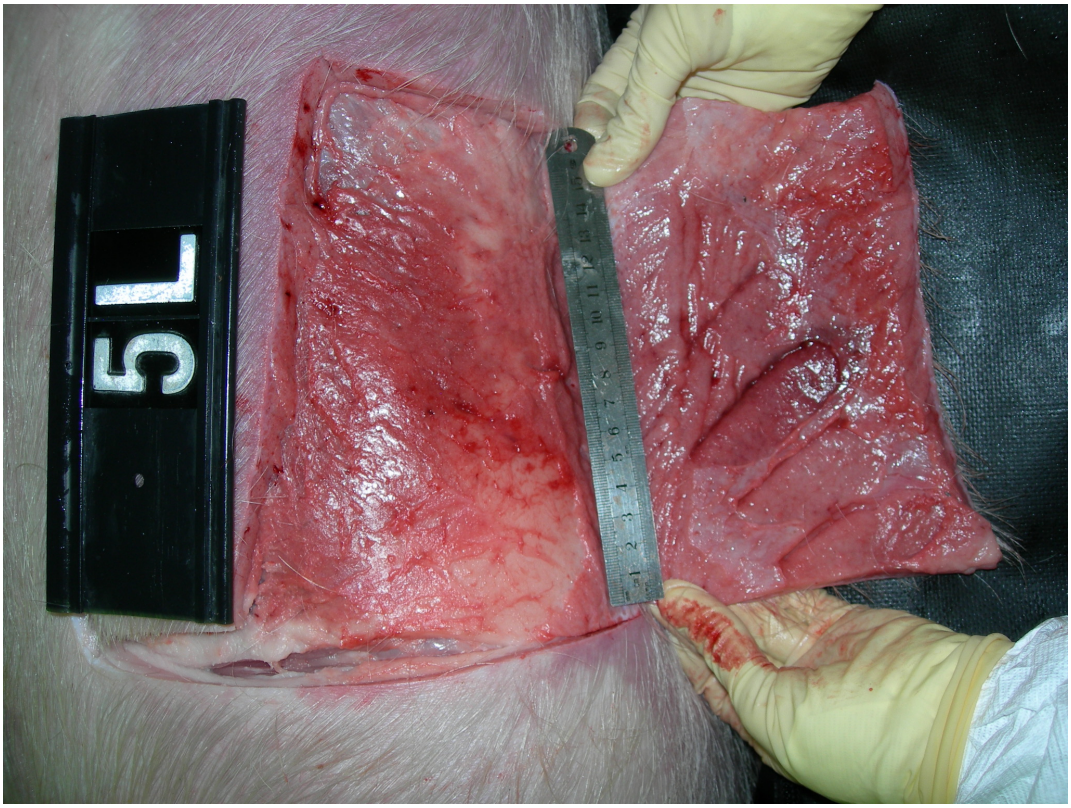

Figure B.16 Laceration to the underlying soft tissue.

19-P6R7R

Porcine specimen six was impacted with a perpendicular hit in the right side with the RingProp at an approximate velocity of 7 mph. The pig was positioned at 90 degrees in the water and secured using three strings. There was no soft tissue or osseous damage from this impact.

20-P6S7L

Pig six was impacted again, this time on the left side using the standard propeller at an approximate impact speed of 7 mph. Again, the pig was positioned at a 90 degree angle for a perpendicular hit. There was no soft tissue or bone damage from the impact.

Appendix C: Personal Watercraft Study

PWC Files 1 and 2.

The accident occurred on August 1996. It involved a six-year-old female, an eighteen-year-old female, and an eleven-year-old male. The six-year-old was riding in front of the eighteen-year-old on a PWC. The eleven-year-old male was riding a stand-up model PWC. He struck the females at a right angle on their left side.

The eighteen-year-old (**File 1**) sustained a fracture of her left proximal tibia, a fracture through the anterior proximal tibia with a level of tibial tubercle oblique fracture. The six-year-old (**File 2**) sustained a comminuted open fracture of her left tibia and fibula with a ten-centimeter laceration of the lateral maleollus. The x-rays were taken on the day of the accident.

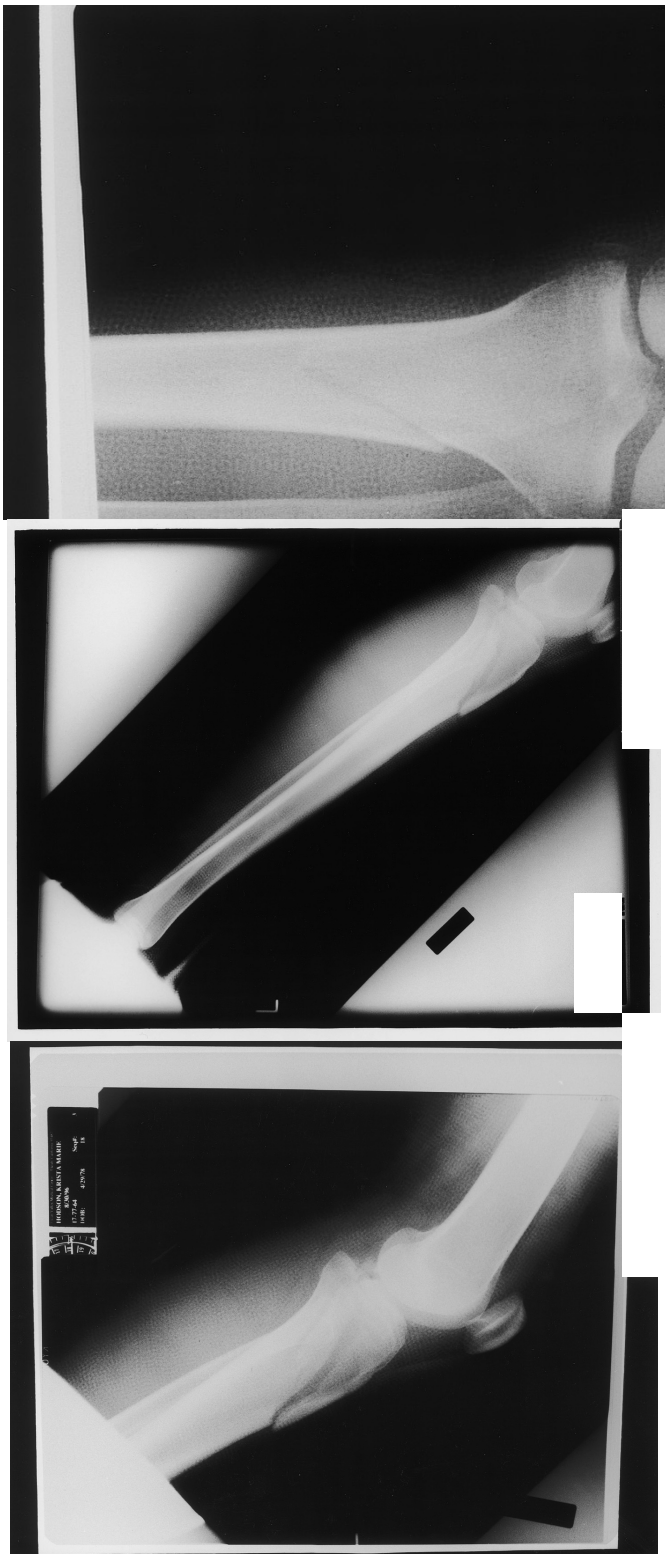

Figure C.1 Radiographs of PWC File 1

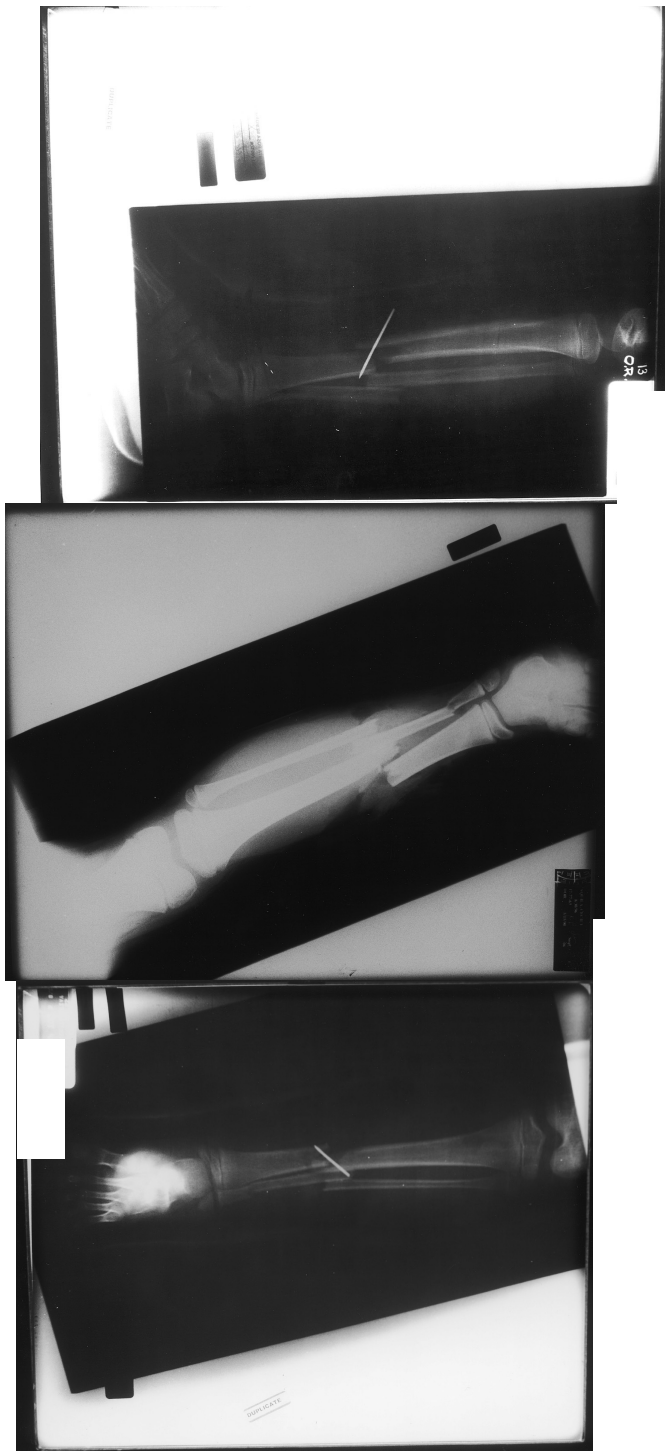

Figure C.2 Radiographs from PWC File 2.

PWC File 3.

This file involves a thirty-four year-old-female. She was riding a PWC in California on the day of the accident. A large wake from a passing yacht hit her PWC broadside. She heard her ankle snap as it hit the inside lip of the foot well. In a letter composed by the injured person to the personal watercraft manufacturer she stated her theory that “the foot well is too deep and narrow, which traps the foot in such a way that any severe jolt puts ones ankle in danger of being broken by the impact of the ankle hitting the adjacent lip of the boat”.

The first physicians to see the patient diagnosed an acute left ankle fracture. The physicians examine radiographs. The findings are that the film reveals a fracture involving the lateral malleolus with only slight displacement of the fracture fragments. The ankle mortise is intact. The impression is a fracture of the lateral malleolus.

On a later date, another physician wrote a report of his visit with the injured thirty-four year-old woman. He states that the woman is seen in orthopedic consultation as referred. In the report he writes that the x-ray films demonstrate an obliquely-oriented fracture involving the lateral malleolus. The ankle mortise appears satisfactory. There is also a 1.0 to 2.0 millimeter displacement of the fracture fragment. His diagnosis is a fracture of the left lateral malleolus. The mechanism that caused the fracture is from a bending motion.

Figure C.3 Radiographs from PWC File 3.

PWC File 4.

It involves a thirty-eight year-old-male riding a 1994 model of PWC. He was injured in a single vehicle accident. His injury consisted of a fracture of the medial tibial plateau on the left side. He also had a fracture of the head of the left fibula.

The medical records from the date of the accident show contain statements by the physicians that the injured man was seen in an outlying hospital and was found to have a proximal tibial fracture and was transported to the larger medical center. In the Emergency Room he was neurovascularly intact in the left lower extemity with obvious swelling of the knee. X-rays show a comminuted tibial plateau fracture. The patient was admitted for further assessment and definitive open reduction and internal fixation. The physicians assessment of the injury is a complex proximal tibial plateau fracture of the left leg.

The radiology report states that a fracture extending from mediolateral tibial plateau extending inferiorly is demonstrated. There are also multiple comminuted osseous fragments present. The fracture extends through all cortices. A depression of tibial spine by approximately one centimeter is demonstrated.

There are also multiple framents depressed on the medial and an avulsion of the tibial spine with fractures into the lateral side. In additon, the head of the fibula is avulsed off.

A consulting physician's report states that the patient's evaluation has shown that there is an extremely comminuted fracture of the proximal tibia with multiple fragments depressed on the medial side and avulsion of the tibial spine with fractures into the lateral side. He goes on to say that the patient is neurovascularly intact, though there have been some paresthesias in the lateral peroneal distribution and a little numbness.

The patient has a significant past history in that he has been diagnosed as having an 80% tear by arthroscopy on the knee that was injured. The physicians then says that he thinks the patient is unstable on the lateral side and that the head of the fibula is avulsed off. He will need to have lateral ligamentous complex opened up and a direct repair as necessary. He also thinks that he would then put on an external type of fixture to hold the multiple fragments. The patient will probably need a small medial incision to elevate the tibial plateau and probably will need bone grafting.

The radiology report from another physician states that there is approximately a one-centimeter lateral offset of the proximal tibia with regard to the tibial shaft, and there is a fracture line extending into the knee joint space itself.

The injured person testified in October two years following the accident that he was making a hard right turn when he fell off the PWC. He speculates that his leg was trapped and the fracture resulted from the leg hitting the "outside wall" of the personal watercraft.

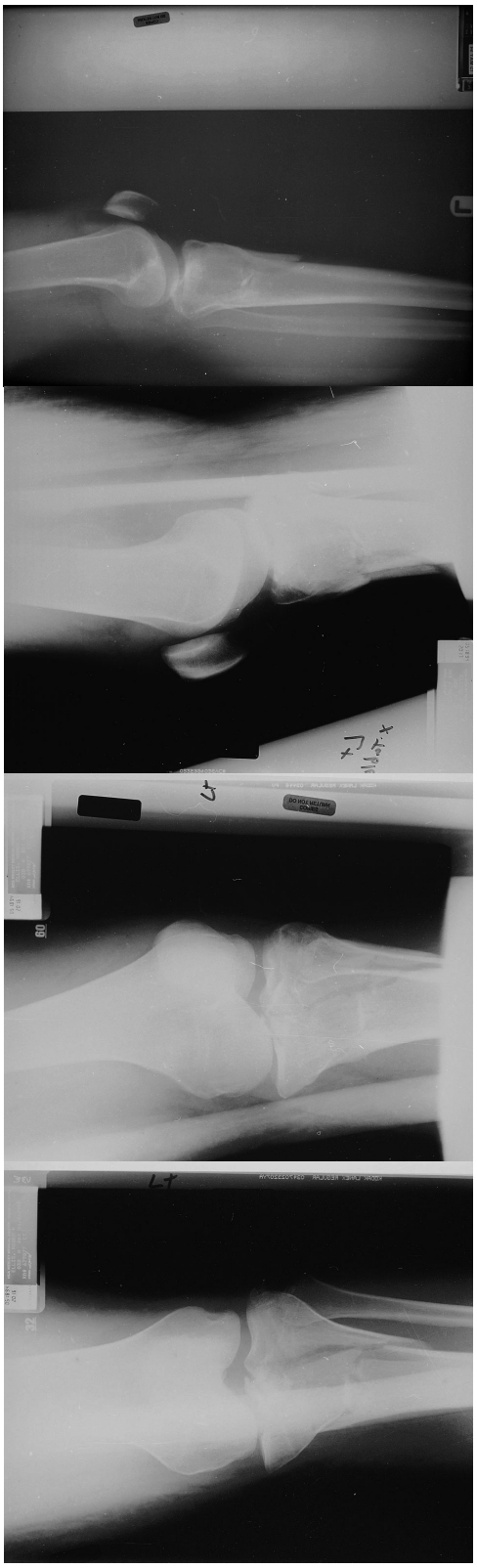

Figure C.4 Radiographs from PWC File 4.

PWC File 5.

The accident involved a thirty-two year-old-male riding a PWC. The emergency department's records state that the patient fell off his personal watercraft sustaining an injury to his right leg in which he could not bear any weight.

The physician stated that the x-rays of the tibia, fibula, and foot were done. The tibia/fibula x-ray shows a spiral fracture of the mid shaft of the fibula. It also shows a fracture/dislocation of the ankle with the tibia displaced laterally. There is also a possible fracture of the talus and fracture of the distal fibula. The foot x-ray did not confirm the talus fracture.

The physician informed the patient of the x-ray results and the need for immediate orthopedic consultations. He explained the possibility that he may need surgery and/or closed reduction that evening. The patient stated that since he lived closer to another hospital, he would prefer to be there in order for his family to not have as far to travel as well as to be closer for follow up visits. Therefore, the patient was given 25mg of Demerol and went by private vehicle to the alternate hospital. The lower leg was placed in a sugar tong splint with OCL, and his x-rays were copied and sent.

The clinical impression of the first physician was a fractured fibula, fractured ankle, and a fractured foot. An new physician agreed to accept transfer of this patient to the Emergency Room at the patient's request.

A radiology report was also written about the thirty-two year-old man's injury. Regarding the right tibia/fibula the radiologist states that the AP and

lateral views of the right tibia and fibula were submitted. He states that there is a comminuted, very minimally displaced fracture of the right fibular shaft at approximately the level of the mid and distal thirds. There is a mild anteromedial subluxation at the tibiotalar joint. The radiologist concludes that there is a comminuted fracture of the right fibular shaft, a posterior malleolar fracture, and subluxation of the right tibiotalar joint.

Regarding the right ankle, he says that three views of the right ankle were obtained. He goes on to say that there is a comminuted fracture of the shaft of the right fibula. There is a chip fracture off of the posterior malleolus, the avulsed fragment measuring approximately 1.5 x 1 centimeter. There is partial subluxation anteromedially at the right tibiotalar joint. The radiologist concludes of the right ankle that there is a small chip fracture of the posterior malleolus, an anteromedial subluxation of the right tibiotalar joint, and a right tibial shaft fracture.

Concerning the right foot, the radiologist states that there are fractures of the right fibula, right posterior malleolus and subluxination at the right tibiotalar joint. Otherwise, no bony abnormalities are seen in the bones of the right foot.

At the new hospital, a physician wrote a report of the injured man. He states that multiple views were obtained of the right ankle and lower one-half of the lower leg. He says that there is a comminuted fracture through the mid-distal junction of the right fibula. The fracture has a minimally displaced oblique component. The longitudinal component of the fracture also seen with its proximal most aspect is not fully delineated on the images.

The physician continues to say that there is a fracture through the posterior malleolus of the tibia as demonstrated on the lateral view. There also are small avulsion fragments from the tip of the medial malleolus. Small bony densities also project over the medial joint space on one of the AP views. These fracture fragments are neither seen on an additional AP view nor on an internal oblique view. Also, there is widening of the medial joint space in the ankle.

The impression of the physician is that there is a comminuted fracture through the mid to distal fibula, a fracture through the posterior malleolus of the tibia, a small avulsion fragment seen distal to the medial malleolus. He also suspects avulsion fracture fragments in the medial joint space. Lastly, he notes the relative widening of the medial joint space.

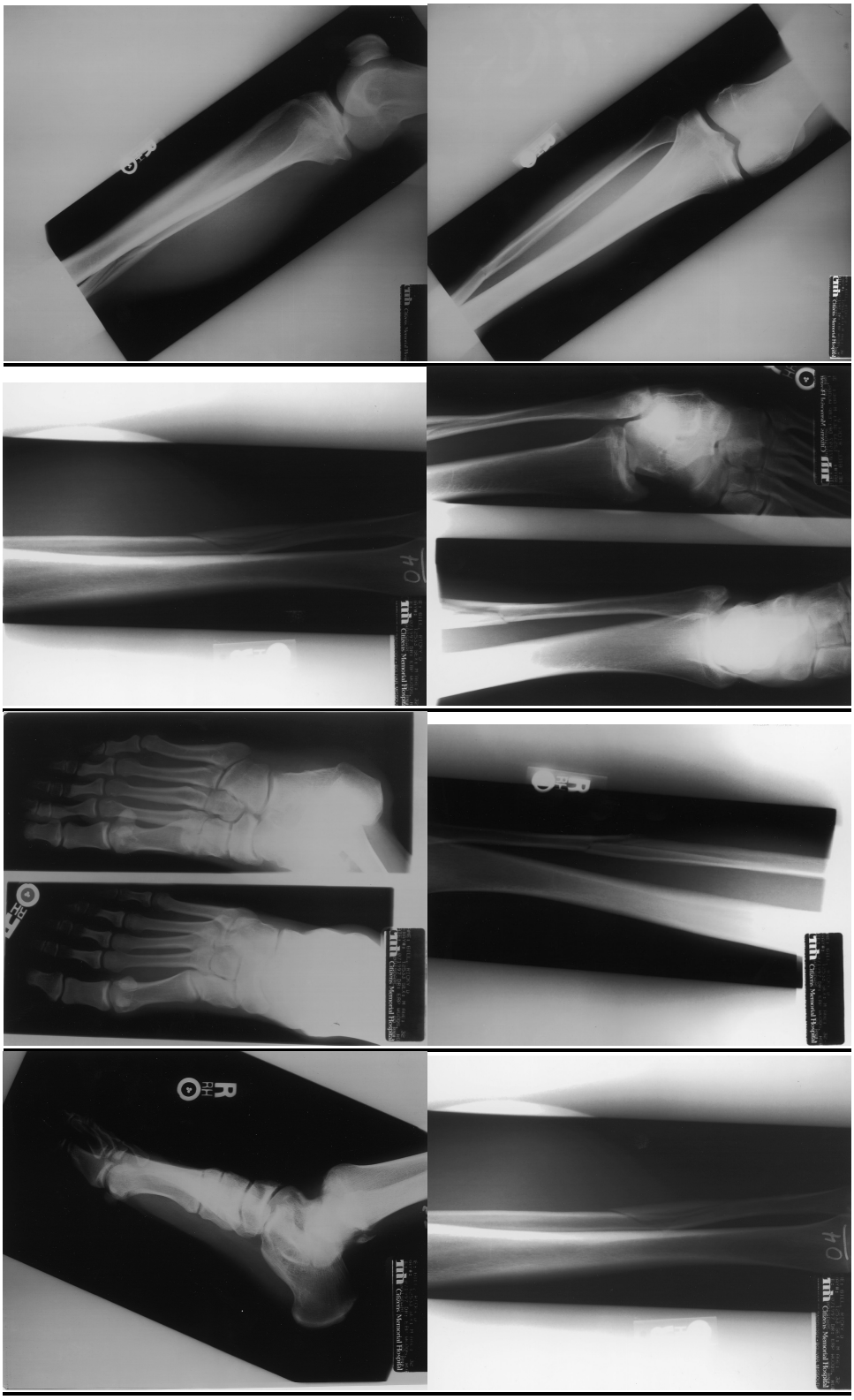

Figure C.5 Radiographs from PWC File 5.

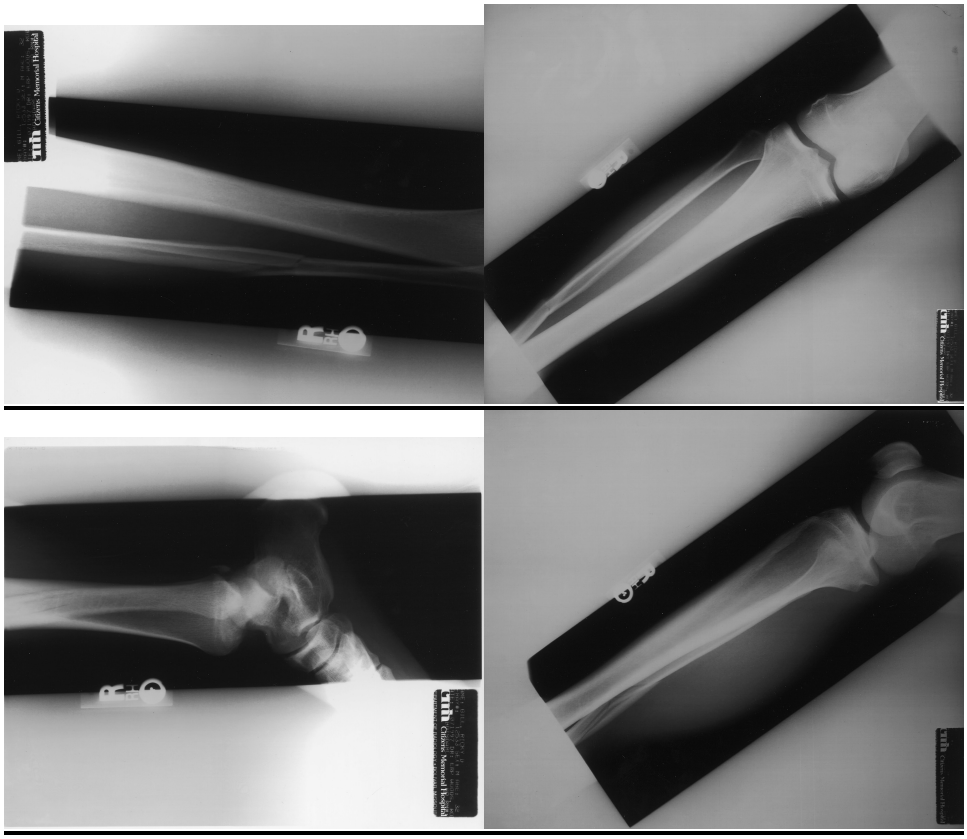

Figure C.6 More Radiographs from PWC File 5.

PWC File 6

It involved a twenty-six year-old-female. The woman owned and was operating a 1993 model of PWC on a lake. The final diagnosis by a physician seeing the patient at a hospital after the accident is a bimalleolar fracture of the right ankle with displacement. The fracture was likely open, which related to a pinpoint wound overlying the medial malleolus.

The radiology report for the right ankle from three views show that there are fractures of the medial malleolus, the distal fibula, and a nondisplaced fracture of the posterior malleolus. There is a slight lateral subluxation of the talus.

In a letter from the injured woman's attorney, he states that while the woman operating the personal watercraft on the day of the accident was, "traveling at a relatively slow speed, she hit a wave and the handlebars on the jet ski jerked completely out of both of her hands. The jet ski jerked to the left, and her momentum continued to carry her forward. Her right ankle became entrapped in the foot well of the jet ski, and as the jet ski turned to the left, her ankle broke."

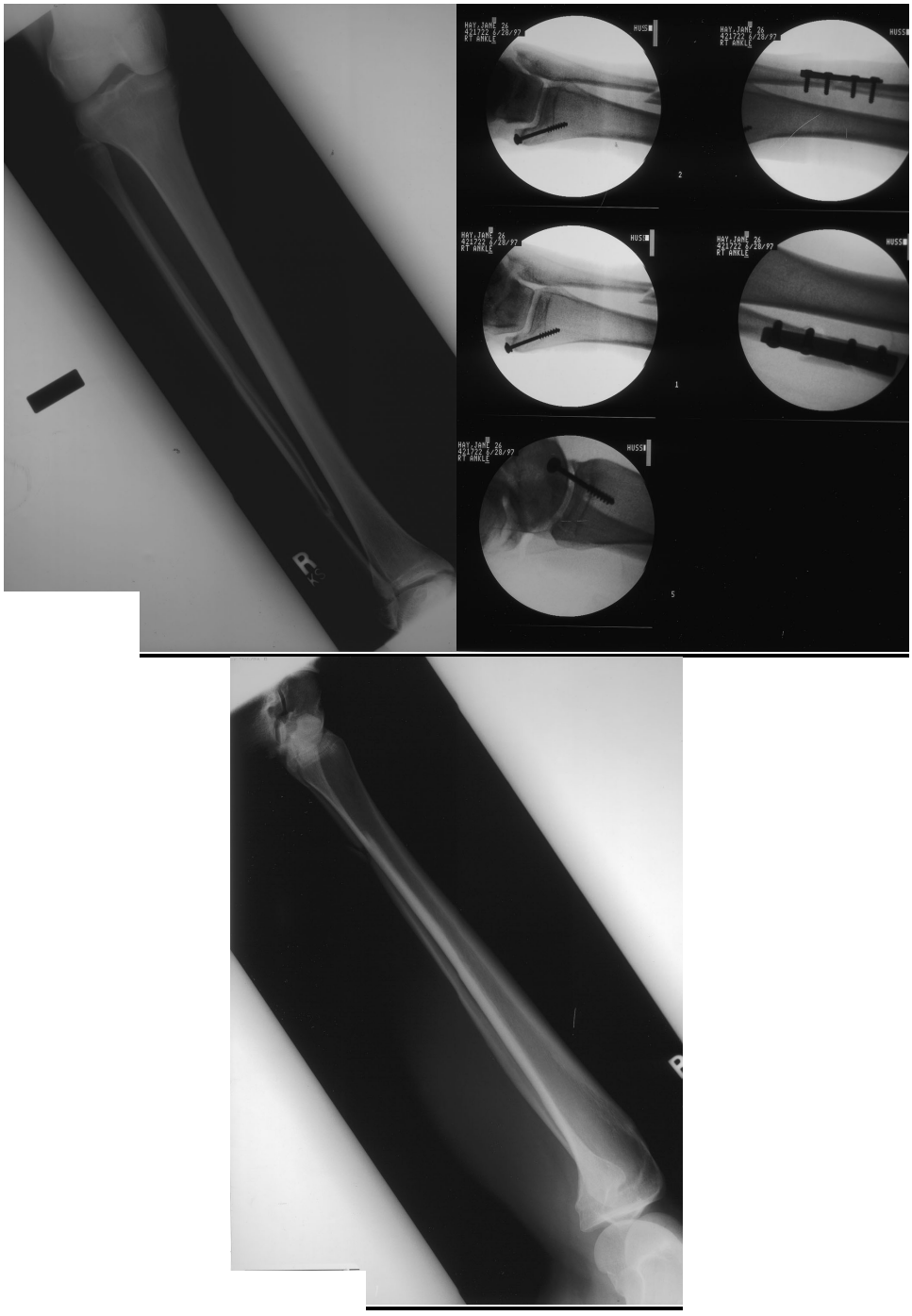

Figure C.7 Radiographs from PWC File 6.

PWC File 7

The person injured is a thirty-eight year-old female in an accident that occurred in 1996. She was the passenger behind her fourteen year-old son on a 1995 PWC. The radiology report from the hospital shows the knee from four views. The physician describes the injury as a left tibial lateral plateau depressed fracture (depressed 3-4 millimeters). His impression is that there is a left lateral tibial plateau fracture, which appears depressed.

The surgeon states that her final diagnosis is a depressed, comminuted displaced lateral tibial plateau fracture of the left knee. The woman also sustained a torn lateral meniscus.

Legal Counsel on behalf of the injured woman. In the letter, the attorney states " the personal watercraft allegedly performed a nose dive. Thereafter, both the claimant and her son were thrown off the vehicle such that the claimant alleges her lower leg became entrapped in the foot well." According to the physician this is a valgus strain, which means that a lateral bending moment caused the impaction of the tibial plateau.

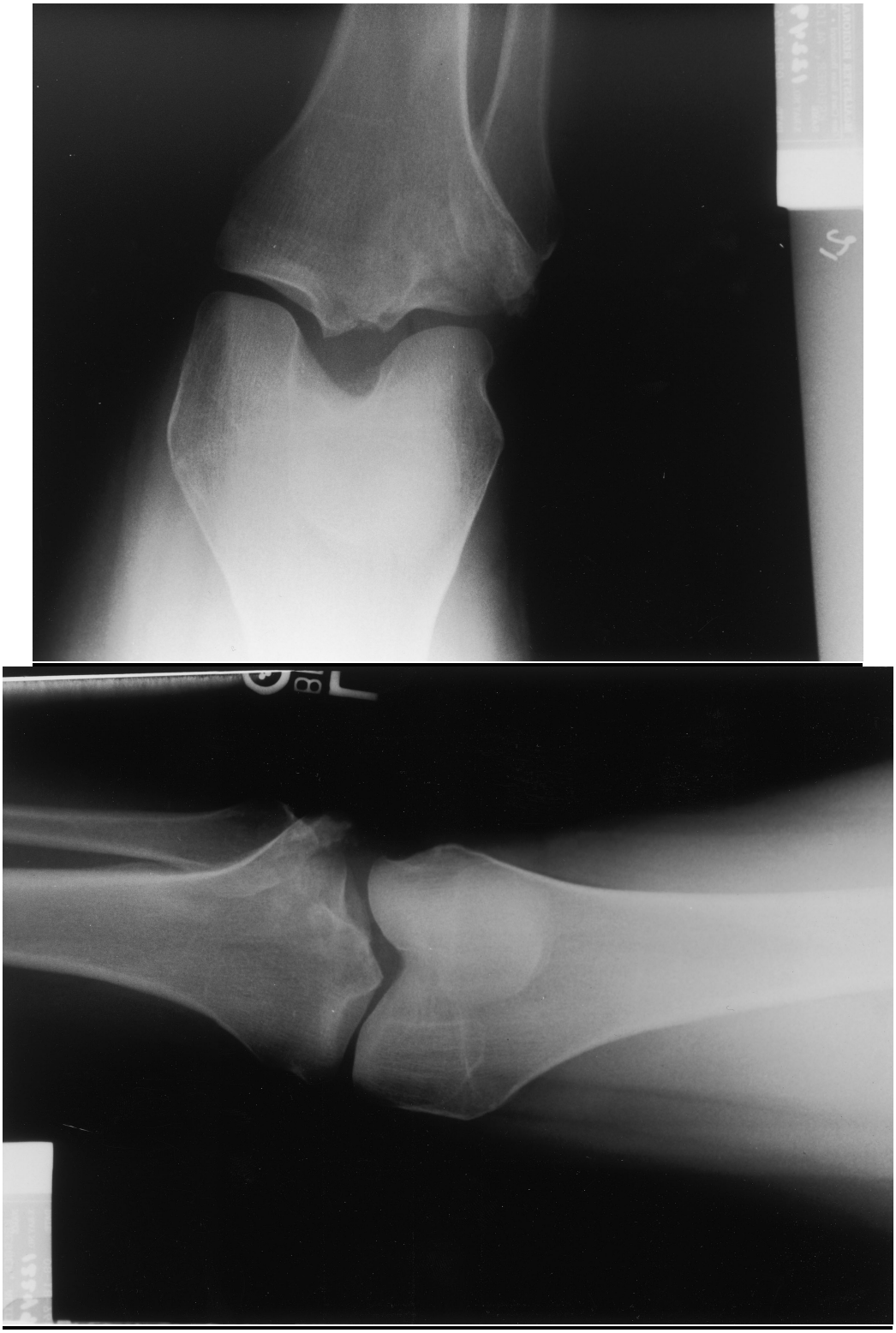

Figure C.8 Radiographs from PWC File 7.

PWC File 8

This file involved a forty year-old male. He was riding a 1994 PWC with his eighty-five pound daughter in front of him, and his one hundred-six pound wife behind him. As the three were at an idling speed, a three-foot wake from another boat hit the side of their personal watercraft. The man's left leg snapped as he and the others fell off the personal watercraft on the left side.

The injured forty-year-old male was taken to the emergency room after the accident. The emergency room report states that the A.P. and lateral views of the lower leg were obtained. An acute spiral type fracture is seen extending through the distal shaft of the left tibia. The A.P. view demonstrates mild displacement of the distal fracture fragment in relation to the proximal shaft fragment by approximately thirteen millimeters. The lateral view demonstrates posterior displacement of the distal fracture fragment in relation to the proximal shaft fragment by approximately four millimeters. An acute comminuted fracture is also seen involving the mid shaft of the left fibula. There is approximately seven millimeters of maximum displacement as seen on the lateral view. The impression is of acute fractures involving the shaft of the left tibia and left fibula.

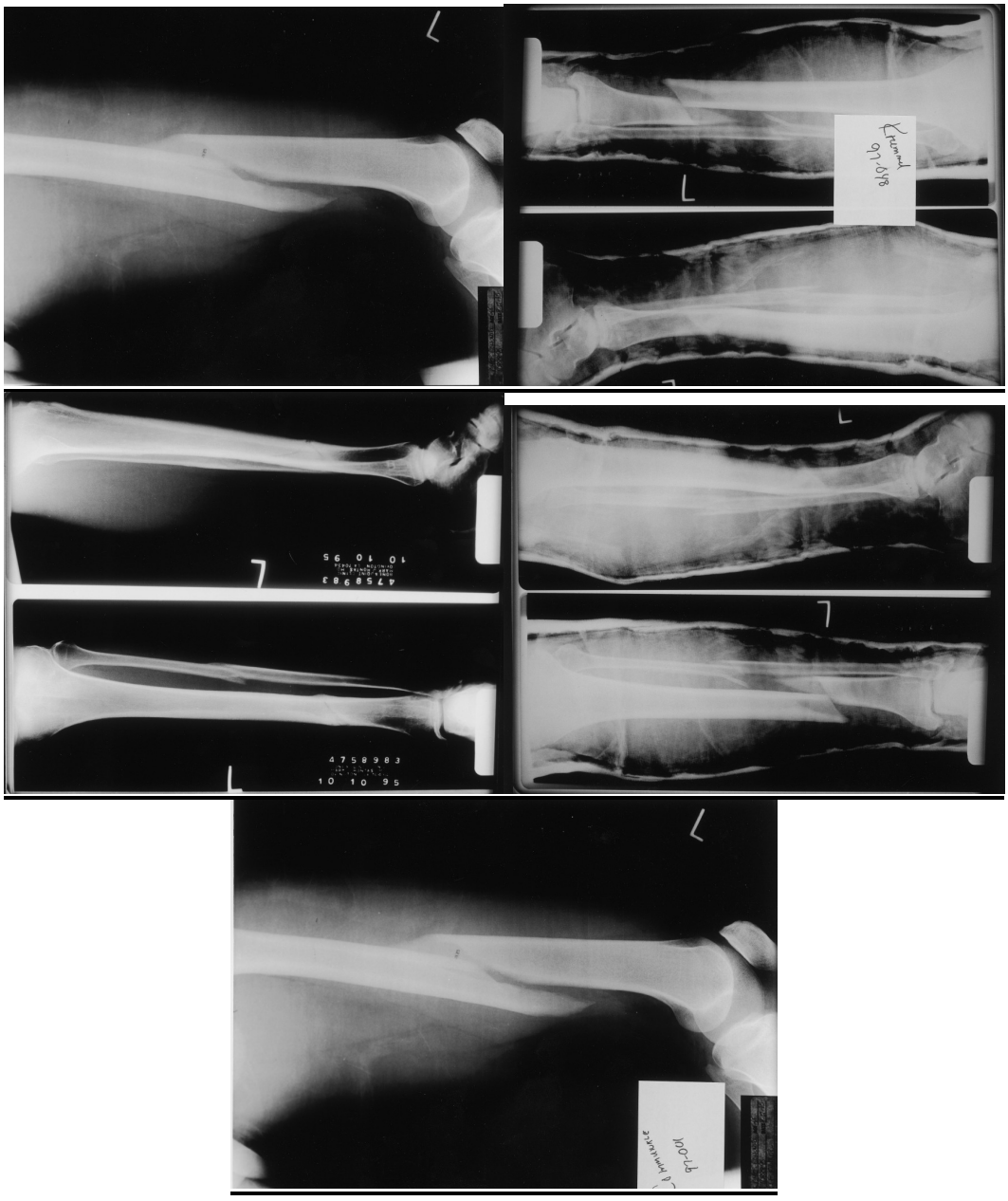

Figure C.9 Radiographs from PWC File 8.

PWC File 9

This accident involves a thirty-seven year-old-male on a 1994 model PWC. Apparently, the man that was injured was riding with two other men at the time of the accident. He claims that while traveling at approximately twenty-five miles per hour, a three-foot wave hit the personal watercraft sending the PWC to the right as he fell to the left. He claims that his leg was trapped in the foot well causing the breaking of his left leg.

The thirty-seven year-old was taken to the hospital. The radiology report states that there is a spiral fracture of the distal shaft of the left tibia with a lateral and posterior displacement of the distal fracture fragments. There is also a comminuted fracture of the proximal shaft of the fibula.

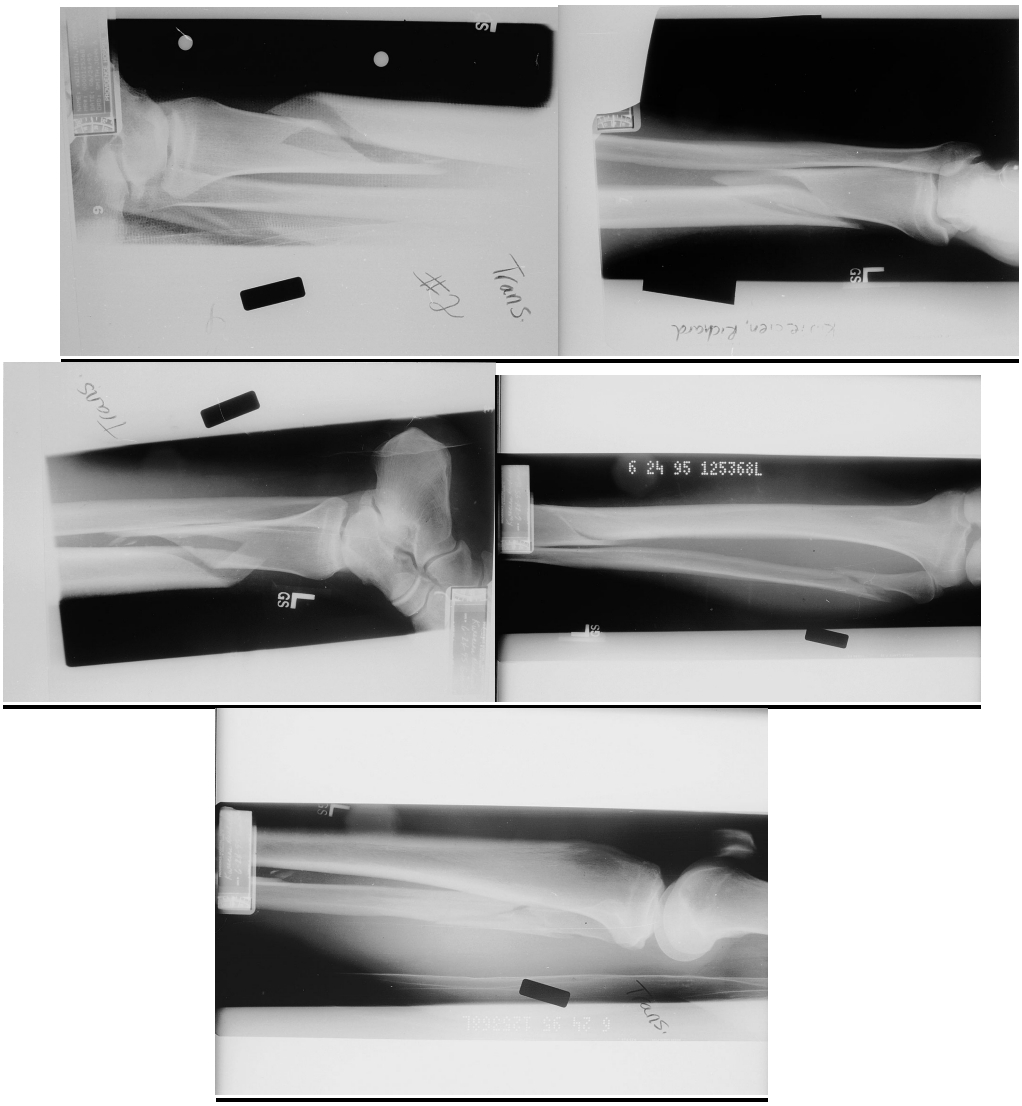

Figure C.10 Radiographs from PWC File 9

PWC File 10

A fifty-seven year-old male was riding a PWC when he hit a wake and was thrown upward as the PWC tilted vertically. Then he came down hard landing back on the seat. The patient was taken first to a regional hospital and seen by an attending physician. However, due to his loss of a testicle, he was transferred to a larger hospital for plastic surgery to be performed on the scrotum. In addition to the testicular trauma, the patient also had an open left tibial plateau fracture.

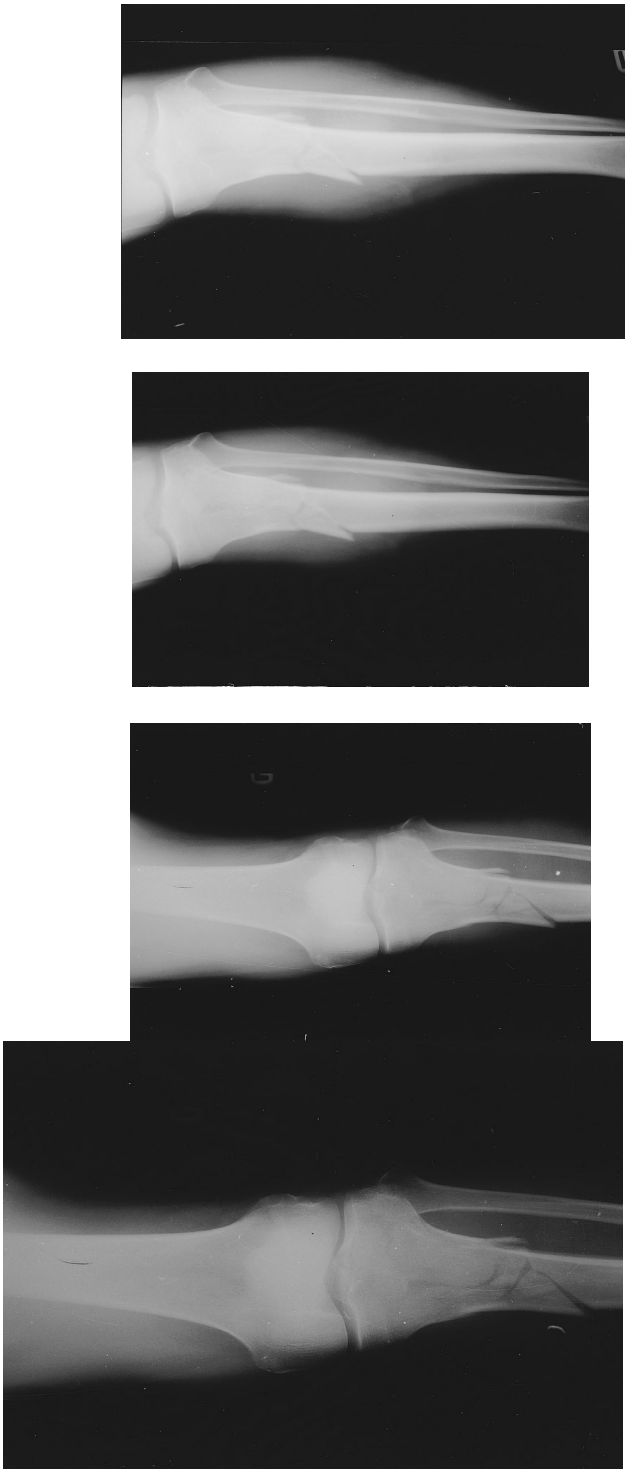

Figure C.11 Radiographs from PWC File 10.

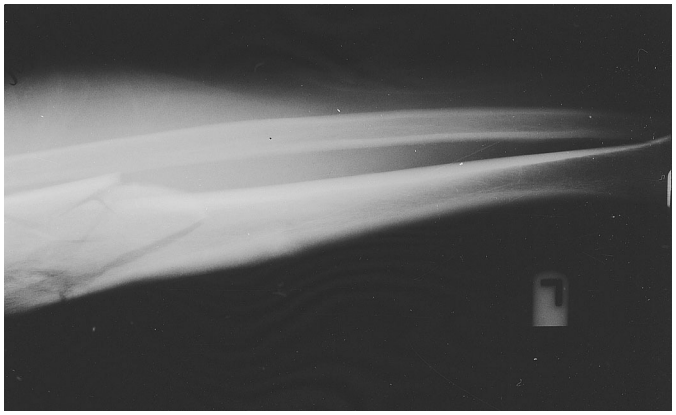

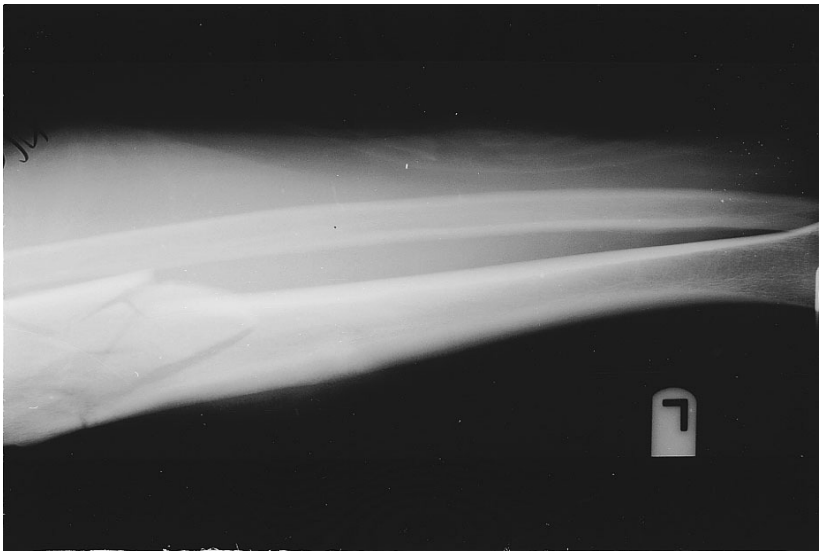

Figure C.12 More radiographs from PWC File 10.

PWC File 11

The file consists of only x-rays, therefore there is no story behind the accident or the injured person. Orthopedic surgeon diagnosed the injury as an oblique spiral fracture of the left distal fibula.

Figure C.13 Radiographs from PWC File 11.

PWC File 12

A twenty-four year-old male was riding his PWC at sixty miles per hour in a straight path. The man hit a wave and lost control, sending him over the handlebars. The patient's injuries consist of a very comminuted fracture of the lateral malleolus and a very thin fairly large post medial butterfly fragment.

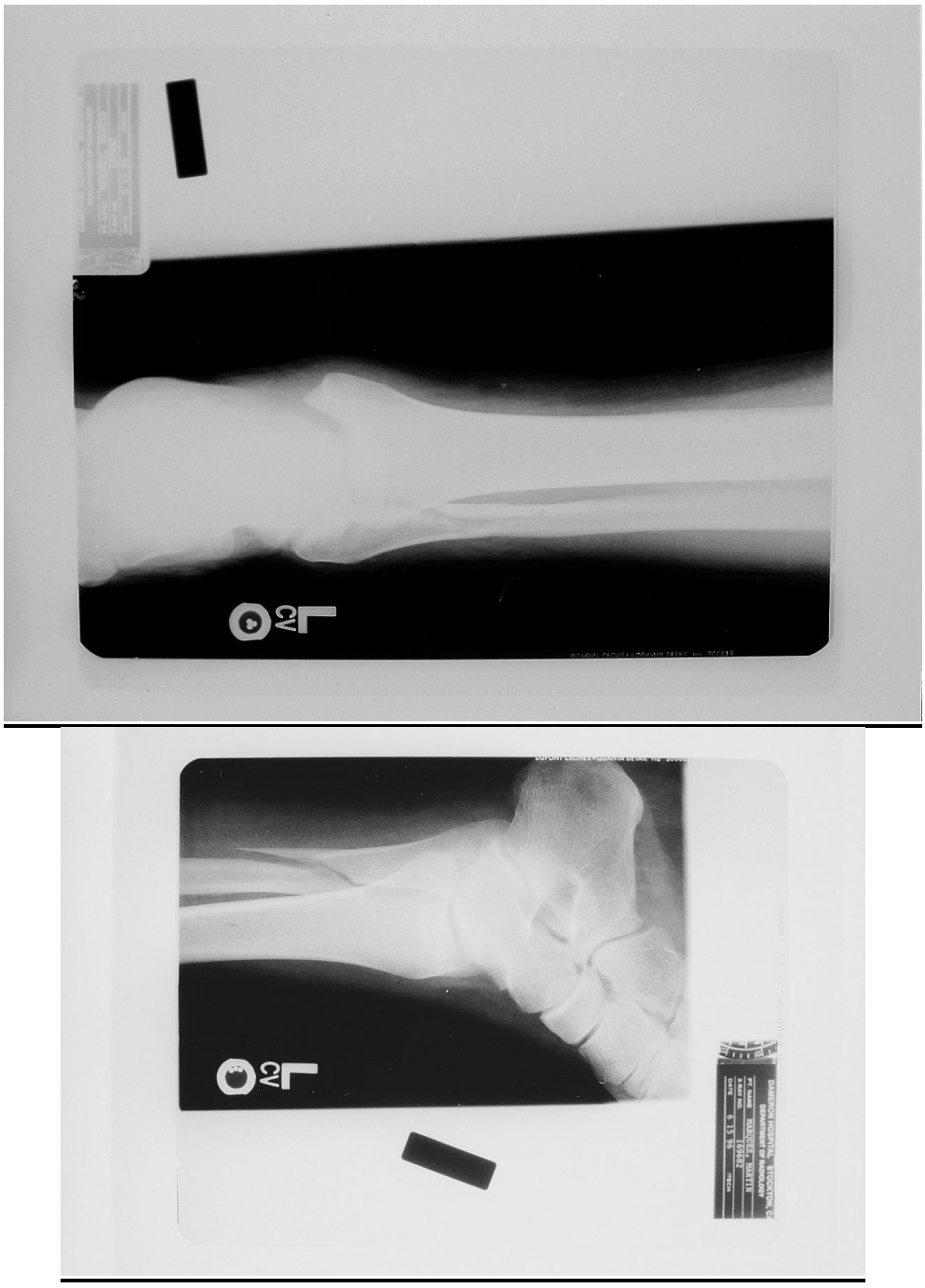

Figure C.14 Radiograph from PWC File 12.

PWC File 13

The sixteen year-old male was riding a PWC. According to a witness, the young man made a very quick turn to the left, throwing him off to the right side of the vessel. As his body went to the right, his left leg was still in the craft going left with the personal watercraft. He was taken to the hospital. The radiologist discussed the injuries to the right tibia and fibula. He stated that there is a Salter IV fracture of the distal tibia. The fracture extends obliquely through the lateral aspect of the distal tibial metaphysis and through the physis as well as the epiphysis. Some posterior and lateral displacement of the fracture fragment is noted. There is an associated oblique displaced fracture of the distal fibular diaphysis. In addition, there is marked soft tissue swelling associated with the fracture.

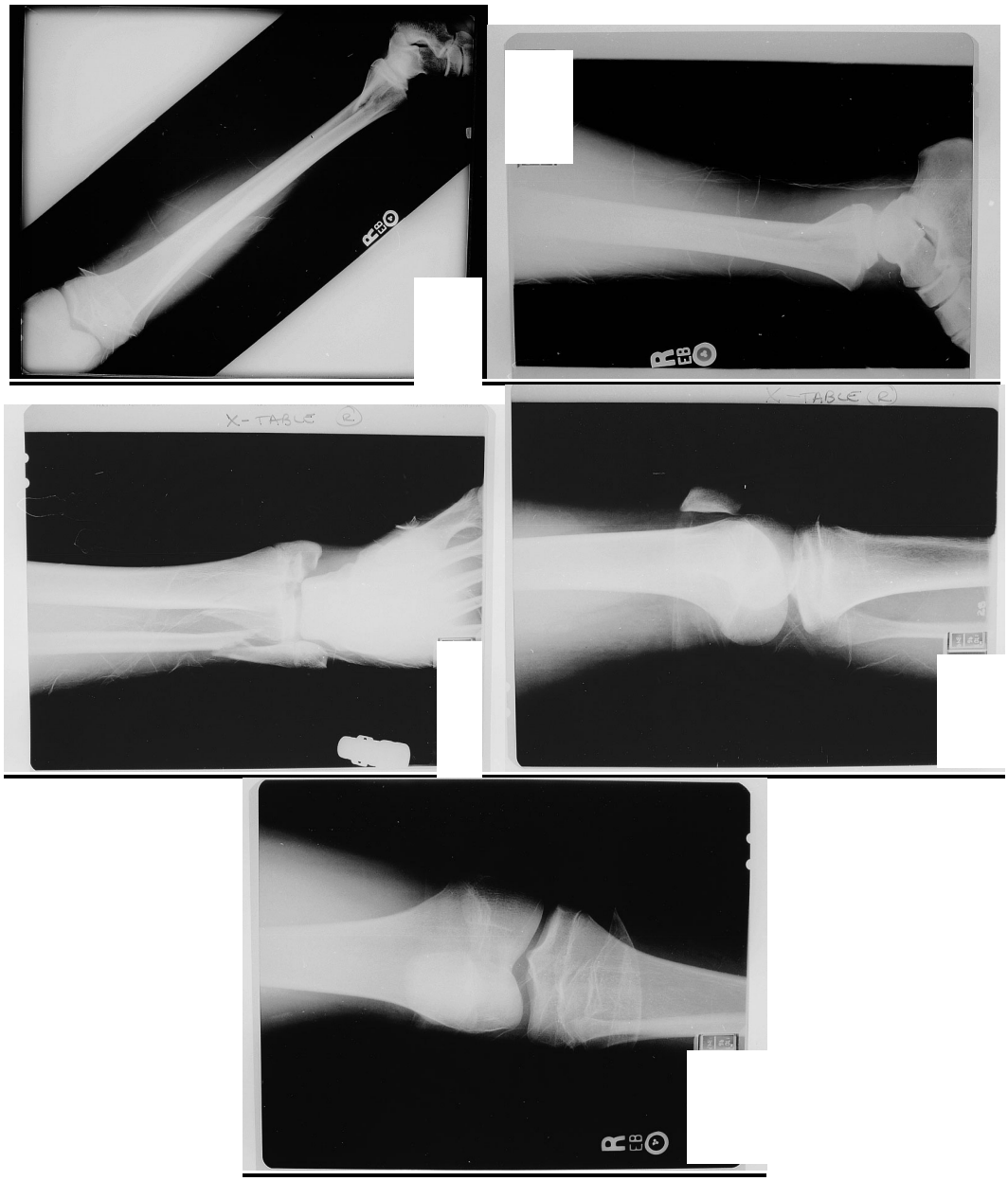

Figure C.15 Radiographs from PWC File 13.

PWC File 14

It involves a thirty-seven year-old male. He was riding a PWC when he made a sudden left turn while traveling between twenty and forty miles per hour. The radiologist states that there is a trimalleolar fracture of the left ankle. There is slight disruption of the ankle mortise, and the talus and calcaneous appear intact.

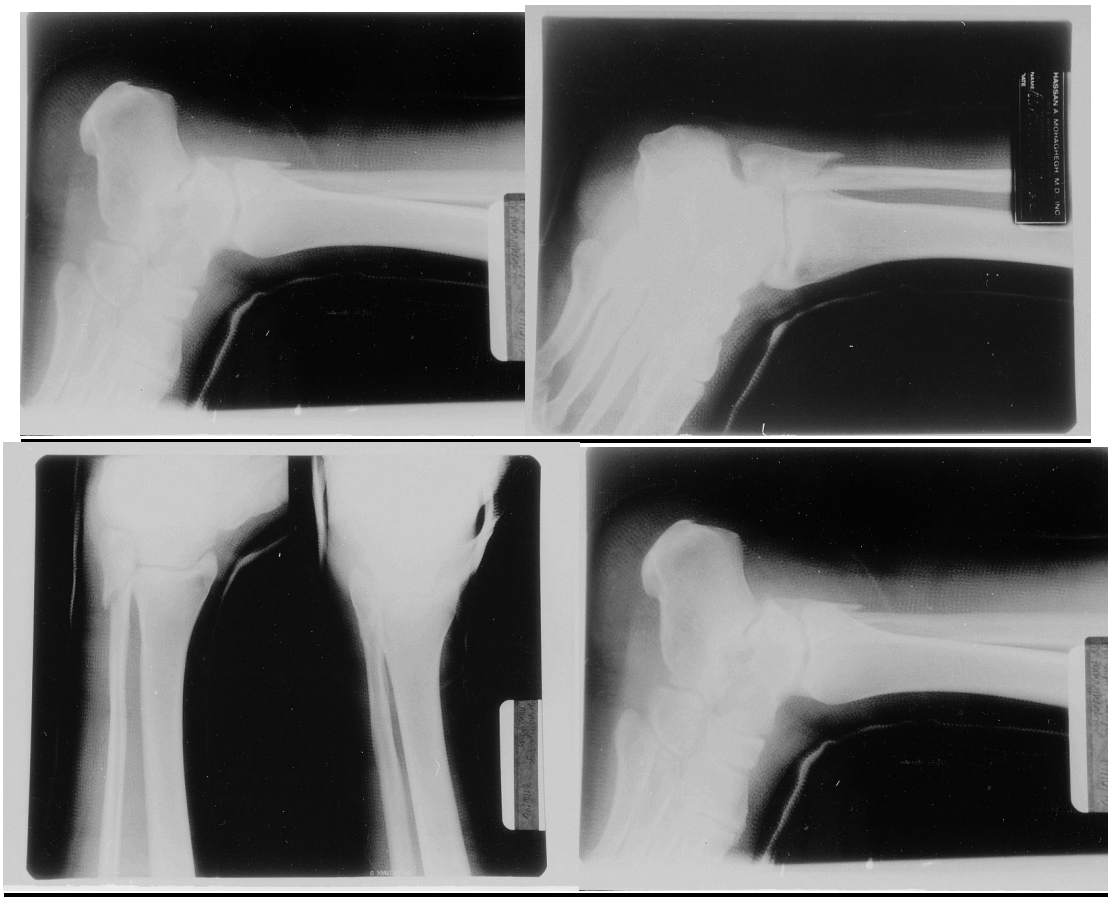

Figure C.16 Radiographs from PWC File 14.

PWC File 15

This accident involves a thirty-four year-old male. There is no explanation of the accident but there is an emergency room x-ray report in which the injury is described as a trimalleolus fracture/dislocation with posterior displacement of the talus. Furthermore, there is a displaced oblique fracture of the posterior malleolus, a non-displaced transverse fracture of the medial malleolus, and an oblique fracture of the distal fibula with lateral displacement distally.

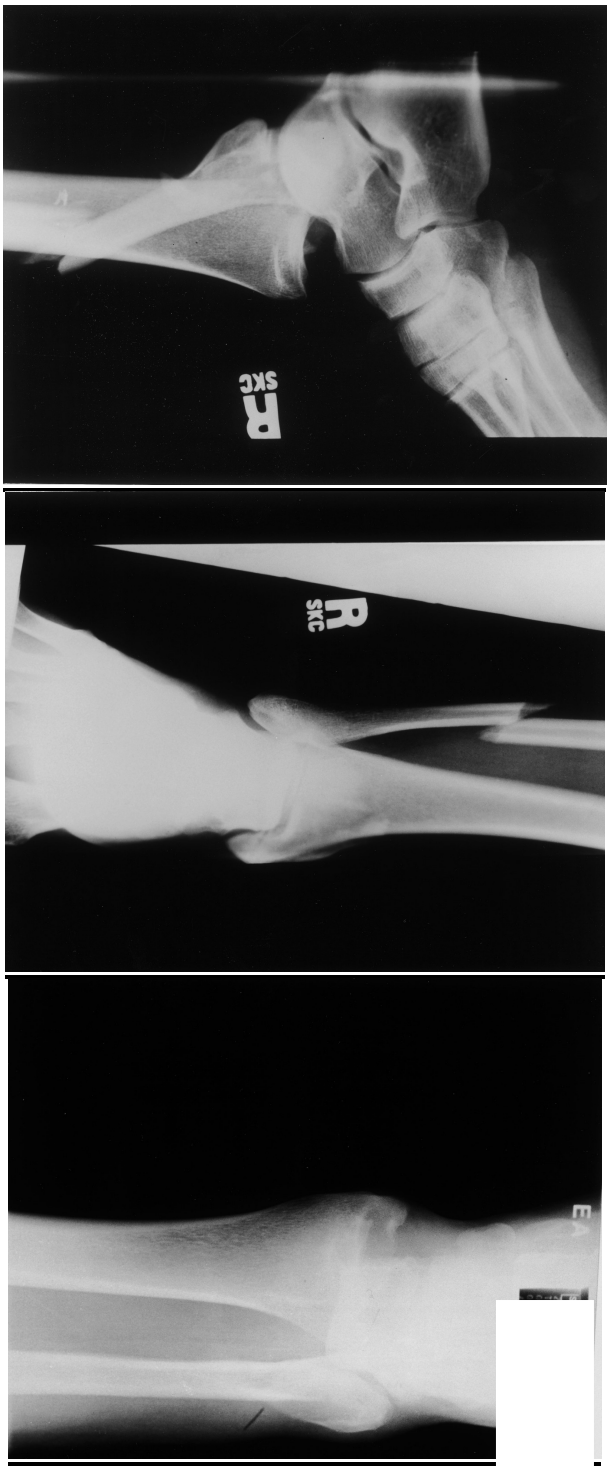

Figure C.17 Radiographs from the PWC File 15.

PWC File 16

This file involves a twenty-seven year-old male. According to the injured man, he was having difficulty making turns and fell five to ten times previously. He was going straight while sitting down, and he made a right turn at one-third throttle. Then, he made a 180-degree turn that took three to six seconds. Next he made a left turn. He started to lose the rear end, so he let off the throttle. Then he went to the right at a 90-degree angle. He felt his leg snap, and he recalled his right foot being stuck in the foot well. The injured man landed six to seven feet away from the PWC. He believes that the inside portion of the wall of the foot well is what caused the fracture to the fibula. He was wearing cross-trekker shoes at the time, and he thinks that the rubber itself may actually have held the foot.

The attending surgeon diagnosed the injury as a trimalleolar fracture/subluxation of the right ankle. The radiology report indicates the injury is a transverse fracture of the medial malleolus, a comminuted spiral fracture of the distal fibula, and a small linear bone density adjacent to the dorsal aspect of the talus, which may represent a small avulsion fracture. The surgeon states in a deposition that this is a very common fracture pattern called a supination external rotation pattern, and it is almost always due to a twisting injury. He also states that axial loading patterns usually fracture the dome of the talus or the tibial plafond, which is the end of the tibia, and is often seen when someone falls or jumps off a roof or ladder. Although these scenarios cause a tremendous axial

load injury that is more devastating than what this patient had, he states that he cannot rule out some involvement of axial loading.

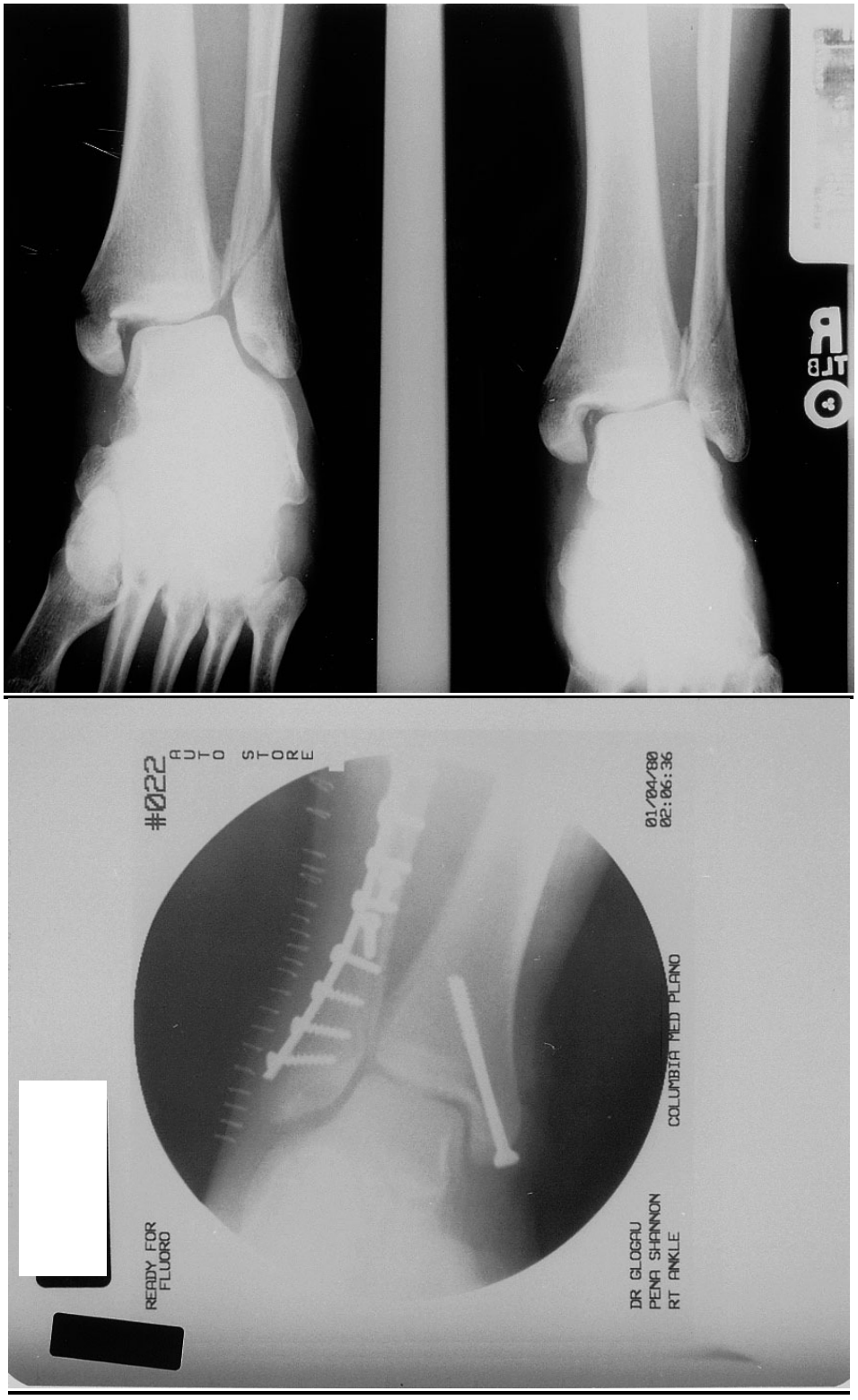

Figure C.18 Radiographs from PWC File 16.

PWC File 17

No history is reported for this case. After viewing the radiographs, an surgeon stated that the injury is a comminuted, spiral fracture of the distal tibia with a fractured proximal fibula.

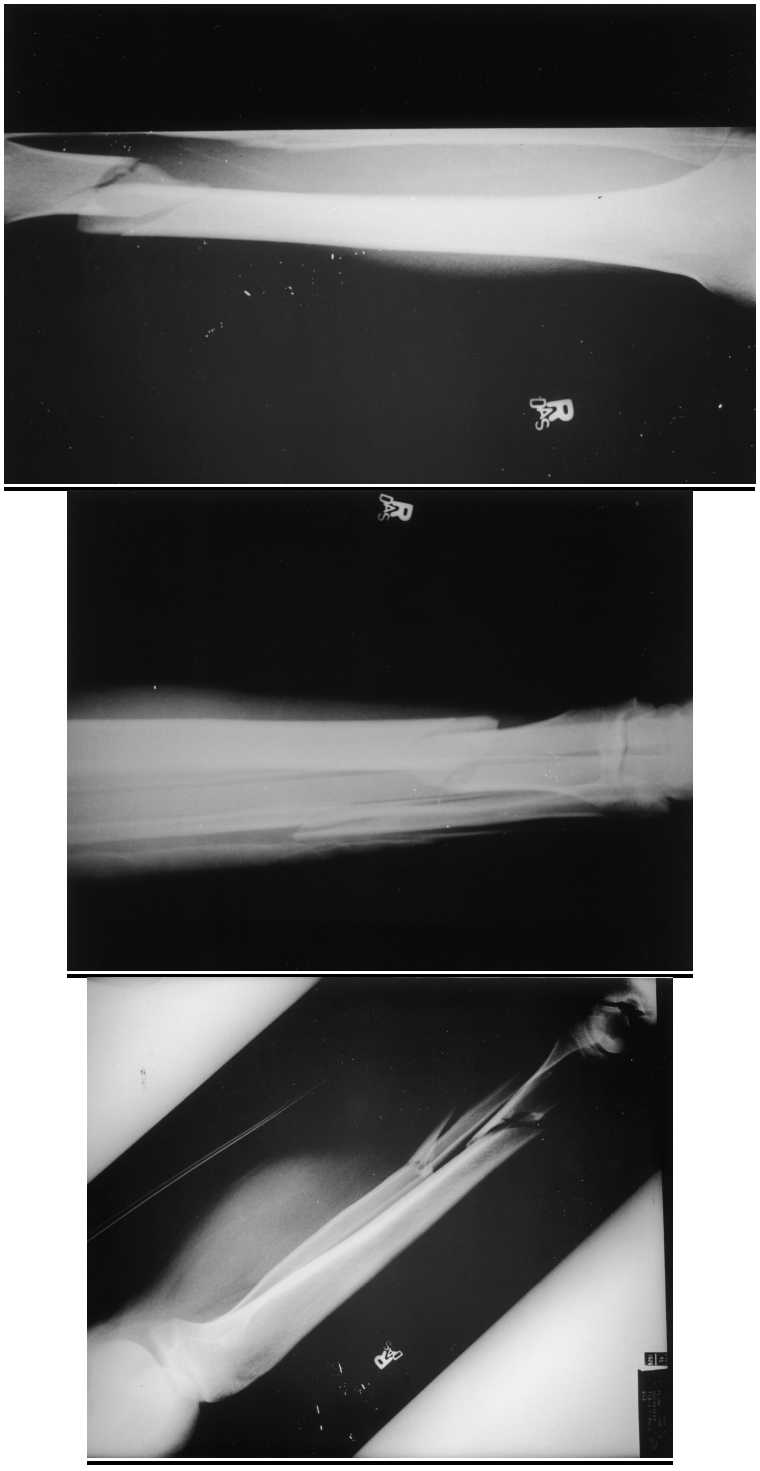

Figure C.19 Radiographs from PWC File 17.

PWC File 18

The accident involving a thirty-three year-old-male occurred on while he was riding a 1993 model PWC. An anatomy professor hired to examine the case composed a letter in which he states, “the injury consisted of a tri-malleolar fracture of the left ankle and non-displaced fractures of the metatarsals of the left foot. It was stated by the injured man in his deposition on June 5, 1995, that he was injured as the result of the handle grip coming off, and his losing his balance. He believes that a part of the machine struck his leg to cause the injury.”

The radiologist who examined the patient after his injury examined the radiographs. He concluded that the left tibia and fibula x-rays show that a horizontal fracture of the medial malleolus is demonstrated with a three-millimeter separation of fragments. Also a fracture of the fibula is noted proximal to the tibia fibula synostosis. In addition, there is an un-displaced fracture of the posterior malleolus. The ankle mortise is asymmetrical with lateral displacement of the talus. No acute bony abnormality is demonstrated in the proximal tibia and fibula. The x-rays of the left foot reveal that an un-displaced transverse fractures of the base of the second, third, and fourth metatarsals are noted.

Figure C.20 Radiographs from PWC File 18

PWC File 19

In this case forty-seven year-old male was injured on a PWC. In relatively calm water, he made a turn to avoid a skier and boat. From the right turn, he fell off the left side of the PWC. According to the radiology report, the examination reveals an oblique fracture through the distal shaft of the fibula. The position and alignment appears adequate. In addition, the ankle joint mortise is anatomic, and calcification is seen in the distribution of the posterior tibial artery.

Figure C.21 Radiographs from PWC File 19.

PWC File 20

The accident occurred in 1996, involving a forty-nine year-old male riding a 1996 model PWC. The patient states that he had just slowed down and throttled off as he was approaching two other boats with skiers nearby. He states that a wave came and pushed him up off the seat, but he still had his hands on the handlebars and he fell to his right. He states that his left leg came out of the well on the left side, but his right foot jammed in the well (he had tennis shoes on, not dock shoes). He felt a snap as he went over the side.

The radiologists states that there is a comminuted spiral variant fracture of the distal tibial shaft extending inferiorly through the metaphysis and posterior malleolus. There is marked posterior displacement of the distal segment as seen on the lateral projection. There is diastasis of the posterior malleolar fragment. There is no widening of the ankle mortise. The medial and lateral malleoli are apparently intact. There is a comminuted fibular neck fracture in the near anatomic position and alignment.

A physician gave a deposition in the case in 1998. In the deposition, he states that there has to be a high vertical loading for such an injury to occur. He also states that there is clearly rotation between the patient's upper body with the foot plant. A spiral fracture can only be developed if there is a vertical component that stops the foot from rotating. The physician believes that it is likely that the body remained still while the craft pivoted.

Figure C.22 Radiograph from PWC File 20.

PWC File 21

According to the history and examination record, the forty-seven year-old man was riding a PWC when he fell off and injured his right ankle. The patient was taken to the hospital where a closed reduction was performed and splint applied. He was transferred to a larger hospital for definitive treatment. The attending surgeon states on the operation record that the injury diagnosis to be a right ankle comminuted, compound, bi-malleolar fracture/dislocation. The orthopedic surgeon gave more detail upon viewing the x-ray. He said that the injury appears to be a transverse fracture of the medial and lateral malleolus. He also stated that the injury is an angular deformity produced by pronation-abduction.

Figure C.23 Radiographs from PWC File 21.

PWC File 22

It involves a twenty-four year-old male riding a 1996 1100 model PWC. The file includes a deposition of the injured man, which has details of the accident. He stated that the PWC's nose (bow) dipped into the water and turned slightly to the left. He was then propelled over the handlebars when he hit the top of his left foot on the left handle bar. The radiologist stated in the report that there is an oblique fracture of the posterior malleolus. There is also a transverse fracture of the base of the third metatarsal, both on the left leg. The physician refers to this type of injury as a plantar flexion eversion injury.

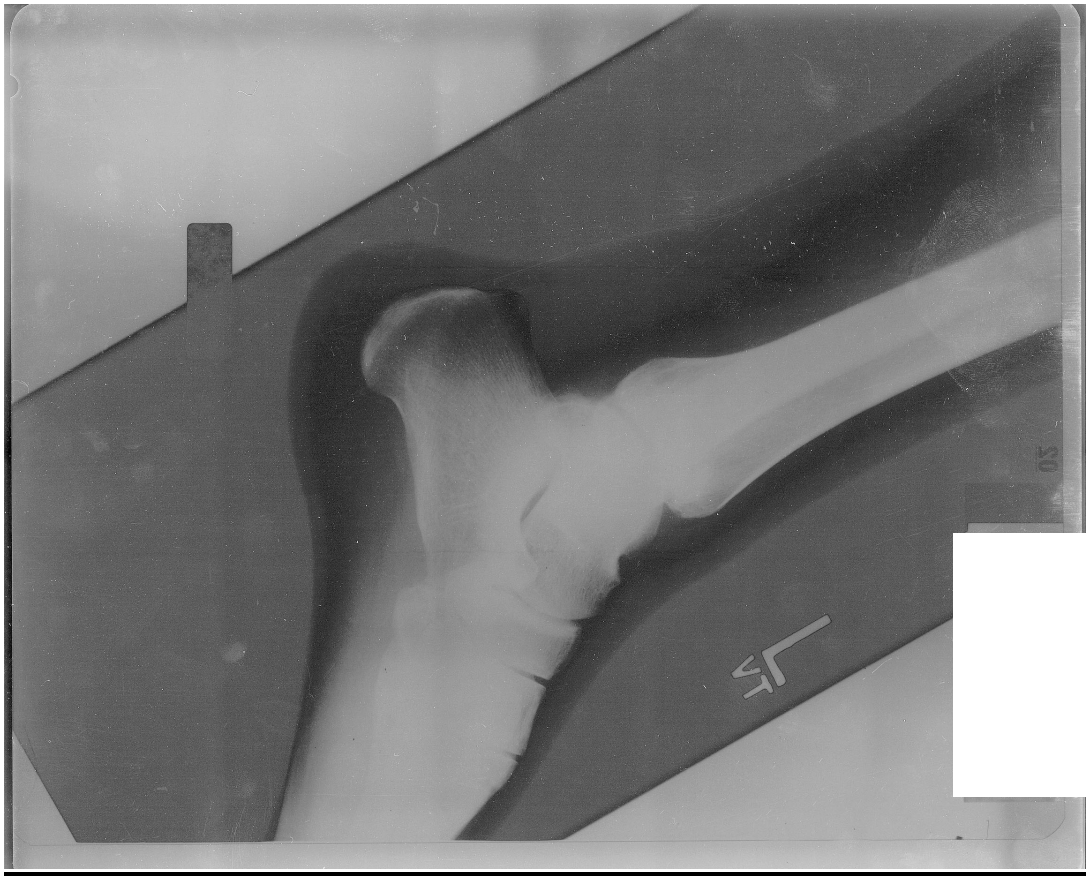

Figure C.24 Radiographs from PWC File 22.

PWC File 23

The accident involves a twenty-four year-old male riding a 1996 PWC. According to the hospital patient history report, the patient was jumping wakes of a boat when he fell off the PWC and landed on his right knee, against a corner of the PWC. However, in his deposition, he claims that he has never jumped a boat wake on a personal watercraft. He then goes on to describe the accident. He was making a left turn at an approximate speed of fifteen miles per hour, and the left handle grip came off. He grabbed the right handlebar hard, and in doing so, squeezed the thumb throttle lever causing the PWC to accelerate rapidly out from under him. His right knee hit the boarding platform in the rear of the vessel back by the transom. The x-rays demonstrate a comminuted fracture of the right patellar.

Figure C.25 Radiographs from PWC File 23.

PWC File 24

The accident involves a forty-one year-old male riding a PWC. According to legal counsel, the man was riding toward shore when he made a sharp left turn in an effort to slow down. While making the turn, he was ejected to the right of the PWC. There are no medical or legal records in this file.

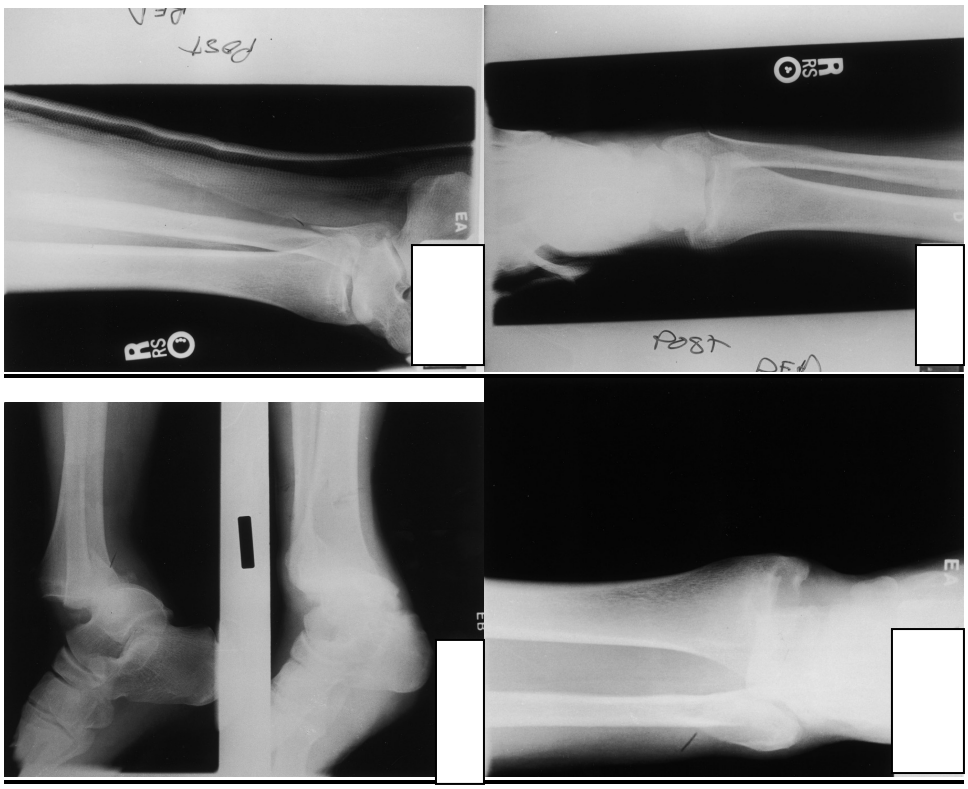

Figure C.26 Radiographs from PWC File 24.

PWC File 25

The accident involved a thirty-five year-old male riding a PWC. According to the emergency department report, the man flipped his PWC at least twice, and he was thrown forward, up over the handlebars, catching his leg against the handle bar. The attending physician diagnosed the injury as a spiral mid-shaft fracture of the left femur. The diagnostic imaging report states that a comminuted laterally and posteriorly displaced spiral fracture of the mid-shaft of the left femur is apparent.

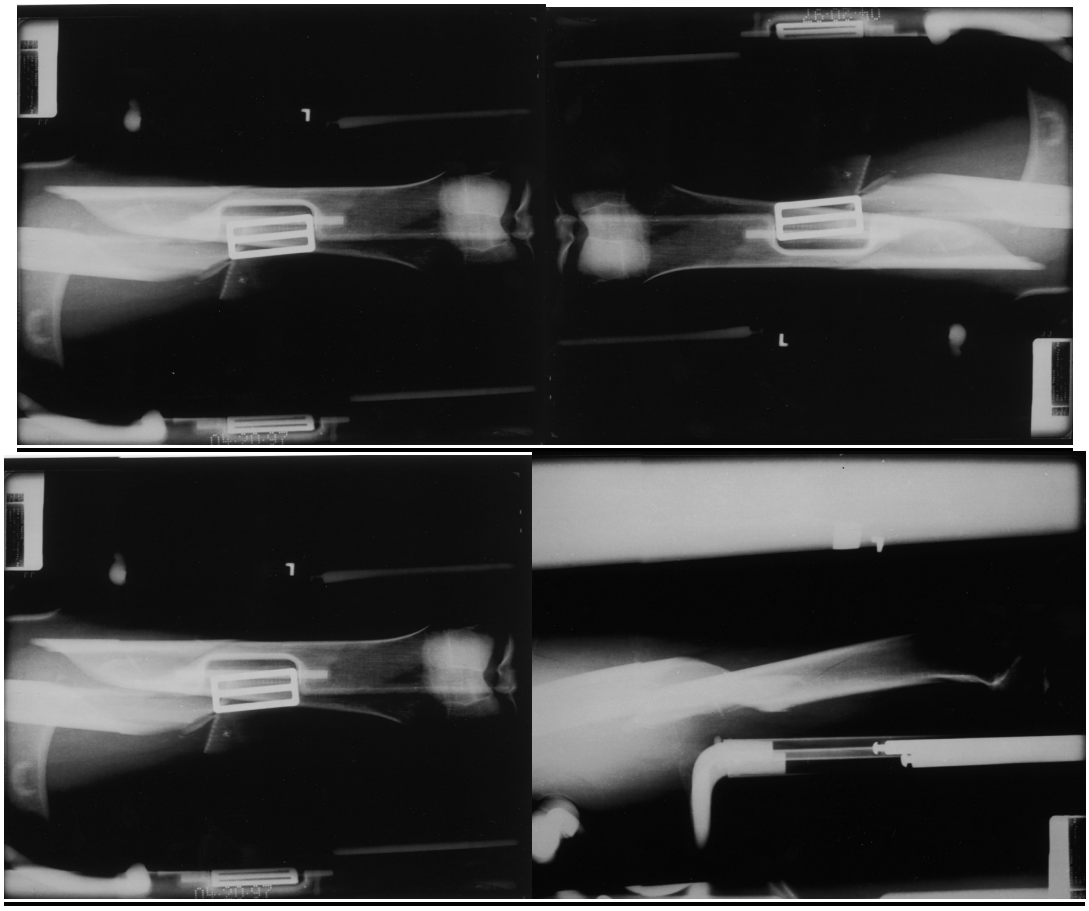

Figure C.27 Radiographs from PWC File 25.

PWC File 26

This accident involves a thirty-seven year-old male riding a PWC. According to the man's deposition taken on October 27, 1998, he hit a six to ten inch wake, and the PWC's nose dipped down. The man was thrown over the front, but he held on with his right hand. The nose of the PWC dipped about a foot. The PWC dipped once or twice before he fell to the right. Emergency room records state that the man sustained a spiral fracture of the right distal fibula. No radiographs are available for this case.

PWC File 27

The accident involves a twenty-nine year-old male riding a PWC. The clinical history report from the hospital states that the man was riding a PWC when it overturned, and he had an apparent inversion twisting injury to his ankle. The emergency room evaluation revealed a displaced fracture of the left fibula with posterior malleolar fragment of the tibia. The articular surface of the tibia was significantly disrupted. The surgeon's preoperative diagnosis found in the operative record is a displaced fracture of the lateral and posterior malleolus of the left ankle. The radiology report states that there is a fracture of the lateral and posterior malleolus. The fracture fragments are essentially undisplaced. There are no radiographs available for this case.

PWC File 28

According to the medical records, a twenty-nine year-old female was riding a 700 model PWC, when she jumped a wave causing her to fall off. The patient states that the kill switch did not operate appropriately, and the PWC came around and struck her in the right femur. She was taken to the hospital where the radiologist wrote a report on the injury. The right femur is examined in the A.P. and lateral projections utilizing the portable imaging apparatus. There is a complete horizontally oriented fracture of the mid shaft of the right femur. There is a lateral displacement of the fracture fragment. Also, there is an approximate one-centimeter area of apposition involving the lateral cortex of the proximal femur and the medial cortex of the distal fracture fragment. A traction device is identified, and the evaluation of the proximal femur is equivocal as is the evaluation of the right hemipelvis.

VITA

Anne Kroman was born May 11th, 1980 in Houston, Texas to Deb and Jim Kroman. While growing up, Anne lived in Houston, Texas; High Point, North Carolina; and Kansas City, Missouri. After high school, Anne attended the University of Kansas in Lawrence, Kansas where she graduated with honors and *Phi Beta Kappa* and a major in Anthropology. After completing her undergraduate degree in 2001, Anne came to The University of Tennessee for her graduate education. She completed her master's thesis on skull trauma in 2003, and remained in Knoxville to work on her Ph.D.

Anne's main area of research is the biomechanics of trauma and injury causation. She has done research in this area since 2000. Anne also has interests in human anatomy, dental anthropology, and evolutionary biology. Currently, Anne is a research scientist for B.E.S.T. Engineering where she works with fracture biomechanics, accident reconstruction, and product safety.

When she is not breaking things, Anne enjoys traveling, photography, running, and boating. Most of all, Anne enjoys spending time with friends and family and relaxing with a good class of red wine.